DISSERTATION

WHAT'S THE MATTER WITH WHITE MATTER? AN EVALUATION OF POSTURAL CONTROL MECHANISMS IN MULTIPLE SCLEROSIS

Submitted by

Sutton B. Richmond

Department of Health and Exercise Science

In partial fulfillment of the requirements

For the Degree of Doctor of Philosophy

Colorado State University

Fort Collins, Colorado

Spring 2020

Doctoral Committee:

Advisor: Brett W. Fling

Daniel Peterson
Heather Leach
Agnieszka Burzynska

ABSTRACT

WHAT'S THE MATTER WITH WHITE MATTER? AN EVALUATION OF POSTURAL CONTROL MECHANISMS IN MULTIPLE SCLEROSIS

Interacting with environments that are constantly varying is difficult and, as bipedal mammals, keeping an upright posture requires a great deal of spatial and temporal acuity. The studies encompassing this doctoral dissertation provide mechanistic insight into the gait and balance of both neuro-typical and -atypical (i.e. people living with multiple sclerosis) adults to understand the neural underpinnings contributing to reduced locomotion and postural control, thereby increasing risks of falls and injury. Enhanced comprehension of the underlying mechanisms for postural control were attained through the abridgment of multiple scientific disciplines including biomechanics, neuromechanics, and neuroimaging to apply advanced concepts to identify biomarkers for future therapeutic interventions. The outcomes from this work demonstrate that, in comparison to neurotypical adults, the people with multiple sclerosis walked with a more conservative and asymmetric gait pattern regardless of speed or cognitive load. Poorer microstructural integrity of transcallosal sensorimotor white matter fiber tracts was strongly associated with these behavioral deficits, thereby establishing a structure-function relationship that comprised both static and dynamic postural control. Implications from this research provide a base of knowledge for how the brain successfully coordinates and controls movements, laying a foundation for future neurorehabilitation approaches that increase independence and overall quality of life.

ACKNOWLEDGMENTS

Research is no one man or woman effort, it takes the collective efforts of a team to produce successful outcomes that can contribute to a productive whole and make an impact to the larger field. This dissertation work was facilitated by the members of the Sensorimotor Neuroimaging Laboratory (SNL) collectively, as each of these individuals over the last three years contributed in one form or another to the success of this project and I thank each of them for their contributions. In research and your career, journeying a new path is not without its own inquisitions and tribulations; the mentorship from Dr. Brett W. Fling (SNL Director) and my committee members (Drs. Daniel Peterson, Heather Leach, and Agnieszka Burzynska) played an invaluable part in making this journey possible. Lastly, achieving a doctoral degree is well established as being a marathon and not a sprint to finish, accomplishing this feat with the support of friends and family is a necessity. The most intracule role in my race came from the encouragement, time, and dedication provided by my wife, her support pushed me to do more than I ever thought possible and finish this academic marathon.

TABLE OF CONTENTS

Chapter 1 | Background

Disclosure Statement: The succeeding information described in background of this dissertation documentation were summarized into a prior published review editorial, see *Richmond and Fling (2019) [1].*

Whether within the spectrum of aging or various neurological impairments, the ability to effectively maintain posture or properly ambulate is essential to the daily lifestyle of a fully functioning adult. Postural stability and locomotor deficits have been related to increases in fall rates and associated injuries that directly contribute to a decreased overall quality of life or reduction in independence. It has been reported that 2.8 million people are admitted to the hospital each year due to a fall-related incident [2] and furthermore, in 2015 fall-related injuries were reported to account for 50 billion dollars of annual medical care costs [3]. More insight into the various mechanisms and neural underpinnings contributing to falls is necessary to develop specific and effective rehabilitation/fall prevention strategies.

The mechanisms of mobility are complex and involve a multitude of sensory inputs and motor outputs to achieve the necessary biomechanical goals of postural control. Whether attempting to stand still while waiting in line to buy a movie ticket or ambulating across the street to that movie theater, our sensory feedback systems (i.e. proprioceptive, vestibular, and visual systems) are constantly relaying information via the central nervous system to the brain enabling motor output (i.e. muscle and tendon) corrections [4]. These corrections are made, in an effort to maintain the center of mass (CoM), also known as the center of gravity (CoG) on Earth, within the base of support (BoS) defined as "the area within an outline of all ground contact points" [5]. If the CoG deviates outside the BoS and is not corrected in a timely manner, this will result in

instability and inevitably a fall [6, 7]. When this BoS becomes dynamic and the ground contact points are fluctuating, as seen in normal gait, the complexity of the mechanics and timing of the movements become imperative. It has been proposed that gait is merely a series of unstable events or a continuous state of imbalance by where each foot fall or step is strategically coordinated to prevent the act of falling [8]. Moreover, these timed corrections become increasingly difficult and dangerous when there is a decline in the ability to regulate or coordinate movements. Any decline in these abilities to regulate the locomotor properties will increase the probability of a fall [9, 10] and therefore result in a declined quality of life [11].

In neurodegenerative populations such as multiple sclerosis (MS), deteriorations of postural control systems predispose these individuals to pathophysiological features that escalate mobility/postural instabilities [11, 12]. These features have promoted MS to being the leading, non-traumatic, neurodegenerative disease among young adults, affecting more than 2.1 million people worldwide and nearly a million people in the United States alone [13, 14]. Its disease course is highly unpredictable, attacking the central nervous system (i.e. brain and spinal cord) through the demyelination of axons (i.e. white matter) without affecting myelination of the peripheral nervous system [15-17]. Gait and postural instabilities/impairments underlie the progression of MS, with more than 50% of people with MS (PwMS) reporting a fall stemming from these instabilities since diagnosis [18]. This inevitably results in the reduction of an active lifestyle and increases in falls, injuries, and even mortality, compromising the ability for PwMS to interact with situations that arise within their everyday surroundings and environment, contributing to a decreased quality of life [19, 20]. Given that the chief compliant filed by 85% PwMS stems from gait or motor disturbances [21, 22] and that a staggering 56% of PwMS will

incur a fall within any given three-month span [23], identification of the postural control mechanisms underlying the shortened health span of these individuals is crucial.

Biomechanics: Postural Control

Human beings are constantly attempting to control (i.e. directing influence upon the postural system [24]), internal and external influential factors initiated in the constructs of our everyday lives. Occupying a world where environments are everchanging and new situations are constantly being encountered, modifications of behaviors both cognitively and physically are required. To physically adapt to these situations, postural changes or alterations in both the static and dynamic domains [4] of body positions are executed in response to conditions that threaten stability with impending fall consequences [12]. Postural control is signified as the act of controlling the position of the body in a given space for the primary purpose of maintaining a stabilized orientation [25] specifically, an upright orientation.

Originally, postural control was hypothesized to be derived from a single system (i.e. the vestibulospinal system) via sets of righting and equilibrium reflexes. However, further field advancement allowed world renowned postural control expert, Dr. Fay B. Horak, to establish a multifaceted model detailing the six important domains of postural control (**Figure 1.1**) [9]. These six domains include biomechanical constraints, movement strategies, sensory strategies, orientation in space, control of dynamics, and cognitive processing. Collectively, the domains describe postural control as a complex motor skill based on the interaction of dynamic sensorimotor processes that are highly situation/task dependent [9]. Within each of the six domains consist individual resources (**Figure 1.1**) and any reduction, deterioration, or loss of these resources would effectively lead to postural instability [9].

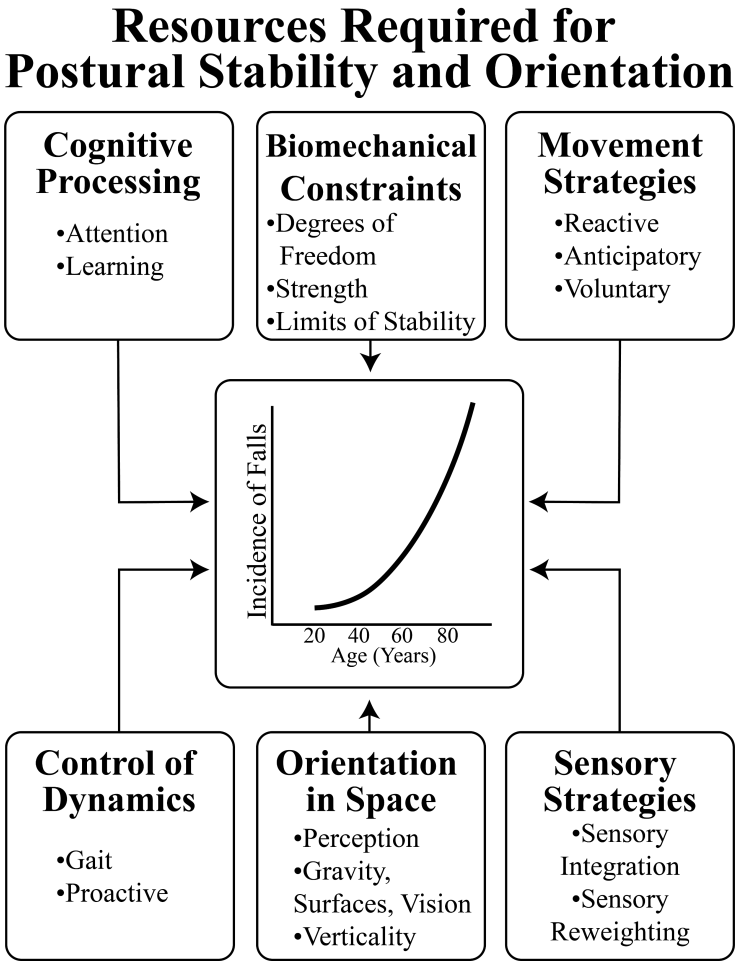

Figure 1.1 | Resources required for postural stability and orientation. A paradigm of the six domains comprising postural control and the resources encompassed by each of the domains. The displayed resources are purposed to be vital for avoiding falls and maintaining the upright bipedal stance. *Figure was adapted from Horak (2006)* [9].

Encompassed within each domain of postural control is the overarching goal to constrain the CoM/CoG within the BoS; this goal can be simplified as achieving states of stability or more generically signified as balance. The CoM is the point where the entire mass of the body is assumed to be concentrated around. Furthermore, on Earth, where there is a strong gravitational presence, the CoM is recognized as the CoG. Stabilization within postural control is affected by

two factors, the height of the CoG and the size of the BoS [26]. For a human being, the CoM (i.e. CoG) is located in a relatively disadvantageous elevated position (~1m above the ankles) atop a comparatively small BoS [27], resulting in a posture that is inherently unstable. To maintain the upright position in the bipedal stance, postural control is dependent upon the neural regulation of both postural equilibrium and postural orientation [28]. The postural equilibrium systems are tasked with stabilizing the CoM within the BoS, requiring the coordination of the sensory and motor strategies to maintain stability during both static or dynamic (locomotive) posture. In conjunction with equilibrium, postural control orientation is attained through central neural interpretation of the sensory reference frames, consisting of the visual, vestibular, and somatosensory (i.e. proprioceptive) system inputs. Visual and vestibular inputs are imperative for orientation of the body, accounting for information derived from body sway (i.e. body movement direction and speed) and gravity, respectively [4]. Somatosensory inputs originate from a number of different receptors and these receptors provide information from "skin in contact with surfaces, limb segment orientation from muscle proprioceptors and joint receptors, as well as muscle length, velocity and force information" [4]. Both individually and collectively, the sensory reference frames provide vital feedback and feedforward information to the body for successful attainment and sustainment of stabilization.

More broadly the aspects/goals of postural equilibrium and postural orientation are independently controlled and sometimes we relinquish one goal for another, often occurring post system re-weighting upon the situation/environmental circumstances encountered [4]. In an optimal environment (i.e. a well-lit room, on a rigid surface) the neurotypical adult has shown to weight the sensory system inputs of somatosensory, vestibular, and visual in a 70%, 20%, and 10% respective system weighting [29]. Through specialized neural circuitry these aforesaid

inputs will facilitate a link between the mind (cognitive) and body (physical). Low-level muscle tension referred to as postural tone is generated to create sound structural force production in both the proximal and distal skeletal muscles required for stabilization of the body segments [27]. When groups of postural muscles are activated at one instance this is deemed as utilizing postural synergies [30]; to avoid the incidence of a fall, different postural strategies are applied. The two primary strategies employed for efficient bipedal postural control are the hip strategy and the ankle strategy. Basis for these strategies is dependent upon the emitted sensory feedback, the immediate sensory conditions, and relevant prior conditions encountered [4]. The ankle strategy is utilized primarily for fine adjustments of postural sway. While larger adjustments or instances where greater torques are required for postural sway corrections, the hip strategy is necessary [31]. Although these strategies are typically nominated upon the magnitude of the sway adjustment required, they are often used in succession of one another. In summation, postural control is more than a single entity, it is a multi-factorial design (referring back to **Figure 1**) contributing to how we maintain static stances and proceed through dynamic ambulation in a safe and effective upright manner.

Static Postural Control

Standing in the bipedal upright position, the human body is constantly combating gravitational forces, requiring constant maintenance which often goes unnoticed. Whether standing in line at the local movie theater or endeavoring the body contortions of the Vrikshasana (i.e. yoga Tree Pose), the body is always attempting to achieve equilibrium and minimize postural sway. Static postural control, also referenced as postural steadiness, is the act of attempting to reach a state where no movement is occurring or as little postural sway as physically possible is being incurred [32]. More specifically from a biomechanical view,

reaching postural steadiness (i.e. the static states) is in reference to a point in time where both the net torques and forces acting on or within the body amount to zero [26]. Although the goal of the static postural control is to attain these zero states (i.e. postural steadiness), it is highly improbable that zero states are able to be sustained for any extended period of time. As previously declared, forces constantly being applied to the body by gravity and other external environmental kinetic factors, thereby hindering any sustainability of postural steadiness. Objective quantification of postural steadiness is completed with the widely-popular utilization of kinetic measurements such as forces, moments, masses, and accelerations. These kinetic measures are determined exclusive of any detailed knowledge regarding position or orientation [33] of the body or its segments.

In 1687, Sir Isaac Newton developed the laws of mechanics; consisting of the 1.) law of inertia, 2.) law of acceleration, and 3.) law of reaction. The third law, based on reaction, states that "when one body applies a force to another body, the second body applies an equal and opposite reaction force on the first body" [34], and is has set the precedence from which all main forms of kinetic quantitative metrics are originated from. When quantifying postural movement, as the body applies forces to the earth, these forces will be signified by a single vector, containing a designated magnitude and direction. Thereby, a force of equal magnitude will be registered in the opposite direction, deemed the opposite reactive force. This single equivalent force, equal to the sum of the distribution of forces applied to a surface, is represented as a ground reaction force. Indirect quantification of changes occurring amongst ground reaction forces projected from the body are recorded via the force platform (**Figure 1.2** [34]) [35, 36].

Force platforms (e.g. force plates) are biometric measuring devices providing technical assessments of balance or postural control/stability [36]. These assessments of balance are umbrellaed under the terminology of stabilometry, the quantification of forces occurring under the feet as a continuous displacement of the CoP [4] and can be completed with two varieties of commercially available force platforms, the strain gauge or the piezoelectric crystal. Both modes of force quantification have been heavily utilized and scrutinized in research over the past four decades. However, the high-frequency responsiveness of the piezoelectric crystal-based platform has revealed to record ground reaction forces with higher ranges and sensitivities compared to its strain gauge counterpart [34]. At its basis, the force platform operates to quantify ground reaction forces, a summation of all the distributed forces applied to the surface of force platform into a single resultant force vector. These resultant forces are surmised from three dimensional components, the *+X (width), +Y (length), and +Z (vertical)* (**Figure 1.2**). The distribution (i.e. the summation) of forces contacting the surface of the plate [34], are a reflection of the CoM

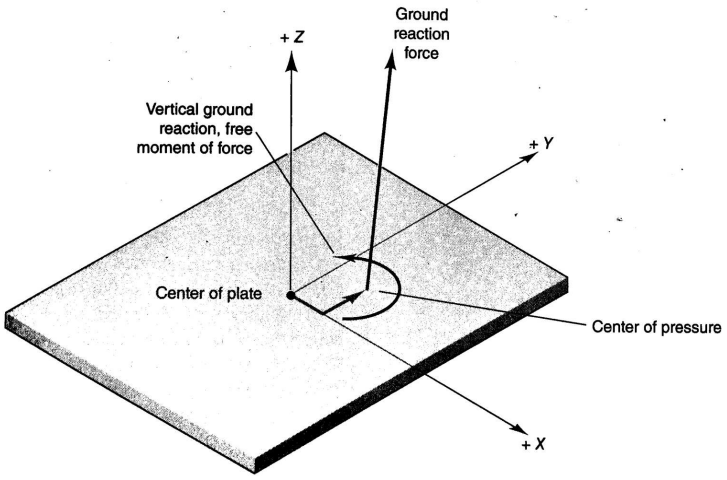

Figure 1.2 | Force components. A diagramed depiction of reaction forces and resultant distributions of the total force when applied to the force plate surface. *Adapted from "Research Methods in Biomechanics" by Robertson et al. (2006) [34].*

trajectory, defined as the CoP [25, 37]. Two-dimensional derivatives (anterior-posterior and medial-lateral) can be originated from the net CoP, allowing for derivation of commonly reported measures such as path length, total excursion, root-mean-square, velocity, and much more [25]. For decades, the laboratory-grade force plate has set the standard by which measures of postural stability are quantified. However, due to the large expense of these devices, costing upwards of ~$5,000-$75,000 or more, lack of portability, and requirement for external power sources, often preclude this option for individuals conducting kinetic assessments in the clinical or field settings [38, 39]. In addition to an AC power requirement, the laboratory-grade force plate is also required to be fixed (bolted) to a surrounding structure, again making this instrument impractical in diverse research or clinical environments.

Figure 1.3 | Portable alternatives. A pictorial of the Balance Tracking System (BTrackS) balance plate; a cost-effective, portable, and validated instrument for quantifying center of pressure displacement. *Adapted from Richmond et al. (2018) [40].*

The advancements procured during the technological revolution has provided countless contributions to biomechanical research, increasing our methodological capabilities to construct more precise objective quantifications. To alleviate some of the drawbacks that accompany the laboratory-grade force plate, portable force platform alternatives have been developed. These mobile replacements are becoming increasingly cost effective ($~795, plus software) and lighter

(<7 kg); leading this portable revolution is the Balance Tracking System Balance Plate (BBP) (Balance Tracking Systems Inc., San Diego, CA, USA) (pictured in **Figure 1.3** [40]). Demonstrating both high accuracy and precision, as well as near perfect inter-device reliability for both X and Y CoP directional components the BBP is vastly becoming a fierce competitor of the "gold standard" laboratory-grade force plate [41]. The BBP enables researchers and clinicians to compute CoP-derived postural metrics outside the laboratory, providing a validated way to deliver these outcomes with near (correlations of 0.98 or greater) perfect precision [40].

Kinetic Outcomes: Traditional Metrics

Traditional CoP-derived metrics are the primary dependent variables utilized in the assessment of postural control [25] and are the result of combining both the anterior-posterior (AP) and medial-lateral (ML) directional components (i.e. two-dimensional (2D) measures). Although the evaluation of each of the directional components are imperative for the discovery of changes in postural control [25], measures of static postural stability are typically separated into discrete spatial (e.g., CoP range or distance) and temporal dimensions (e.g., duration or average CoP velocity). These discrete measures represent different aspects of postural control within the entire CoP time-series and include:

- **Path Length:** the magnitude of two-dimensional displacement based on the total distance travelled [42].

$$PL = \sum_{i=1}^{N-1} \sqrt{(CoP_{x_{i+1}} - CoP_{x_i})^2 + (CoP_{y_{i+1}} - CoP_{y_i})^2} \qquad [43]$$

- **Root-Mean-Square (RMS):** the variability of the postural movement more specifically, mathematically derived as the "standard deviation of the displacement of the CoP" [25, 42].

$$RMS = \sqrt{\frac{\sum_{t=1}^{N}(\overline{x}-x_t)^2}{N}} \qquad [43]$$

- **Total Excursion:** "the total distance traveled by the CoP over the course of the trial duration" [25].

$$TOTEX = \sum_{n=1}^{N-1}[(AP[n+1]-AP[n])^2 + (ML[n+1]-ML[n])^2]^{\frac{1}{2}} \qquad [44]$$

- **Velocity:** the CoP excursion or distance travelled divided by the trial time [25, 42].

$$MVELO = TOTEX/T \qquad [44]$$

- **Ellipse Area:** total area covered in the ML and AP direction using an ellipse (often reported as the 90% or 95% ellipse) to fit the data [42].

$$AREA - CE = \pi ab = 2\pi F_{.05[2,n-2]}\,[(s_{AP}^2 s_{ML}^2) - s_{AP\,ML}^2]^{1/2} \qquad [44]$$

- **Frequency:** the rotational frequency of the CoP if it travels the total excursions around a circle with a radius of the mean distance, in revolutions per second or Hz [44, 45].

$$MFREQ = \frac{TOTEX}{2\pi MDIST * T} = \frac{MVELO}{2\pi MDIST} \qquad [44]$$

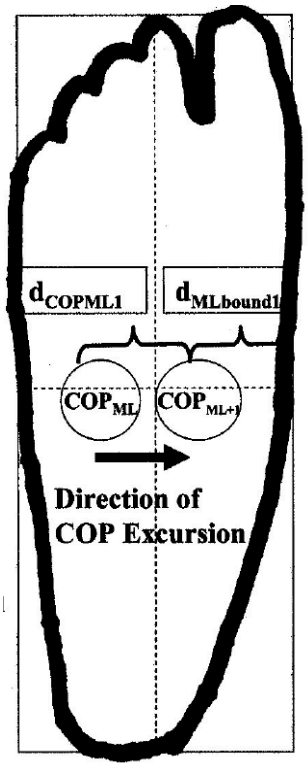

Figure 1.4 | Foot Model. A graphical representation of the foot exterior parameters being modeled as the boundaries, comprising a rectangular representation of the base of support. Interior calculations are representative of the medial-lateral two-dimensional analysis. *Adapted from Hertel et al. (2006) [52].*

These dimensions have proven to be vital in indicating postural unsteadiness and increases in dependent variables like velocity (a temporal dimension) have been found to be in direct correlation to the reduction in the ability to control posture [25, 46-49]. Likewise, reductions in spatially derived metrics such as path length, RMS, ellipse areas and total excursion of the CoP path are synonymous with minimized distances traveled by the CoP (e.g. a smaller amount of total excursion) [49-51] or better postural control. However, caution and carefully established context should always prelude interpretations of CoP-derived measures. For

nearly half of the last century biomechanists have been engrossed with different elucidations of the meaning of many of these measures, thus interpretations need to be navigated carefully and continually evaluated to reduce the convolution of outcomes.

Kinetic Outcomes: Time-to-Boundary

Coinciding with the advancements in measurement technology, outcome analyses have also progressed with the turn of the new century. Instead of separating each of these dependent (traditional) variables into spatial or temporal dimensions, more sophisticated measures are revolutionizing how we evaluated postural control, in particular time-to-boundary (TTB). TTB is multi-dimensional measure of postural control, incorporating both spatial and temporal (i.e. distance and time) dimensions into a single measure along the entire CoP time series. This measure considers both the trajectory and velocity parameters of each CoP data points relative to the edge of the BoS. The instantaneous velocity of the data point is calculated (see **Equation 1a**) in each direction of the two-dimensions (i.e. AP and ML). TTB for each direction is computed via dividing the distance by the aforementioned instantaneous velocity (see **Equation 1b**) [52]. Boundaries for these calculations are established by a modeled-rectangle representative of the foot (**Figure 1.4** [52]), this foot model allows for the CoP in each two-dimensional (AP and ML) component to be measured [52-54].

Equation 1a.) AP: $V_{CoP\_AP_1} = d_{CoP\_AP_1} / T$ [52]

ML: $V_{CoP\_ML_1} = d_{CoP\_ML_1} / T$

Equation 1b.) AP: $TTB\_AP_1 = d_{AP\_bound1} / V_{CoP\_AP1}$ [52]

ML: $TTB\_ML_1 = d_{ML\_bound1} / V_{CoP\_ML1}$

The TTB measure represents the amount of time available to make corrective postural adjustments prior to the incidence of a fall (e.g. the CoM traveling outside the BoS). This measure allows clinicians to track when, how often, and the magnitudes of the minimum time available to make these adjustments. It is expected that a higher frequency of recorded minima values and the smaller TTB magnitudes (i.e. a lower time recorded, less time until an individual reaches the boundary (edge) of his/her BoS) is indicative of a reduced aptitude of postural control. TTB has displayed inverse relationships with age; indicating that reduced margins of stability likely play a key role in reductions of postural control [55, 56]. Regardless of how postural steadiness or control is quantified, the scope of information achieved by this type of analysis goes beyond the parameters of the neurotypical aging population and has potential to be instrumental as a fall prevention aid for atypical neurodegenerative populations.

Postural Steadiness of People with Multiple Sclerosis

As described above, the mechanisms of postural control are complex and involve a multitude of sensory inputs and motor outputs to achieve the associated biomechanical goals required to maintain an upright postural position. Our sensory feedback systems (i.e. proprioceptive, vestibular, and visual systems) are constantly relaying information via the central nervous system to the brain for the coordination of motor output corrections [4] to accomplish the aforementioned biomechanical goal. If these output corrections are not executed in a timely manner and the CoG (ipso facto the center of pressure) deviates outside the BoS, this will inevitably result in instability and inevitably a fall [6, 7]. Highlighted by the importance of the sensory feedback system, proprioception is transmitted for input/interpretation via the cortical spinal tract (CST), otherwise referred to as the cortical proprioceptive tract. This white matter relay tract is highly conductive and relies on time sensitive information transference and

becomes hindered, inconsistent, and potentially dangerous when demyelination occurs. Demyelination is the hallmark disease characteristic of MS; an auto-immune disease causing a wide variety of structural, connective, and activation challenges causing further functional (i.e. gait and balance) deficits. Postural unsteadiness is embedded within the pathology of MS, as PwMS demonstrate decreased postural control amongst a multitude of dependent variables compared to a neurotypical population (refer to **Table 1.1**) [12]. PwMS exhibit postural deficits stemming from larger postural magnitudes, leading to an inability to control the CoM within their BoS. Proprioceptive information for quiet standing is initiated in the lower extremities, traveling up spinal cord via the dorsal columns and decussating at the ipsilateral nucleus gracilis post synapse. The neural transmission ascends the medial lemniscus to the ventral posterior-lateral nuclei located within the thalamus, before arriving at the post-central gyrus and dispatched to the primary somatosensory cortex (Brodmann Area 3a) [57]. Dr. Brett W. Fling and colleagues have implicated that diminished quality of microstructure in this pathway as the origin for insufficiencies leading to increased postural instability [58]. Within this path lye the ascending dorsal column-medial lemniscus of the CST, responsible for the transmission of fine touch, vibration, and conscious proprioceptive information to the cerebral cortices [58]. Dr. Fling establishes further that poorer proprioception is associated with poorer CST microstructural integrity (see **Figure 1.5**) and is implicit with diminished postural steadiness [58]. Although blossoming associations are prevalent between the neural circuitry/sensory feedback and traditional postural kinetic outcomes; correlations between proprioceptive neural circuitry and

more advanced multi-dimensional measures of postural control (i.e. TTB) have yet to be established.

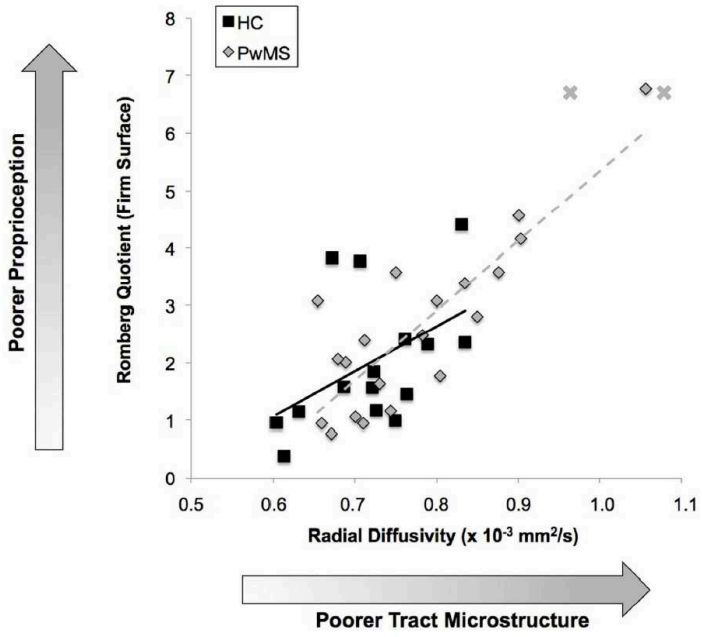

Figure 1.5 | Poorer microstructure integrity of the proprioceptive pathway is associated with poorer proprioceptive-based balance performance in PwMS. A strong association was established between increasing RD (i.e. poorer white matter tract integrity) and poorer static postural performance (i.e. increased sway area) proprioceptive sensory reference frames in PwMS. *Adapted from Fling et al. (2014) [58].*

Table 1.1: Primary Postural Stability Deficits in PwMS (Adapted from Comber et al. (2018) [12])

Dependent Variables	Neurotypical vs. Atypical Neurodegenerative Adults (PwMS)
General Postural Outcome	
CoP Path Length	Longer
CoP Velocity	Higher *(in the ML direction)*
Sway Area (or 95% CE)	Longer
Quiet Stance with Eyes Open (on Rigid Surface)	
CoP Displacement	Higher*: raw displacement, & RMS
CoP Velocity	Higher*: raw, larger SD, & Higher RMS
Quiet Stance with Eyes Closed (on Rigid Surface)	
CoP Displacement	Larger (AP&ML) raw displacement, path length, & RMS
CoP Velocity	Higher
Time-to-contact boundaries (TTB)	Lower
CoP Area	Larger
Trunk Sway	Greater
CoG Movement	Larger
Sway Acceleration	Greater
Sway Jerk	Greater
Sway Path	Larger
Quiet Stance with Eyes Open (on Compliant Surface)	
Postural Sway	Higher
Time-to-contact boundaries (TTB)	Shorter Times
CoG Velocity	Higher
Quiet Stance with Eyes Closed (on Compliant Surface)	
Postural Sway	Higher
Time-to-contact boundaries (TTB)	Shorter Times
Total Area Covered	Larger Area
CoG Velocity	Higher Velocity
Limits of Stability	
Reaction Times	Larger
Movement Velocities	Higher
Max Excursion	Lower

Note: **Not Significant*

Dynamic Postural Control

Brooks (1986) blurs the line between posture and movement by saying, “movements are the transition from one posture to another” [59]. In the upright bipedal position, the body is propelled forward through the ambulation of the lower extremities, the legs carry out propulsion

and add structural support of the movement; Dr. David Levine terms this action as 'normal walking' [33]. Different neural circuitry, muscles, and tendons produce the aforesaid transitions of postural position, creating a BoS that remains in a state of continuous modification, attempting to synchronize or keep up with the undulating movement of the CoM. Given the complexity of these movements, to coordinate the activities related to the manipulation of the BoS with the CoM, there is an inherent constant state of imbalance. During ambulation, each foot strike or placement of the foot is strategically completed, consciously or unconsciously, in order to prevent a fall [37]. The ability to successfully place the swing foot in a proper orientation and distance from the plant foot with the expectation of controlling the CoM motion, thereby regulate the body's momentum is the act of dynamic postural (balance) control [60]. Often this action can be described through the manner or style in which the movement (i.e. walking) is carried out, popularly defined as an individual's 'gait' or more specifically, the depiction of coordinated footfall patterns and the biomechanical properties (e.g. interaction between internal and external factors) within the movement through neuromusculoskeletal actions [33, 61].

The gait cycle (**Figure 1.6**) is "the time interval between two successive occurrences of one of the repetitive events of walking"; these occurrences, also known as major events, include the 1.) initial contact, 2.) opposite toe off, 3.) heel rise, 4.) opposite foot initial contact, 5.) opposite toe off, 6.) feet adjacent, and 7.) tibia vertical [33]. These seven major events can be abridged into two distinct phases, the stance phase and the swing phase. Each phase is subdivided into distinct parts; encompassed within the stance phase is the loading response, mid-stance, terminal stance, and pre-swing, while the swing phase can be broken down into the initial swing, mid-swing, and terminal swing (**Figure 1.6**) [33]. Due to the intricate nature of these complex movements, gait cycle timing is critical and signifies the different phases of gait. When

proceeding through the 'normal walking' gait cycle, 60% of the gait cycle is spent in the stance phase, prior to entering the final 40% of the gait cycle, the swing phase, demarked by the toe off action (occurring at 60% mark of the gait cycle (**Figure 1.7** [62])) [33, 61]. Considering the complexity of these actions and the delicate timeframes to which these actions must be executed within, coordination between mind and body is pivotal. Unaccounted alterations of gait timing will enviably result in the reduction of ambulation aptitude (i.e. poorer bilateral coordination), thereby constructing a cascading effect of biomechanical consequences piloted by an upsurge of postural unsteadiness escalating the likelihood of incurring a fall.

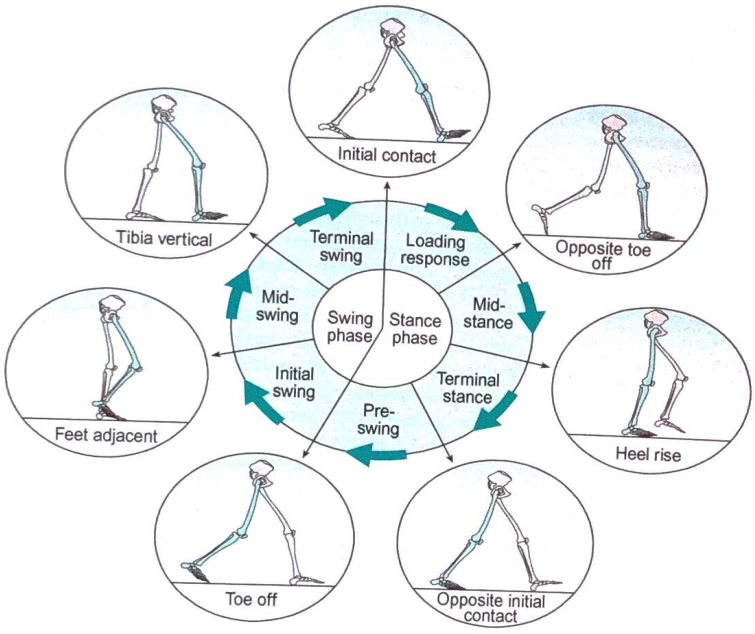

Figure 1.6 | Events of the gait cycle. The major events of the gait cycle with the subdivided phases. The highlighted leg is represented in teal and demonstrates each of the signified stages. *Adapted from "Whittle's Gait Analysis" by Levine, Richards and Whittle (2012) [33].*

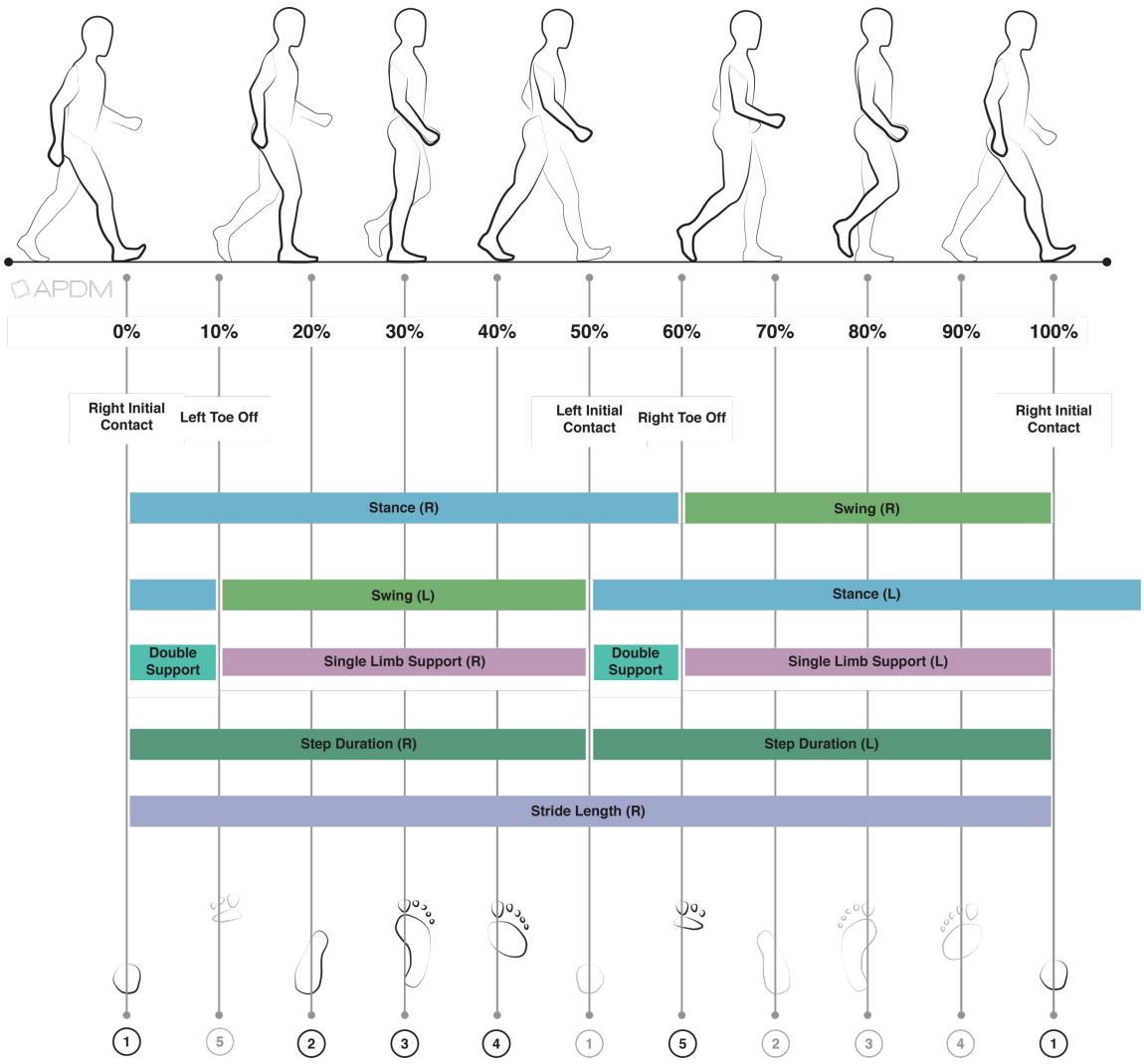

Figure 1.7 | Temporal phases of the gait cycle. A temporal representation of the events derived over two step (a gait cycle) and the various phases (i.e. stance, swing, and double support) comprising these intricate movements. *Adapted from APDM, Inc. [62].*

Neural Circuitry of Gait

Like the mechanics of the gait cycle, the neural circuitry of gait consists of several multifaceted components (diagramed in the **Figure 1.8** schematic [63]) occurring simultaneously and are dependent upon the difficulty of the task being executed [61]. There are three core structures/regions at the levels of the brainstem and spinal cord involved in the postural control

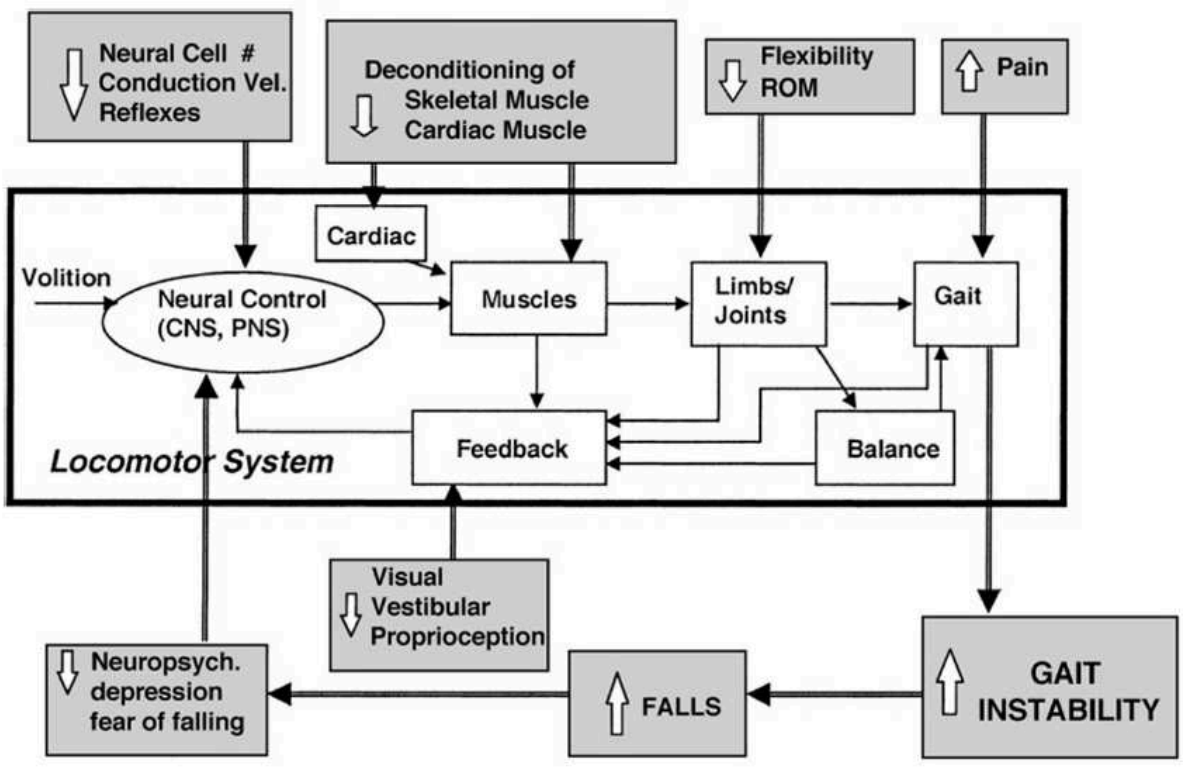

Figure 8 | Gait instability schematic. A detailed schematic identifying the prominent physiological and neurological factors that are associated with gait instability. *Adapted from Hausdorff et al. (2001) [63].*

of gait, including the "midbrain locomotor region [64-66]; the subthalamic locomotor region [67]; and the cerebellar locomotor region located in the midpart of the cerebellum [68]" [61]. Regulation of gait through these neuroanatomical areas can be voluntary (i.e. the act of intentional motor movements) or involuntary (i.e. unconscious motor movements) via both cognitive and automated functions. Originally, gait has been viewed as a predominantly automated process via the central pattern generators, select sensory feedback, and 'low-level' brain inputs acting as the primary driver of rhythmic alternating leg movements through the phases of the gait cycle [67, 69]. The central pattern generators located in the neural network of the spine are proposed to be the lower-extremity coordinating entities, independent of sensory feedback or higher supraspinal inputs [61]. Although it is certain the central pattern generators

do contribute to sustained gait, their importance as the primary or dominate functioning entity within locomotion has been downgraded. More recent models accentuating the roles of high-level goal-orientation and intentional cognitive function in gait have been theorized to play a more dominate role in gait than initially assumed. To demonstrate the executive effect that physiological and neurological factors have on the reduction of dynamic postural control (i.e. gait), Dr. Jeffery M. Hausdorff provided a detailed schematic (**Figure 1.8**) [63].

High-level functioning is encompassed by movements that require executive function; this type of function is responsible for the initiation or intention of action, planning, working memory, and directing attention. Executive functioning requires both awareness and attention for performing actions within the parameters of the gait cycle. As we go through our daily routines, walking in these environments, we voluntarily encounter fixed obstacles (e.g., a curb or stairs) and others obstacles that are continuously changing (e.g., avoiding vehicles on the road or pedestrians when navigating a crowded sidewalk) [61]. Add-on the distracting social aspects of life and it is easy to understand the importance of the role that cognitive functioning plays in the postural control of gait. In addition to the core structures of postural control of gait are four cognitive processes: (1.) Cognition of bodily information (e.g. orientation of the body), (2.) Transmission of body information (e.g. generating a correct motor response), (3.) Motor programming (e.g. structural collaboration) and (4.) Postural control [61]. Detailed explanations of each aforesaid cognitive processes and the roles they play in allowing us to function within the confounds of our environments can be found in the chapter entitled Gait of the *Handbook of Clinical Neurology* [61]. Propagation of the cognitive processes occur along two separate locomotor neuropathways, the dorsal pathway of cognitive locomotor control and ventral pathway for emotional locomotor control. These neuropathways are responsible for facilitating

both dopaminergic (i.e. the excitatory projections) and inhibitory neuronal projections. Recalling that the neural network of locomotion or neural circuity composing gait is highly complex and requires collective labors from a multitude of neuronal structures, Dr. Anat Mirelman (2018) details this neural circuitry, identifying that

> "The dorsal lateral prefrontal cortex encodes the goal or plan for movement and regulates and controls the movement. The supplementary motor area (SMA) then decides the sequence of movements after input from the posterior parietal association areas and superior temporal gyri (perceptual integration). The hippocampus and parahippocampal regions contribute to spatial planning. The plan is then transferred to the primary motor cortex with simultaneous processing subcortically in the basal ganglia (long-term storage of motor programs) and cerebellum (control of timing and adaptation) with subsequent transfer to the spinal cord interneurons, thought to be responsible for control of activation of muscle firing patterns, and finally to the motor neurons in the anterior cord and the neuromuscular junctions. There is constant feedback and communication at all levels with the sensory system, particularly in regard to spatial information. The anatomic network of motor control is thus interlinked with the network of higher-level cognitive function" [61].

Clearly the complexity of the locomotive neural networks goes beyond the scope of the central pattern generators and furthermore, dispels the theoretical notion that our gait is completely automated. Many of the neural aspects of gait are still being researched and discovered, including how the body effectively coordinates and controls ambulation performance in gait through transcallosal interhemispheric communication.

Bilateral Coordination and the Corpus Callosum

The brain consists of two hemispheres (i.e. a right and left) connected by the largest white matter fiber bundle in the human nervous system, the corpus callosum [70-72]. This neuroanatomical structure is comprised of approximately 250 million axons [72] facilitating the propagation of complex movements. Communication occurring between hemispheres, interhemispheric communication, transpires via the commissural fibers composing the corpus callosum deriving control of the contralateral distal extremities. This means that control of the

right distal extremities is facilitated by the left hemisphere and vice versa for the right hemisphere (**Figure 1.9**) [72]. Control of these contralateral communicated movements stem from a designated balance of excitatory and inhibitory neurotransmission [73, 74], effective and efficient mobility/task execution. Performing tasks that require bimanual (i.e. upper extremities)

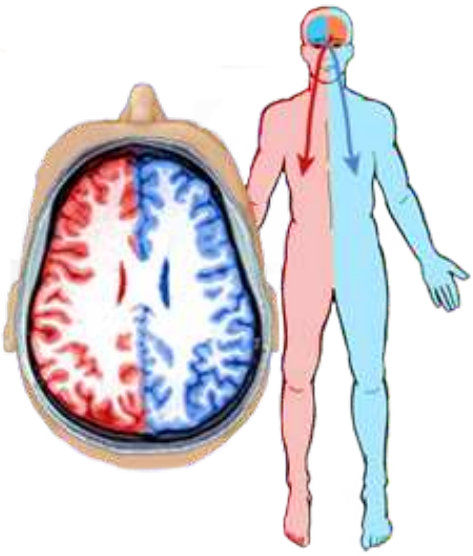

Figure 1.9 | Contralateral control. An illustration depicting the ability of each brain hemisphere to control the contralateral side of the body, imperative for bimanually or bilaterally coordinated activities.

or bilateral (i.e. lower extremities) coordinated movements, adds a layer of spatial and temporal complexity that requires effective interhemispheric communication. Many of these types of activities arise daily, tasks such as, opening a bottle of water or tying the laces of a shoe [74]. Although bimanual coordinated movements have been highly publicized over the last thirty years, bilateral coordinated movements which follow similar coordination principles to perform lower extremity ambulatory actions remain largely understudied.

Coordinated bilateral movements require the execution of specific spatial and temporal actions in larger muscle groups (verse the finer muscle movement of bimanual coordinated movements) to generate desired, optimal, and effective walking patterns. Utilizing both sides of the body, as the legs progress through either the stance or swing phases of the gait cycle, specific interhemispheric communication of neurotransmitter signaling must occur to enable ambulation to occur in a symmetrical fashion. During the initiation of gait, an increased excitation at the primary motor cortex (M1) transpires creating the swing phase in the initiated leg (e.g. right leg). After which, there is a simultaneous influx of inhibition transpiring in the opposite stance limb (e.g. left leg) [75] followed by continual repetitions of this ambulatory process. The entirety of the process is purposed to be facilitated by interhemispheric communication and principally accomplished through the corpus callosum [72].

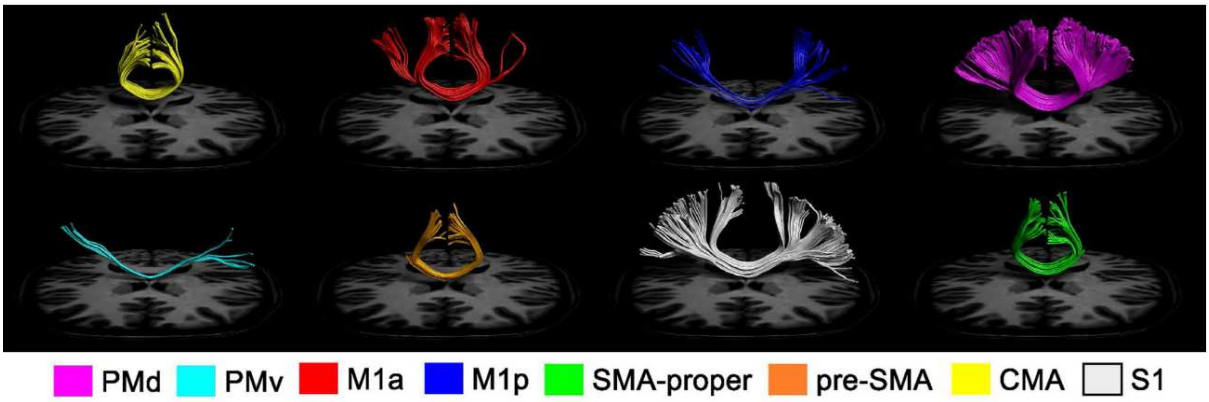

Figure 1.10 | Transcallosal sensorimotor white matter fiber bundles. Segmentation of the eight transcallosal white matter fiber bundles composing sensorimotor tracts of the corpus callosum. The parcellated transcallosal bundles (dorsal premotor cortex (PMd), pre-supplementary (pre-SMA) and supplementary motor areas (SMA proper), anterior and posterior primary motor cortices (M1a, and M1p), cingulate motor areas (CMA), and the primary somatosensory cortices (S1)) were derived using diffusion tensor imaging and the Ruddy_Template built within the ExploreDTI (University Medical Center Utrecht, Netherlands, Version 4.8.6; www.exploredti.com) graphical toolbox atlas. *Adapted from Ruddy et al. (2016) [70].*

Advancements in diffusion tensor image analysis, a magnetic resonance imaging-based technique, have allowed for a better understanding of the fiber orientations comprising the transcallosal bundles (**Figure 1.10** [70]) and the sensorimotor regions the bundles bridge [*Ruddy_Labels:* dorsal premotor cortex (PMd), pre-supplementary (pre-SMA) and supplementary motor areas (SMA proper), anterior and posterior primary motor cortices (M1a, and M1p), cingulate motor areas (CMA), and the primary somatosensory cortices (S1)] [70]. Heavily entrenched in movement, these connections are recognized as being essential parts of the early phases of motor preparation/planning (PMd, SMA proper, pre-SMA, and M1) [76] and extending to motor execution (M1) [77]. Traditionally, the corpus callosum is segmented into five anatomical sub-regions; the rostrum, genu, body, isthmus, and splenium, respectively listed in their anterior to posterior orientation. These sub-regions of the corpus callosum entertain properties that lead to the facilitation, alteration, and cultivation of predictions with respect to bimanual coordinated performances [74]. Anterior portions of the corpus callosum have been associated with upper extremity temporal coupling movements [78] as well as internally guided movements [79]; conversely, the posterior portions of the corpus callosum are associated with spatial coupling [80] and externally-guided movements [79] (for a more in depth review of these concepts refer to *Transcallosal Control of Bilateral Actions [1]*). Each sub-region is essential for the intricate movements and timing associated with coordination, although with time these parameters are inherently affected by the aging process. Like reductions in muscle tone or plasticity that accompany the aging process, the corpus callosum and its encompassed white matter fiber tracts experience a reduction in microstructural integrity across all sub-regions. Accompanying these age-related reductions are slower/less accurate movements with increased variability, and less synchronistic fluidity [81-83].

Although neurodegeneration is seen as a distinctive neuropathological principle of the aging process, it occurs at a progressively faster rate in the pathology of MS and is demarked as a hallmark of the disease. PwMS have demonstrated poorer structural connectivity of the corpus callosum with or without the prevalence of a lesion [81, 84] and poorer interhemispheric inhibition between the primary motor cortices (M1a & M1p) compared to age-matched neurotypical adults [85]. Pertaining to movement, these individuals display slower in- and anti-phase bimanual movements in relation to decreased integrity of the corpus callosum [86]. Beyond motor execution deterioration, these issues can be amplified in the supplementary and/or premotor cortices that play vital roles in the planning, coordinating, and execution of the complex events involved in both locomotion and postural stability [72]. However, a limited understanding exists regarding the underlying microstructural architecture of the transcallosal white matter fiber tracts and the effect these tracts have on the gait bilateral coordination in both neurotypical and atypical adults.

Methods of collection: Kinematic, Kinetic Spatial Temporal (APDM)

Health experts have deemed gait performance as global health marker, enabling professionals to use gait performance measures to predict survival, cognitive decline, overall quality of life and falls statuses [87]. How a fully functioning adult approaches daily life activities and generates their livelihood is manifested by movement and how they produce these actions neutrally and mechanically is necessary. Given the complexity of gait, it would be obtuse to surmise gait with a single method of quantification. There are multiple domains of biomechanics to derive these measures from and furthermore, there is a multitude of equipment used to make these quantifications. Listed in the respective biomechanical domains below, are common methodological indices used to explain gait.

- **Kinetics**: “the study of the causes of motion; the study of forces and moments of force and their characteristics such as work, energy, impulse, momentum, and power” [34].
- **Kinematics:** the study of motion, disregarding the causes or quantities of motion (i.e. any reference to forces). Examples of kinematic derived variables include velocity, speed, acceleration, or angular displacement [33, 34].
- **Spatial-Temporal:** having both spatial and temporal qualities such as cadence and/or cycle time, stance and stride time, swing time, stride length, stride width, etc.
- **Additional Methods of Mobility Quantification:** Phase Coordination Index and Gait Asymmetries, pressure values occurring under the foot during gait, Gait phase, and step detection.

The equipment used to extrapolate these measures has continually developed with the evolution of technology. Apparatuses like instrumented walkways (e.g. GAITRite), electrogoniometers, force platforms, electromyography (EMG), pressure mapping technology (e.g. Tekscan F-Scan system (electronic insoles)), and even stopwatches have all shaped the analysis of gait. However, the gold standard of both kinematic and spatial-temporal gait analyses is produced by three-dimensional motion analysis systems. This variety of quantitative analysis is completed with the use of high-speed infrared cameras, anatomically placed reflective markers, and special interface boards that synchronize frames together. The positioned reflective markers are followed within each frame by a minimum of two cameras at any given time to cultivate three-dimensional marker positions in both time and space. This type of analysis allows for the accuracy of kinematic measures that is unrivaled by other methods of movement analysis, registering errors of less than one millimeter, enabling accurate limb position coordinates and joint angles, in addition to calculated linear/angular velocities and accelerations [33]. Although the advancement

of motion capture technology throughout the last few decades has permitted resolutions to many of biomechanics greatest questions, three-dimensional motion analysis is not without a plethora of downsides. This type of system is highly dependent upon the quality of the equipment (e.g. cameras or interface boards), in addition to the introduction of a great deal of variability between system setups. Finally, these systems come with a high financial expenditure, costing often tens of thousands of dollars and needing the allowance of fixed position, therefore limiting the "real-world" applications they can achieve.

More recently, the technological advancements of accelerometers have attempted to resolve these "real-world" application concerns, by allowing spatial-temporal measures to be completed outside the laboratory. Furthermore, these devices extend research capabilities by making out-of-lab longitudinal (static or dynamic) assessments of postural control a reality. An accelerometer directly measures the accelerations embodied by the mass it's adhered to and are devised by the number of axes available to quantify the movement. The accelerometers can be uni- or tri-axial (able to quantify movements in the x, y, and z axes), the widely-popular tri-axial accelerometer has become the industry standard for acceleration quantification [34]. Commonly paired with gyroscopes and magnetometers, accelerometers capture/store each segment of movement in six degrees of freedom [88] for the primary purpose of quantifying 3D linear accelerations, angular velocities, and orientation [89]. Specifically, the gyroscope allows for description of the body segment in space (angular accelerations), whereas the magnetometer, quantifies orientation of the movement upon magnetic field, for directional purposes [33]. Collectively, the tri-axial accelerometer, gyroscope, and magnetometer comprise the components of the inertial monitoring unit (IMU) (aka movement monitors) and provides the ability to assess what Dr. Horak describes as the "quality of body motion by characterizing the kinematics and

spatiotemporal aspects of mobility, both in the clinic and in real-life conditions" [88]. Beyond environmental testing factors, IMUs offer accurate metrics of impairment levels, the ability to increase the sensitivity of measures for clinical evaluated comparisons, and immediate biofeedback to enhance treatment efficacy [88].

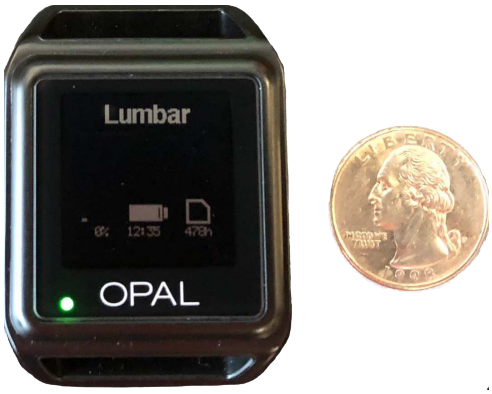

Figure 1.11 | Inertial monitoring unit. A dimensional representation of the Opal, a wearable IMU developed by APDM, Inc. (APDM Inc., Portland, Oregon) to characterize the kinematics and spatiotemporal aspects of movement.

IMUs developed by APDM, Inc. (Portland, Oregon) and their proprietary analysis software have quickly become an industry favorite, their validated [89, 90] wearable alternative to the assessment of gait and balance has changed how we are to approach scientific exploration. Their wearable tri-axial system (**Figure 1.11**) allows researchers and clinicians to characterize mobility by obtaining reliable and sensitive acquisitions of spatial-temporal/kinematic data at high sampling rates, while permitting the access of continuous longitudinal data (up to twenty-four hours of streamed data on a single charge) [91]. 3D spatial/temporal gait (e.g. gait speed, step duration, elevation at mid-swing, and much more) and balance (e.g. ranges of motion in the coronal, sagittal, and transverse planes) outcomes are derived on site within a matter of seconds

succeeding acquisition with proprietary algorithms built within the Mobility Lab (APDM Inc, Portland, Oregon) software [92]. Outside of the neurotypical population, these IMUs enable researchers to evaluate/objectively quantify validated clinical mobility assessments commonly utilized in both MS [93, 94] and Parkinson's disease [95]. Like any method of quantification, IMUs are susceptible to limitations; for decades their inability to measure higher level kinematics (e.g. joint angles) compared to the "gold standard" have been a glaring drawback. However, endeavors to remedy this shortcoming are being developed with the APDM, Inc. Moveo Explorer software (a successor to Mobility Lab) enabling full-body kinematics to be procured [91] for both the lower and upper extremities [93, 96, 97] .

Spatial-Temporal Outcome Measures

Widespread biomechanical differentiation in population mobility has stemmed from spatial-temporal measures, contributing to the fundamental understandings of how and why a person moves; measures that enable the characterization of the effectiveness of gait among neurotypical and atypical (impaired) populations. Traditional spatial-temporal measures entail:

- **Stride length (m) (spatial):** "the distance between two successive placements of the same length"; a stride is consisting of two consecutive steps (e.g. a right and a left or vice versa) [33].
- **Step length (m) (spatial):** "the amount by which the foot can be moved forwards during the swing phase" [33]., so that a short swing phase on one will generally reduce the
- **Cadence (steps/unit time) (temporal):** "the number of steps taken in a given time", usually recorded in steps per minute [33].
- **Cycle time (s):** the time taken to complete single gait cycle (e.g. heel strike of the ipsilateral leg) [33].

- **Walking speed (m/s) (spatial and temporal):** "the distance covered by the whole body in a given time" [33]. The walking can be calculated via two separate equations:
  A. Speed (m/s) = stride length (m) x cadence (steps/min) / 120 [33]
  B. Speed (m/s) = stride length (m) / cycle time (s) [33]

Deteriorations of the spatial-temporal characteristics of gait (i.e. lower cadences, shorter stride and step lengths, wider steps and slower walking speed) are initiated within the aging (post-puberty) process and followed by a progressive decline in dynamic postural control [98]. This decay in control and eventual debilitation stemming from a reduction of an active lifestyle via an increased fall risk or the fear of falling.

Similar to the aging paradigm PwMS commonly display reduced step lengths, [11] and like stroke or Parkinson's disease, PwMS often develop a more effected side pending lesion location and disease duration, developing asymmetries associated with power, strength, muscle activity, or limb loading [99-105]. More pronounced lateral gait deficits are implicated by the affected side during single support, whereby a reduction in step length is fabricated and the ensuing mechanics generate asymmetries in the gait pattern. Inevitably, the generated mechanisms force the adoption of compensation techniques to enable the individual to spend less gait cycle time on the affected side (i.e. less time in stance phase on the affected limb) exuding descriptions of gait pathology [33]. Although, the length or width of a step does present inclinations about gait deficits, these traditional spatial measures neglect to distinguish how the extremities are moving in relation to the overall coordination or the identification of asymmetrical ambulation. To rectify this dearth of knowledge, quantification of bilateral coordination and asymmetrical differences have been instituted via Phase Coordination Index (PCI).

Phase Coordination Index (PCI)

PCI allows for the quantification of bilateral coordination throughout the entirety of the gait cycle (i.e. a stride: heel strike to heel strike with the same foot) by modeling each step as a phase (φ). φ generation incorporates the time from the initiation of the gait cycle (initial first heel strike) to the heel contact of opposite the foot (**Figure 1.12 [1]**). The objective of PCI is to assess the accuracy and consistency of φ generation via the φ relationship between step timing of both legs respectively, in a normalized gait cycle [106]. A single gait cycle is modeled as 360° (i.e. one complete stride) and a perfect φ as precisely half of the cycle, 180°. Accuracy of the φ generation is defined as the absolute difference between the φs occurring at each stride and 180°. While the variation (i.e. consistency) between φs in the gait cycle can be with the coefficient of variation for the mean φ on a participant by participant basis [106].

Mathematically, PCI phases is calculated by deriving the average swing time values for each of the legs, then utilizing the leg with the higher average swing time as reference for the gait cycle (pictured as the left leg in **Figure 1.12**). Computation of φ values occur in the leg opposite

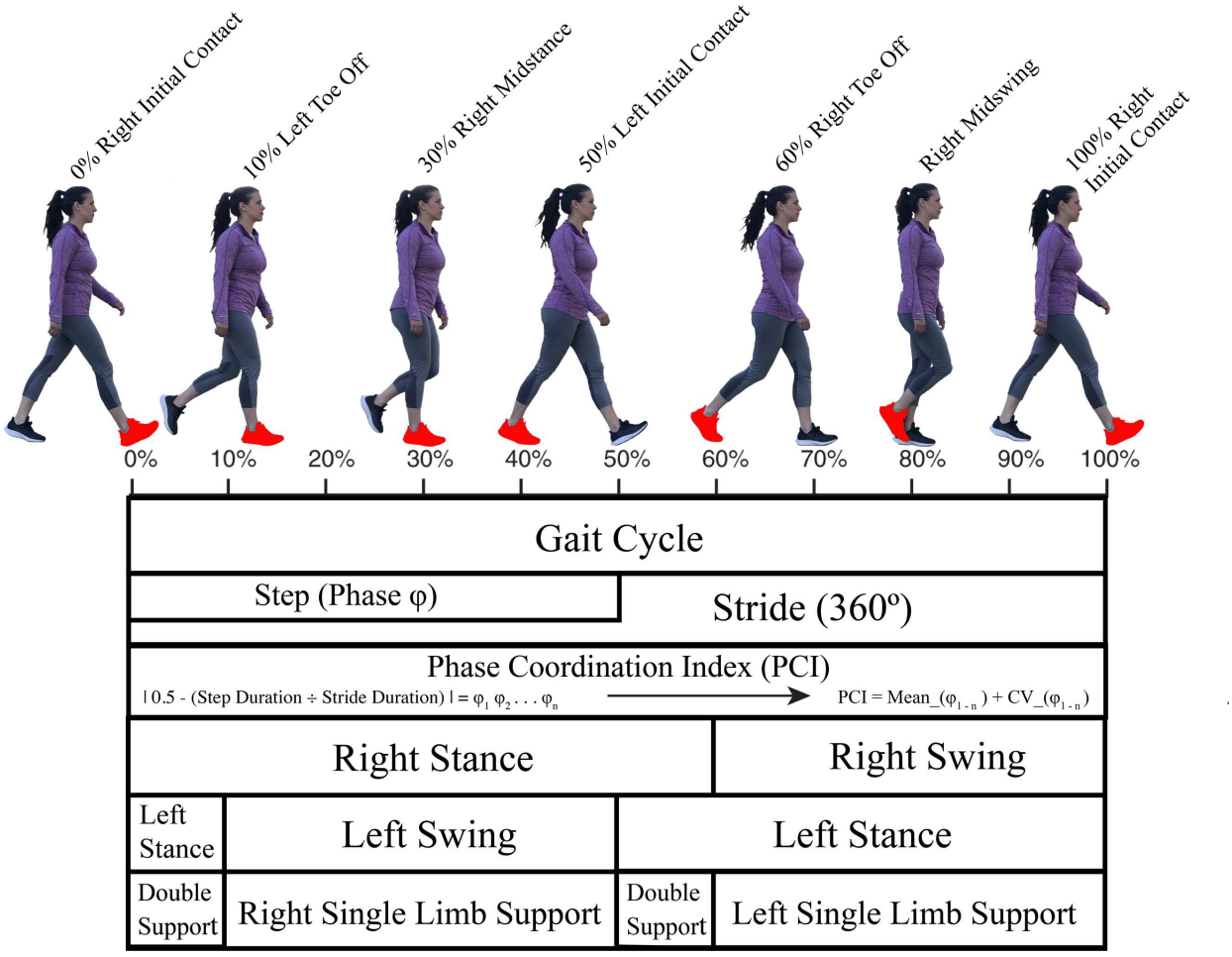

Figure 1.12 | Phase coordination index. A time-lapse representation of the gait cycle and the temporal bilaterally coordinated phases comprising it. PCI is an assessment the accuracy and consistency of phase (step) generation with an optimal being represented as 180° when the gait cycle (a single stride) is modeled as 360°. *Adapted from Richmond & Fling (2019) [1].*

of the reference leg (pictured as the right leg in **Figure 1.12**). Swing timing for each leg is referenced from the toe off to the *ith* heel strike. The φ of the *ith* stride is then calculated by the normalization of step time in respect to the stride time and transformed into degrees by multiplying by 360° (**Equation 1A & 1B**) [106].

A. $\varphi_i = 360° * (\frac{t_{Si} - t_{Li}}{t_{L(i+1)} - t_{Li}})$ [106, 107]

B. $Phase\ (\varphi) = \left(\frac{Step\ Times}{Stride\ Times}\right) * 360°$ [108]

Equation 1. (A) The original phase calculation and (B) the commonly simplified version of equation.

To attain the PCI outcome, the summation of accuracy and consistency (**Equation 2**) from the originated φs established in **Equation 1A and 1B** is calculated with the aim being to generate φs as close to zero (180°) as possible [106].

$$\text{PCI} = \varphi\_CV + \text{P}\varphi_{\text{ABS}} \quad [106]$$

Equation 2. Calculation for the primary outcome measure of PCI.

The accuracy (φ_ABS) of phase generation is represented by the absolute value of the φ and presented as a percentage in the $\text{P}\varphi_{\text{ABS}}$ outcome variable (**Equation 3**). The second half of the equation is represented by consistency (φ_CV) or the coefficient of variation for the φ generation (*Equation 4*) across all recorded strides [106].

$$\varphi\_ABS = |\varphi - 180°| \rightarrow \text{P}\varphi_{\text{ABS}} = 100 * (\frac{\varphi\_ABS}{180}) \quad [106]$$

Equation 3. Calculation for the level of *accuracy* of phase generation

$$\varphi\text{\_CV} = \frac{SD_{\varphi}}{mean_{\varphi}}\ [\%] \quad [106]$$

Equation 4. Calculation for the level of *consistency* in phase generation

An approximate minimum of 23 strides (~46 steps) or more are required to accurately derive a PCI outcome with no gait speed limitations attached to this stride/step requirement [107].

Interpretation of PCI outcomes are as follows:

- A **LOWER** PCI value depicts that the individual has *better* coordination possessing an enhanced ability to generate phases with more consistency and/or more accuracy [109].

- A **HIGHER** PCI value indicates that the individual has *worse* or impaired bilateral coordination, possessing phase generation deficiencies [109].

PCI has been utilized to quantify bilateral coordination in a multitude of studies involving both neurotypical [106, 108-110] and various neuroatypical [111-114] populations. In neurotypical adults, coordination abnormalities are a common result of the aging process. Older adults have revealed significantly poorer (i.e. higher PCI) ability to coordinate the lower extremities scores compared to their younger counterparts (**Figure 1.13**) [110]. Likewise, inferior aptitudes (i.e. higher PCI) to coordinate left–right stepping have also been well-known

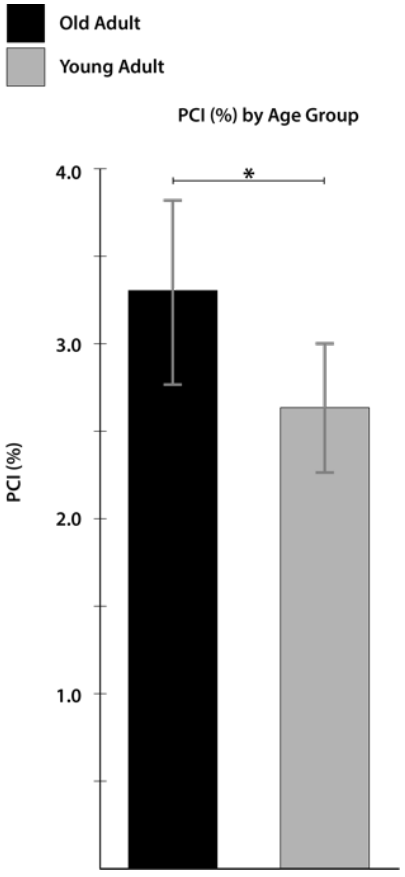

Figure 1.13 | Poorer bilateral coordination identified in older adults. Older adults display reduced ability (i.e. increased PCI) to generate accurate and consistent phases during self-selected walking compared to young adults. *Adapted from Swanson & Fling (2018)* [103].

hallmarks of Parkinson's disease [111-114] and known prognosticator of disease severity concerning mobility pathology [113] and cognitive disability [112] in this population. Although, MS presents similar mobility deficiencies to Parkinson's disease, to the knowledge of this authorship, there have been no established publications relating to PCI and PwMS.

Dynamic Postural Control (Mobility) in Multiple Sclerosis

Comparable to Parkinson's disease, a wide breadth of research has revealed that PwMS develop defined spatial-temporal gait abnormalities. When walking at self-selected or fast walking speeds, PwMS exhibit decreased gait velocity [115-123], cadence [115, 117-123], step length [119-122], stride length [116-119, 121, 122], and time spent in the swing phase [115, 118], while additionally demonstrating augmented step width [116, 117, 119-122] and time spent in double support [115, 117-122] (**Table 1.2**) in an effort adapt a more conservative gait pattern.

Table 1.2: Primary Gait Deficits in Neuro-degenerative (PwMS) vs Neurotypical adults [11]

Dependent Variables	Self-Selected Walking Speed	Fast Walking Speed
Velocity	Slower	Slower
Cadence	Reduced	Reduced
Stride Length	Reduced	Reduced
Step Length	Reduced	Inconclusive
Double Support Duration	Increased	Increased
Step Width	Increased	Inconclusive
Stride Time	Longer	Inconclusive
Swing Phase Duration	Shorter	Shorter

However, these divergent gait patterns are multifactorial and extend beyond motor control impairments to a plethora of additional confounding impairment factors (e.g. "visual impairments, vestibular symptoms, weakness, spasticity, ataxia, imbalance, sensory loss, pain, and fatigue" [17]). Mobility deficits in PwMS can be boiled down to deficits stemming from three primary systems: motor, sensory, and cognitive; resulting in gait and postural control

impairments with an increased likelihood of a fall [12]. Given the heterogeneity of MS in conjunction with its inept pathology and early onset (diagnosed onset: 20-40 years old [17] & peak onset: 45-49 years old [15]) the neural underpinnings contributing to gait and postural abnormalities and subsequent falls in PwMS remain poorly understood. This is an unfortunate because reductions in mobility generate a cascading effect economically from indirect factors and direct medical costs, thereby impacting socioeconomical statuses and overall quality of life [124, 125]. Therefore, it is imperative that improved identification of gait abnormalities and the neural mechanisms underlying mobility impairments be pursued to advance neurorehabilitation techniques for PwMS. Also due to its heterogeneity, the rehabilitation of mobility impairments in PwMS is incredibly difficult and therefore a 'one size fits all' rehabilitative approach is less likely to be effective. To stratify individualized rehabilitative efforts and alleviate mobility impairments, the acquisition of mechanistic comprehensions concerning the microstructural integrity of the neural underpinnings of mobility deficits is essential.

Neuroimaging: Diffusion Weighted Imaging

Diffusion is the state of being spread out or transmitted especially through contact [126], a principle definition founded by Botanist, Dr. Robert Brown in 1826. Since Dr. Browns' scientific breakthrough, the diffusion concept has evolved well-beyond the scope of botany with the focused efforts of history's greatest minds including Thomas Graham, Adolf Fick, and Albert Einstein. Their scientific labors provided theoretical equations that have proven to be pivotal to the foundations of diffusion weighted imaging (DWI), a magnetic resonance imaging (MRI)-based technique [127]. By utilizing the diffusion of water molecules dispersed throughout the brain, derived quantitative measures furnish an in-vivo representation of the neuroanatomical structures.

The basics of how a DWI is acquired begins at an atomic level within the human body, which is predominantly comprised of water molecules. Each water molecule consists of two hydrogen protons attached to an oxygen. The hydrogen protons go through a spin concept, where by in-phase spins become coherent (i.e. resulting in a strong output signal) or out of phase and spins become incoherent (i.e. sums of the signal cancel). When the body is placed inside the primary magnetic field (B_0) ranging in strength from 0.5 - 7T [128], these nuclear spins align with that magnetic field and emit a signal that is proportional to the magnetic field ($\omega = \gamma * \beta$), deemed the Larmor frequency [129]. A rotating magnetic field (B_1) or localized gradient field is then applied to evoke excitatory signals (i.e. tipping the proton). The applied gradient fields are designed to be multi-dimensional (G_x, G_y, and G_z) allowing for the differentiation of anatomical or neuroanatomical structures to be localized [129]. In diffusion imaging, manipulation by the applied gradients effects the signal strength allowing for detailed interpretations to be visualized. Magnetic field alterations in spin frequency occur when the gradient is turned "on", aligning the protons via a 90° knock down occurrence. When the gradient is turned back "off", the protons will spin back up to their desired Larmor Frequency. The rates at which these up-spins transpire is dependent upon the type of tissues they are contained within, a process aptly termed frequency encoding [129]. In order to achieve optimal image acquisition, general diffusion procurement with these gradients require appropriate spacing, so that they are sampling in non-collinear directions [130]. The emitted RF signal from this spin back is received by the RF coil then undergoes an analog to digital conversion, before being condensed into a k-space [131]. Prior to image depiction, the k-space is sorted via a Fourier Transformation and retrieved as a set of DWIs (diagramed in **Figure 1.14**).

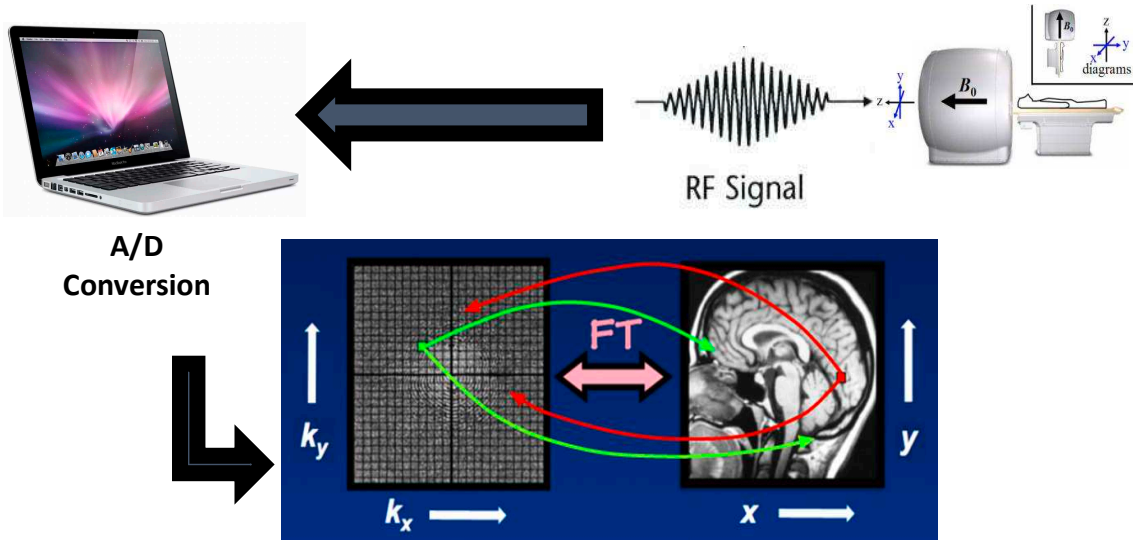

Figure 1.14 | Basics of DWI acquisition. Starting with initiation of image via MRI-based acquisition with emittance of the RF signal (*top right*), going through an analog to digital conversion (*top left*), collection of the signal within the k-space, and ending with the fourier transformation (*bottom*) to output the DWI image.

When acquiring DWI's, it is imperative to abide by the b-values (i.e. the number of gradients applied or more specifically, the applied diffusion weighting [127]) and the pulse sequences (i.e. the sequence required to achieve optimal signal to noise ratios (SNR) with minimal artifact introduced). A 'b-value' of 1000 s/mm^2 is recommended as the minimal value required for optimal results [128] however, b-values exceeding 2000 s/mm^2 are increasing in popularity when applying more advanced post acquisition techniques [127]. Additionally, the quantity of non-collinear gradient directions being applied in conjunction with the 'b-value' is central to the quality of the image output. Drs. Jacques-Donald Tournier, Susumu Mori, and Alexander Leemans suggest that a minimal b-value of 1000 s/mm^2 will require at least 28 non-collinear gradient directions to achieve optimal image quality. Although, the minimum gradient numbers applied will often climb over 45 directions with more intermediate b-values (e.g.

upwards of 3000 s/mm^2) [128]. A rule of thumb is that the more gradient directions that can be applied increases the overall SNR thereby improving the quality of the output image [128].

Beyond DWI acquisition, it is imperative to consider the type of diffusion being characterized. During the diffusion process, diffusion can be classified as free (isotropic) diffusion, where water molecules disperse throughout a space without hindrance from external structures; hindered (anisotropic), where the molecules come in contact and are slowed down by the external structures; or lastly, when a molecule is restricted within an internal structure it is considered to have restricted diffusion [127]. When the diffusion is isotropic it is commonly associated with the cerebral spinal fluid, where no hinderance is observed. External structures such as white matter (myelinated axons or bundles of axons) will hinder the path of molecule, ergo providing an anisotropic view of the microstructure. In summation, DWI measures reflect the amount of hinderance/restriction experienced by water molecules moving with a component of displacement along the axis of the applied gradient and averaged over the voxel [132].

Diffusion Tensor Imaging

Diffusion tensor imaging (DTI) is a DWI-based mathematical approach allotting for the in-vivo identification of ischemic changes and the mapping of white matter microstructural architecture. As the only imaging technique known to map the orientation of white matter fiber bundles [127], DTI is based around the mathematical representation of water-flow directionality within a given voxel. Recorded from the scanning gradients during the diffusion sequence, water flow is modeled as a tensor on a voxel-by-voxel basis. The “shape” of the tensor allows for the characterization of the underlying microstructure and origin of the tensor requires at least six or more gradient directions. The geometrics and quantitative outputs are depicted by the length

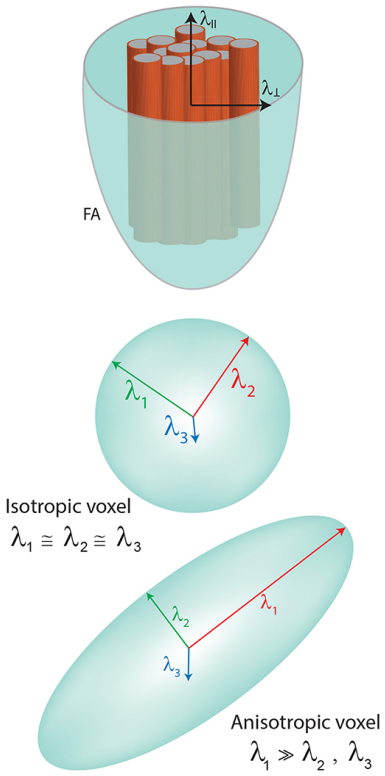

Figure 1.15 | Tensor composition. Illustrated representation of the tensor model as it displays the eigenvalues for an isotropic (*middle*) and anisotropic (*bottom*) voxel. *Adapted from Moura et al. (2019) [126].*

measures of the tensor, these are referred to as the eigenvalues (i.e. $\varepsilon_1\sqrt{\lambda_1}, \varepsilon_2\sqrt{\lambda_2}, \varepsilon_3\sqrt{\lambda_3}$) and the orientations of the tensor (i.e. the global location in the x, y, and z planes) are represented by the eigenvectors (identified in **Figure 1.15** [133]) [134]. The combination of the eigenvectors and eigenvalues enable the procurement of axial diffusivity (AD), radial diffusivity (RD), mean diffusivity (MD), and fractional anisotropy (FA) quantitative outcome measures. AD is associated with the first eigenvalue ($\varepsilon_1\sqrt{\lambda_1}$), embodying the principle direction of the tensor. The average of the second and third eigenvalues ($(\varepsilon_2\sqrt{\lambda_2} + \varepsilon_3\sqrt{\lambda_3})/2$) construct RD and the average

of all three eigenvalues ($(\varepsilon_1\sqrt{\lambda_1} + \varepsilon_2\sqrt{\lambda_2} + \varepsilon_3\sqrt{\lambda_3})\ /3$), comprising a single average diffusivity within a particular voxel is recognized as MD. Lastly, FA quantifies on a voxel by voxel basis, how much isotropy (e.g. a more spherical tensor) or anisotropy (e.g. a more elongated ellipse or increased binding to a single axis) there is within the given voxel. Unlike the previously three measures, FA is differentiated by being a normalized measure and ranges from 0 (isotropic) to 1 (anisotropic) [127, 135].

In addition to devising a voxel-by-voxel interpretation of the underlying microstructural architecture, the tensor aids in connecting distant regions of the brain and parcellating white matter fiber pathways via an approach termed tractography [136]. Tractography can be described as utilizing a collection of

> "algorithms that are designed to combine local discrete (voxel-based) models of fiber orientation (derived from either the principal eigenvector for the diffusion tensor, peaks in the dODF or peaks in the fODF) and reconstruct continuous fiber pathways" [132].

Although tractography presents an enhanced view of the composition and integrity of underlying microarchitecture of neuroanatomical structures, fiber arrangement is chaotic throughout the brain and crossing fibers are inevitable. The presence of crossing-fibers can alter or constrict the ability to accurately tract fiber orientations and has been widely recognized as a common pitfall associated with DTI analysis [132]. To better account for crossing or complex fiber orientations, the implementation of higher order models of acquisition (e.g. High Angular Resolution Diffusion imaging (HARDI)) allow for the registration of angular portions of the DW signal to be incorporated into the tractography algorithm [128]. The continual evolution of DTI high-order models has allotted for the fashioning of comprehensive interpretations of the microstructural architecture via constrained spherical deconvolution (CSD) tractography. A sophisticated higher-order model, CSD is able to depict white matter microarchitecture with high accuracy by

utilizing HARDI signals in conjunction with spherical deconvolution. The combination of CSD with higher-order modeling increases the parameter of possible fiber populations to infinity, thereby increasing the ability to account for crossing-fibers. Beyond the postulation of tractography outputs that incorporate augmented fiber orientations [128], CSD allows for quantification of connecting the homologous/non-homologous regions of the cortical motor networks stemming from these models [70]. However, CSD is not without pitfalls; often requiring higher order models (i.e. HARDI) for enhanced acquisition to provide a more robust accountancies of complex fiber configurations. Though this technique is optimal for fitting multi-tensor models (i.e. CSD), it will require enhanced acquisition parameters such as more non-collinear diffusion directions, higher b-values or higher spatial resolutions which increase scan times and drive the SNR down [127]. However, if properly fulfilled, HARDI acquisitions and CSD-based tractography allot for the complex fiber characterizations of the fibers incorporated within the corpus callosum, cortical spinal tract, and other highly fiber dense neuroanatomical structures [127]. Additionally, from the framework of CSD, apparent fiber density (AFD) can estimate the intra-axonal volume fraction within each of the single fiber bundles and enabling the differentiation among single fiber bundles within a regions containing crossing-fibers [137], giving a more inclusive view of the tract-specific differences in fiber density [127]. Obtaining quantifiable in-vivo measures is the initial step to furthering our understanding of the quantity or quality of the brain neural networks however, fitting the correct interpretation to these quantitative measures is imperative to the question being asked.

Interpreting Diffusion Tensor Metrics

Fractional anisotropy (FA) is a normalized description of the diffusion properties quantified from all three eigenvalues and providing a depiction of diffusion directionality in any

given tissue [138]. Recalling that an FA closer to one indicates a more anisotropy or a definitive direction of diffusion (i.e. bound to a single axis) and closer to zero is indicative of equal diffusion in all directions. FA has traditionally been the most frequently reported DTI measure however, FA is highly influenced by a number of unregulated factors and presuming any direct interpretation of white matter integrity as an index of myelination or myelin damage is cited as being "a mere oversimplification" [127]. Therefore, FA should be interpreted solely as benefactor to the magnitude of diffusion tractography configurations whereas the diffusion rate (the average of all three eigenvalues$((\varepsilon_1\sqrt{\lambda_1} + \varepsilon_2\sqrt{\lambda_2} + \varepsilon_3\sqrt{\lambda_3})\ /3)$) within a voxel, regardless of the direction is achieved from the mean diffusivity (MD). A higher MD value (e.g. damaged tissue) will equate to higher diffusion rates from increased free diffusion throughout the tissue. Whereas in this same tissue, the damage will construct decreased FA (i.e. less anisotropy) due to a loss of coherence of the primary diffusion direction [135].

Segmenting out the eigenvalues, the first eigenvalue ($\lambda_{\|}$) embodies the principle (axis) direction or axial diffusivity (AD) of diffusion occurring in the specified voxel and the average of the second and third (minor axes) eigenvalues ($\lambda_{\perp}$) construct the radial diffusivity (RD) of the tensor. A decrease in the principle direction (AD) has been interpreted as a representation of axonal loss [127, 132]. Inversely, an increase in tensor RD indirectly signifies a reduction in myelin (i.e. a reduction of myelin integrity or myelin damage) [127, 139]. Further research has postulated RD relationships between indirect measures of axonal density, axonal diameter, and the fiber coherence [140, 141]. Both AD and RD allow for intuitive information to be acquired about specific microstructural features of white matter connections within the brain however, these measures neglect to contribute to insight about how an increased intra-axonal volume equates to a denser axonal structure, cueing the evolution of AFD. Increased densities have been

associated with both amplified AD and RD quantifications, identifying augmented abilities for white matter bundles to effectively transmit information. Raffelt et al. [137] denotes that interpretations of AFD should be approached with caution and "not be interpreted in terms of axons per unit area, but rather in terms of the space occupied by these axons (i.e. the intra-axonal cross-sectional area per unit area)". Regardless of the quantitative measure or complexity of fibers composed, DTI permits the parcellation of white matter tracts and of the encompassed microstructural integrity for both neurotypical and neuroatypical populations.

Diffusion Tensor Imaging and Multiple Sclerosis

As an autoimmune-based neurodegenerative disease, PwMS exhibit large scale alterations or reductions in white matter microstructural integrity [142] along with postural control deficits (both static and dynamic) [11, 12]. These neurophysiological declines accompany disease progression [143, 144] and are synonymous with increased RD, MD, and AD outcome values, in addition to reduced FA values [145]. Interpolations of DTI microstructural outcomes continue to cultivate; nevertheless, additional mechanistic insights are warranted for connecting declines in microstructural integrity to postural control reductions in PwMS, which is imperative to the efficacy of the neurorehabilitation of mobility deficiencies.

What has DTI told us about the neural control of gait and balance in PwMS?

Maintenance of a fixed position requires a significant reliance on the vestibular, visual, and proprioceptive sensory reference frames to maintain an upright position [4, 146] and any forfeiture of this aptitude impinges an active lifestyle. PwMS have been known to express larger postural sway patterns (i.e. increases in center of pressure path length or sway area) over their disease progression [12] and structural DTI analyses have revealed neuroanatomical tract degradations in sensory reference frames that are related to postural unsteadiness [58].

Unlike neurotypical adults, PwMS display increased width in sway displacement (i.e. more medio-lateral displacement) that has been linked to reduced integrity of the white matter tracts in all three (inferior, middle, and superior) cerebellar peduncles, the general cerebellar white matter, pons, thalamus, anterior and middle cingulum, and the corpus callosum [147]. This relationship was illuminated by our laboratory, discovering a positive correlations between increased postural instability (i.e. increased sway area) and an enlarged proprioceptive tract RD, indicating reduction of myelin integrity in PwMS (**Figure 1.5**) [58]. In addition to the proprioceptive tract, the periventricular regions, corticospinal, and callosal fiber tracts all displayed reduced white matter microstructural integrity in connection with poorer proprioception. Specific affiliations between microstructural degradation related to balance control were localized to the right hemisphere of PwMS compared to the left [58]. This is particularly significant because the right hemisphere accounts for the generation of visual/spatial awareness, a sensory reference frame heavily weighted upon for postural stability. If the proprioceptive system becomes deficient, sensory re-weighting could potentially increase the reliance of these individuals on vision and in conjunction with proprioceptive deficits, increase the probability of instability [148].

Beyond static instability, gait impairments are reported in 85% of PwMS [21]. Gait or dynamic postural control is a sequence of continuous events designed to recover from constant imbalances in order to prevent a fall [60] and like the other aspects of postural control, gait involves regulatory strategies meant to contain the CoM within a constantly changing BoS. Gait spatial-temporal characteristics and clinical assessments have detailed ambulation impairments in PwMS, establishing affiliations between these impairments and white matter microstructural integrity.

The widely-popular, expanded disability status scale (EDSS) describes disease progression in reference to mobility [149] but, has identified no meaningful relationships to the mean or tensor directional measures (i.e. MD or RD) of microstructural integrity [150, 151]. However, normalized DTI-based integrity outcomes (i.e. FA) have provided positive correlations to this validated clinical scale [152]. A possible explanation for these conflicting results, may be driven by augmented inter or intra-rater variability comprising the subjectively surmised EDSS scores [149]. Further clinical explorations have revealed that more objective measures of gait such as the timed twenty-five-foot walk (T25FW (for gait speed)) [151-156], two [151] or six-minute (for endurance) walks [155], and timed up and go (to assess turns and transitions) [155, 157] [151] have all provided significant associations to poorer white matter microstructural integrity based upon DTI outcomes. Outside of clinical investigative outcomes, traditional spatial-temporal characteristics albeit limited in MS, have displayed significant correlations to tract microstructural integrity outcomes. Like EDSS, declines in gait velocity, a reputed prognosticator of gait performance [87], has similarly been (negatively) correlated to diminished corticospinal tract white matter tract microstructural integrity computed via FA [151]. More distinct (non-normalized) calculations of tract integrity (i.e. AD, RD, and MD) have revealed a structure-function association with motor pathway damage and reduced step length and stride time in PwMS. Specifically, distinguishing MD/AD measures as biomarkers of stride length and MD/RD measures as being positively associated with stride time [155]. Hubbard and colleagues have further elaborated that significant negative correlations between MD declines (structural deficits) and the 6MW, T25FW, and gait velocity but, were unable to identify significant relations between FA and any of the gait parameters assessed [155]. This concluding result

contradicts previously established [151] associations in PwMS, supporting the need for more in-depth investigations into the intricacies of these interactions.

Corresponding with static postural instabilities (i.e. sway increases) [58, 147] and decreased automatic postural responses (i.e. increased latency) [158], gait demonstrates similar structure-function relationships that encourages future kinetic and kinematic biomechanical investigations to cement these conceived mechanisms. Beyond MS literature, we can continue to derive further explorations from neurogenerative aging paradigms. These aging models have been successful in utilizing structural integrity metrics as biomarkers to gait performance and are detailed in *The neural correlates of discrete gait characteristics in ageing: A structured review* [159].

In summation, more knowledge is a prerequisite to drawing parallels between the neurological underpinnings of neurotypical/-atypical adults and mobility, we are continually growing this knowledge aided by technological developments (e.g. IMUs and DTI) to figuratively connect these dots. Strong evidence suggests that PwMS display increased degeneration of white matter (e.g. indirectly measured as a rise in RD or decrease in FA) [160] in conjunction with postural control deficiencies [147, 158, 161, 162]. Although scientific comprehension has systemically surrounded interactions involving more traditional postural control measures, a dearth in the literature involving more complex (i.e. multi-dimensional) measures of mobility in PwMS has been acknowledged. Additionally, establishing enhanced connections to non-normalized microstructural DTI metrics (i.e. AD, MD, and RD) [151, 155] is imperative for bolstering biomarkers as a means of individualizing neurorehabilitation programs and improving the health span of PwMS.

Dissertation Aims and Hypotheses

Study 1 | A Temporal Analysis of Bilateral Coordination in Neurotypical and Atypical Adults

Specific Aim 1: The primary objective of this investigation was to assess IMU-derived measures of gait temporal phase measures in neuro-atypical (i.e. PwMS) and neurotypical age-matched adults to identify the contributions these phases make to bilateral coordination. *I hypothesized that PwMS will demonstrate poorer bilateral coordination derived from loftier gait cycle phase temporal means and variance measures within the stance and double support gait phases than in the neurotypical population.*

Specific Aim 2: The secondary objective was to comprehend how these relationships are altered under a cognitive load and when walking speeds are augmented. *I hypothesized that further conservative gait adaptations associated with ascertaining increased dynamic postural control will be enhanced with the augmentation of gait speed and cognitive loading in both populations*.

Study 2 | Bridging the Callosal Gap in Gait: A Mechanistic Evaluation of White Matter in Bilateral Coordination

Specific Aim 1: To assess MRI-derived measures of transcallosal sensorimotor fiber tract quality and quantity (via diffusion imaging) and identify their relation to gait coordination using novel methods of ecologically-valid mobility assessments in 30 healthy adults. *I hypothesized that poorer quality of white matter fiber tracts connecting the right and left sensorimotor cortices of the brain (i.e. transcallosal tracts) will be strongly associated with increased lower limb asymmetries quantified via the Phase Coordination Index (PCI), a novel and comprehensive metric to evaluate bipedal coordination by assessing both the accuracy and consistency of phase generation in locomotion (i.e. gait asymmetries).*

Specific Aim 2: To assess MRI-derived measures of transcallosal sensorimotor fiber tract quality and quantity in 30 PwMS and identify their association with gait and balance performance. *I hypothesized that PwMS will have reduced transcallosal sensorimotor fiber tract quality and quantity, as well as reduced gait coordination compared to the age- and gender-matched neuro-typical cohort from Aim 1. Further, I hypothesize that associations between sensorimotor transcallosal structure and lower limb coordination in PwMS will be greater than those observed for the neuro-typical cohort in Aim 1.*

Study 3 | Advanced Characterization of Static Postural Control Dysfunction and Associated Neural Mechanisms in Persons with Multiple Sclerosis

Specific Aim 1: To assess the microstructural architecture of the sensorimotor pathway quality and quantity (via diffusion imaging) and identify their relation to the multi-dimensional postural control measure of time-to-boundary in neurotypical adults. *I hypothesized that poorer quality of microstructural architecture of the sensorimotor pathway would be strongly associated with decreased time quantified via time-to-boundary (TTB), a novel and comprehensive metric to evaluate postural control by assessing both the velocities and positions of the center of pressure.*

Specific Aim 2: Additionally, we sought to identify how the proprioceptive neural underpinnings of this multi-dimensional postural control measure is different between PwMS and neuro-typical adults. *I hypothesized that in addition to displaying poorer sensorimotor pathway microstructural integrity, PwMS will exhibit shorter TTB values (i.e. poorer postural control) compared to their neurotypical counterparts across all postural conditions and emphasized during proprioceptive manipulated conditions.*

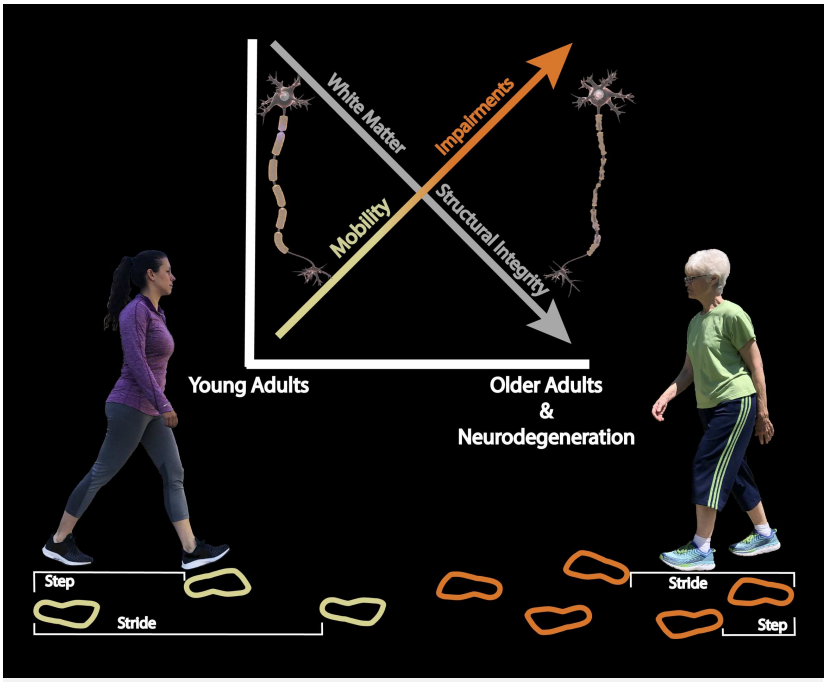

Figure 1.16 | Graphical hypothesis for the overarching aim. A pictorial representation of the prediction that as tract microstructure degeneration intensifies, mobility impairments will elevate in both static and dynamic biomechanical modalities. *Adapted from Richmond & Fling (2019) [1].*

Collectively, the three purposed examinations were designed to provide mechanistic insights into the gait and balance of both neuro-typical and -atypical (i.e. PwMS) adults and achieve a better understanding of the neural underpinnings contributing to reduced locomotion and postural control, thereby increasing risks of falls and injury. Predictively, these mechanisms will manifest through associations between substandard microstructural integrity and impaired mobility (graphically depicted in **Figure 1.16**). The novel outcomes expected from this study will provide comprehensive and mechanistic insights into both dynamic and static postural control for healthy and neurodegenerative populations. These studies will provide specific knowledge about how the brain controls aspects of mobility and will indicate specific neural targets to improve future mobility rehabilitation strategies.

Chapter 2 | A Temporal Analysis of Bilateral Coordination in Neurotypical and Atypical Adults

Chapter Summary

Background: Gait performance dictates the functional aspects of navigating the dynamic environments of everyday living. With each stride the lower extremities move through phases of stance, swing, and double support; coordinating these motions with high accuracy and consistency is imperative to constraining the center of mass within the base of support, thereby staying in an upright position. Gait abnormalities accompany neurodegeneration, impeding stride to stride cohesion and increasing the likelihood of a fall. *Research Question:* This study sought to better understand the temporal mechanisms underlying bilateral coordination and furthermore, how the temporal parameters of bilateral coordinated movements are affected by neurodegeneration. *Methods:* Bilateral coordination was quantified with the Phase Coordination Index (PCI). Both PCI and temporal phases of the gait cycle were acquired with inertial measurement units while walking at a self-selected pace, a fast pace, and under a cognitive load. A 'backwards' multiple regression and derived correlations between the PCI and gait phase characteristics were produced in thirty neurotypical (21 females and 8 males) adults and twenty-seven neuro-atypical (i.e. people with multiple sclerosis (PwMS)) (20 females and 7 males) adults. *Results:* PwMS displayed significantly worse bilateral coordination compared to neurotypical adults regardless of cognitive loading or speed augmentation and deficits from the left-right stepping predicated from higher temporal gait cycle phase variances. While walking under a cognitive load, PwMS performed poorer than the neurotypical adults, yielding a higher performance cost. Additionally, PwMS established a more protective gait strategy while coordinating the left-right stepping patterns derived from specific temporal phase of the gait

cycle. *Significance:* This temporal analysis of bilateral coordination in PwMS, indicates poorer ability to derive symmetrical left-right stepping pattern and provides potential therapeutic targets for individualized rehabilitation strategies aimed at improving health span and overall quality of life.

Introduction

Mobility reflects the aptitude to control the displacement of the center of mass (CoM) during bipedal locomotion and the detailed aspects of these actions is known as gait [163]. During bipedal gait, the summation of specific spatial and temporal movement parameters transpires ambulation to effectively constrain the translating CoM within a continually re-establishing base of support. Gait performance has been deemed a "global health marker" and reputed predictor of survival, declines in cognition, falls status, and overall quality of life [87].

During ambulation, each leg works independently through successive phases of stance and swing to establish gait patterns, thereby enabling individuals to interact within a dynamic daily living environment. The stance phase of the gait cycle (i.e. two successive steps or heel strike to heel strike on the same foot) consists of the events occurring while the foot is in contact with the surface, beginning with initial contact (i.e. heel strike) and ending with toe off; times when both feet are in contact with the surface comprise the double support stance phase [33].The stance phase encompasses 60% of the gait cycle (10% of which is double support) with the swing phase constituting the remaining 40%. The swing phase composes the time when the foot is not in contact with surface, from toe off to heel strike [33]. Sustainment of effective gait requires left-right coordination between bilateral stance and swing phases to effectively constrain the CoM and regulate velocity at the moment of foot placement (i.e. stepping) [164, 165]. The precision and consistency of the steps generated during the engagement of locomotion dictate the

efficacy of sustaining the CoM position within the stability region thereby preventing the forfeiture of postural stability.

The degree of accuracy and consistency of left-right step coordination can be quantified with the Phase Coordination Index (PCI) [106] and recorded by a number of biomechanical modalities. Technological advancements have provided a transition from fixed laboratory-based kinematic modalities to more portable evaluations using instrumentation like the inertial monitoring unit (IMU). The IMU utilizes accelerometer-derived measures to establish spatial-temporal quantification of movements allowing for transpiration of kinematic characterizations to be completed outside the laboratory environment, in a more community-dwelling setting that further representative of daily living [94]. IMU-based measures provide temporal signatures to establish quantitative measures of bilateral coordination via PCI. Associations between traditional broad-based spatial-temporal measures (e.g. gait speed and stride length) have been identified [166] however, a dearth of knowledge encompassing the specific temporal phase mechanisms deriving these broad associations exists. Further understanding of the phasic events encompassing changes in bilateral coordination is a prerequisite to establish a basic scientific understanding of coordinated gait and eventually specify rehabilitation aims to improve bilateral coordination. To our knowledge, no known IMU-based study exists exploring the aforementioned subject matter and furthermore, we believe an absence in the comprehension of these mechanistic associations extend beyond the neurotypical populations to those living with neurodegenerative diseases. Neurodegeneration stemming from the aging process or a neurological disease are known contributors of reduced bilateral coordination (i.e. higher PCI) [111, 112, 114].

Multiple sclerosis is an auto-immune based neurodegenerative disease that instigates mobility deficits in 93.7% of affected individuals [18]. The majority (63%) of people with multiple sclerosis (PwMS) incur a fall within any twelve-month span and 45% of those individuals will develop into recurring fallers [10]. Given that there are nearly one million adults living with MS in the United States [14] and the quality of life impacts that succeed falls, further attention is required of the event mechanisms establishing bilateral coordination and how these degrade with neurodegeneration.

The purpose of this investigation was to assess IMU-derived measures of gait temporal phase measures in neuro-atypical (i.e. PwMS) and neurotypical age-matched adults to identify the contributions these phases make to bilateral coordination. Furthermore, we sought to comprehend how these relationships are altered under a cognitive load and when walking speeds are augmented. We hypothesized that PwMS will demonstrate poorer bilateral coordination derived from loftier gait cycle phase temporal means and variance measures within the stance and double support gait phases than in the neurotypical population. Furthermore, we believe that further conservative gait adaptations associated with ascertaining increased dynamic postural control will be enhanced with the augmentation of gait speed and cognitive loading in both populations.

Methods

Participants: Twenty-seven neuro-atypical adults with a confirmed diagnosis of relapse-remitting MS (20 females & 7 males; 48 ± 12 years, 1.66 ± 0.08 m, 68.6 ± 9.2 kg, body mass index 24.9 ± 3.8 $kg{\cdot}m^{-2}$) and thirty additional sex- and age-matched neurotypical adults (21 females & 8 males; 47 ± 15 years, 1.69 ± 0.08 m, 72.4 ± 14.2 kg, body mass index 25.3 ± 4.0 $kg{\cdot}m^{-2}$) were included in this study. Participants were excluded if they were unable to safely walk

unassisted (an Expanded Disability Systems Scale < 4.0; PwMS median [3.5] and range [0 - 4.0]) or if they had a joint replacement, musculoskeletal or vestibular disorder, or any additional neurological impairment outside of MS. This study was approved by an institutional review board and all participants gave their informed written consent before beginning participation.

Walking Procedure: Participants performed three separate over ground walks for a duration of two-minutes; each walk was performed in the following in order: 1.) at a self-paced speed, 2.) while at a self-paced speed under a cognitive load, and 3.) while walking as fast as possible without initiating a flight phase in their gait. The two-minute walk is an alternative to the six-minute walk for adequately and accurately evaluating gait performance while reducing the effects of fatigue [167], a common concern for PwMS. All trials were completed while walking barefoot down a 110-foot hallway, free of any distractions or obstacles. Spatial-temporal parameters for the primary outcomes were acquired by six tri-axial Opal™ body-worn IMUs

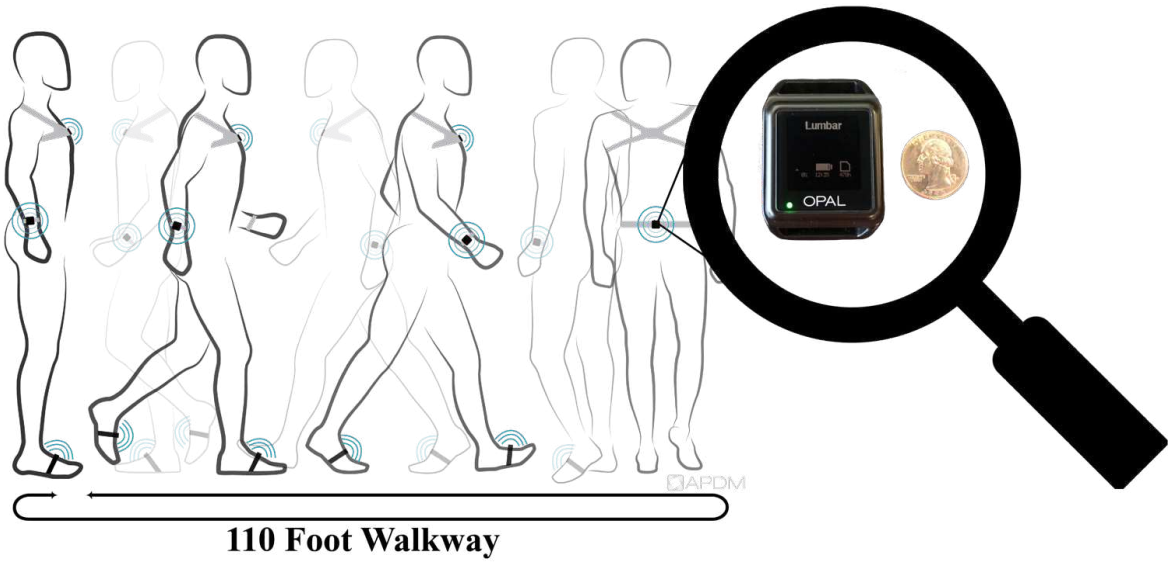

Figure 2.1 | Walking protocol. A depiction of the APDM, Inc. IMU system utilized with a six-sensor placement (sternum, lumbar region, wrists, and feet). These IMUs were utilized for all three continuous walking trials (self-selected, dual-task, and fast) that occurred down a 110-foot walkway. *Image was adapted from APDM Inc, http://apdm.com.*

(Version 2.0, APDM Inc, Portland, OR, USA) sampled at 128 Hz [168]. IMUs were placed on the sternum, lower back (L4/L5 region), wrists, and feet (depicted in **Figure 2.1**); prior to each walk, participants were given instruction on the walking pace, the inclusion of the dual-task (i.e. cognitive loading), and to avoid deviating their gaze away from the forward position.

Dual-Task Procedure: Prior to initiating any walking trials, a two-minute baseline examination of cognitive performance was recorded while in the seated position. While seated, each participant counted down from a randomized number by sevens (i.e. serial sevens), during this task, participants counted aloud into db9PRO VR1.0 (dB9PRO and Arcos Global Ltd., UK) audio recorder that was adhered to the shoulder. During the dual-task cognitive loaded walk, participants began the serial seven counting and then were instructed to begin walking at their own self-selected pace, counting aloud into the adhered db9PRO VR1.0 was sustained until the end of the two-minute duration. All post-error analysis of the single and dual task recordings was analyzed by a single trained analyst, whom established a record of total achieved values and errors. Single and dual task performance (**Equations 1** and **2**) was calculated and a prioritization paradigm was utilized for task dependencies (i.e. performance cost equation (see **Equation 3**)). Decreased performance when going from single to dual task conditions were indicated by a negative performance cost value conversely, performance improvement was specified by a positive value [169].

$$\text{Single Task Performance} = Total\ Numbers\ Achieved_{\ seated} * Percent\ Correct_{\ seated} \quad (1)$$

$$\text{Dual Task Performance} = Total\ Numbers\ Achieved_{walking} * Percent\ Correct_{walking} \quad (2)$$

$$\text{Performance Cost} = \frac{(Dual\ Task\ Performance - Single\ Task\ Performance)}{Dual\ Task\ Performance} * 100 \qquad (3)$$

In the event of any incomplete dual-task audio stemming from technical audio difficulties or inabilities to complete the task, these participants were discarded from dual-task analysis. There were three PwMS (n = 24) and a single neurotypical (n = 28) adult excluded from the cognitive analyses due to complications.

Gait Analysis: PCI was utilized as the primary outcome measure of bilateral coordination, measuring the accuracy (φ_ABS) and consistency (φ_CV) of phase (step) generation within the gait cycles of each two-minute walk. Utilizing the spatial-temporal parameters derived from the IMUs; PCI outcomes were generated via a custom MATLAB (MathWorks, Natick, MA, USA, version R2017a) script from equations originated by Dr. Mier Plotnik and colleges [106]. In PCI, a gait cycle is modeled as 360 degrees and a step (i.e. heel strike to toe off on the same foot) equating a phase (φ) within the cycle (see **Equation 3** and **Figure 2**) [106]. PCI calculation comprises the accuracy and consistency (seen in **Equations 4 and 5)** of φ generation and completed by quantifying the φ relationship between the step timing of both legs respectively [106]. A PCI score closer to zero indicates better bilateral coordination or better φ generation accuracy and/or consistency within the gait cycle [106, 166].

$$\text{PCI} = \varphi\_CV + \text{P}\varphi_{\text{ABS}} \qquad (4)$$

$$\varphi\text{\_ABS} = |\varphi - 180°| \rightarrow \text{P}\varphi_{\text{ABS}} = 100 * (\frac{\varphi\_ABS}{180}) \qquad (5)$$

$$\varphi\_CV = \frac{SD_{\varphi}}{mean_{\varphi}} [\%] \quad (6)$$

Beyond PCI, the generation of temporal gait cycle events were derived by APDM's Mobility Lab™ (APDM Inc, http://apdm.com), a validated customized analytical software using data acquired by the IMUs [89, 90, 168]. From Mobility Lab™, mean times (as a percentage of the gait cycle) was calculated for each of the major gait phases: stance, swing, and double support. Additionally, coefficients of variation (CV) was calculated (CV = (standard deviation /mean) * 100) outside Mobility Lab™ using the for each walking trial in both populations.

Statistical Analysis: A 2x3 repeated measures analysis of variance (RMANOVA) was employed to identify differences in overall PCI outcomes for all three walking conditions between groups. Additionally, RMANOVAs were also completed between groups for the consistency and accuracy of phase generation and gait speed during all three walking conditions. In the event that a Mauchly's test of sphericity indicated a violation ($p < 0.05$), a Greenhouse Geisser correction was applied. Where appropriate, Bonferroni post hoc tests were performed to determine which of the walking conditions differed. All cognitive performance costs were configured in Microsoft Excel (Microsoft Office 2018, Version 16.16.18) and differentiation between groups for achieved values, errors, and performance costs were identified by Student independent t-tests.

A backward selection multiple regression model was employed to explain the amount of variance or contributions to PCI scores could be explains by their swing, stance, and double support mean and CV gait phase measures for all three walking conditions. Pearson product moment correlations were then calculated for all performance variables obtained from the PCI and each gait phase measure in all three conditions. The product moment correlation coefficients

(r) establishes the relationship between PCI outcomes and phase metrics from the gait cycle timing (GCT). All statistical applications were computed using JASP (University of Amsterdam, Amsterdam, Netherlands, Version 0.11.1), and calculated with the risk of type I error set at $\alpha = 0.05$. Statistical plots and outlier identifications were derived in GraphPad Prism 8 (GraphPad Software, La Jolla, CA, Version 8.3.0).

Results

Across all three walking conditions, PwMS displayed significantly higher PCI values (**Tables 2.1A & 2.2A**) compared to their neurotypical counterparts. Additionally, this atypical population comparatively generated these phases composing bilateral coordination with significantly lower accuracy and consistency (**Tables 2.1A, 2.2B, & 2.2C**) for each walking condition. Paralleling bilateral coordinated gait deficits, PwMS performed each walking condition at a significantly slower pace than the neurotypical adults (**Table 2.1B**).

Table 2.1 | Summary of Means (Standard Deviations) for (A) Bilateral Coordination and (B) Gait Speed for the Self-Selected, Dual-Task, and Fast Walking Conditions.

A.

Walking Conditions	**Self-Selected**		**Dual-Task**		**Fast-Pace**	
Group	*Neurotypical*	*PwMS*	*Neurotypical*	*PwMS*	*Neurotypical*	*PwMS*
PCI (%)	1.84±0.64	2.70±1.71	1.76±0.56	2.66±1.56	2.02±0.58	2.64±1.46
φ_ABS (deg)	1.82±0.64	2.68±1.70	1.74±0.56	2.64±1.56	2.00±0.58	2.61±1.46
φ_CV (%)	0.02±0.01	0.03±0.01	0.02±0.00	0.03±0.01	0.02±0.01	0.02±0.01

Note. PCI: Phase Coordination Index; φ_ABS: Accuracy of φ generation; φ_CV: Consistency of φ generation.

B.

Walking Conditions	**Self-Selected**		**Dual-Task**		**Fast-Pace**	
Group	*Neurotypical*	*PwMS*	*Neurotypical*	*PwMS*	*Neurotypical*	*PwMS*
Gait Speed (m/s)	1.25±0.11	1.12±0.20	1.16±0.13	1.02±0.21	1.67±0.18	1.42±0.29

Note. Gait Speed (mean ± SD). Data show a Group × Condition interaction ($p = .022$); neurotypical adults walked significantly faster than PwMS across all three conditions ($p < .001$).

Table 2.2 | Repeated Measures Analysis of Variance (RMANOVA) for the Components of Bilateral Coordination Across Walking Conditions and Between Groups.

A. Overall Phase Coordination Index

Within Subject Effects

	Sum of Squares	df	Mean Square	F	p
Walking Condition	0.375	2	0.187	0.935	0.396
Walking Condition ✻ Group	0.675	2	0.337	1.685	0.190
Residual	21.632	108	0.200		

Note. Type III Sum of Squares

Between Subject Effects

	Sum of Squares	df	Mean Square	F	p
Group	26.588	1	26.588	7.059	0.010
Residual	203.385	54	3.766		

Note. Type III Sum of Squares

B. Accuracy of Phase Generation

Within Subject Effects

	Sum of Squares	df	Mean Square	F	p
Walking Condition	0.362	2	0.181	0.916	0.403
Walking Condition ✻ Group	0.653	2	0.327	1.653	0.196
Residual	21.342	108	0.198		

Note. Type III Sum of Squares

Between Subject Effects

	Sum of Squares	df	Mean Square	F	p
Group	26.226	1	26.226	7.031	0.010
Residual	201.426	54	3.730		

Note. Type III Sum of Squares

C. Consistency of Phase Generation

Within Subject Effects

	Sum of Squares	df	Mean Square	F	p
Walking Condition	4.838e -5	2	2.419e -5	1.593	0.208
Walking Condition ✻ Group	7.568e -5	2	3.784e -5	2.492	0.087
Residual	0.002	108	1.518e -5		

Note. Type III Sum of Squares

Between Subject Effects

	Sum of Squares	df	Mean Square	F	p
Group	0.001	1	0.001	5.776	0.020
Residual	0.010	54	1.885e -4		

Note. Type III Sum of Squares

Means and standard deviations for all temporal dependent variables during each of the three walking conditions are presented in **Figure 2.2**. PwMS demonstrated significantly poorer performance for each of the dependent gait temporal outcomes compared to their neurotypical counterparts.

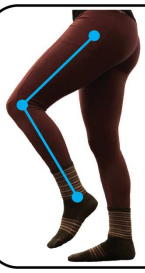

Swing (%GCT)

	Mean		CV	
	PwMS	*Neurotypical*	*PwMS*	*Neurotypical*
Self-Selected	39.94 ± 1.90	40.46 ± 1.11	2.25 ± 0.78	1.71 ± 0.32
Dual-Task	39.06 ± 2.06	39.85 ± 1.19	2.31 ± 0.85	1.72 ± 0.46
Fast	41.97 ± 2.22	42.77 ± 1.77	2.31 ± 0.60	1.88 ± 0.36

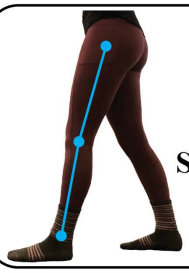

Double Support (%GCT)

	Mean		CV	
	PwMS	*Neurotypical*	*PwMS*	*Neurotypical*
Self-Selected	20.11 ± 3.77	19.06 ± 2.22	6.60 ± 1.97	5.64 ± 1.51
Dual-Task	21.88 ± 4.11	20.29 ± 2.36	5.94 ± 1.55	4.94 ± 1.03
Fast	16.66 ± 3.68	15.10 ± 3.68	8.56 ± 2.15	7.89 ± 1.94

Stance (%GCT)

	Mean		CV	
	PwMS	*Neurotypical*	*PwMS*	*Neurotypical*
Self-Selected	60.06 ± 1.90	59.54 ± 1.11	1.48 ± 0.46	1.16 ± 0.21
Dual-Task	60.95 ± 2.06	60.15 ± 1.19	1.45 ± 0.44	1.13 ± 0.27
Fast	58.15 ± 1.87	57.99 ± 2.00	1.65 ± 0.37	1.41 ± 0.30

Figure 2.2 | Gait cycle timing. A summary of means/ coefficient of variations ± standard deviations of the temporal gait phase (as a percentage of the gait cycle) composing bilaterally coordinated gait for each walking condition in both participant populations.

Self-Paced: When walking at a self-selected speed, a significant amount of variance in PwMS PCI score was explained by swing CV ($R^2 = 0.584$), F (1, 25) = 35.09, $p = < 0.001$. In neurotypical adults, the amount of variance in their PCI score was explained by the double support mean, stance mean, double support CV, stance CV, and swing CV ($R^2 = 0.458$), F (5, 23) = 3.89, $p = 0.011$ (**Table 2.3A** & **2.3B**).

Dual-Task: During both the baseline and dual-tasked walk, PwMS exhibited counting deficiencies; collectively, these individuals achieved less numbers within the two-minute time frame and compiled more errors compared to the neurotypical population (**Figure 2.3**). Furthermore, these individuals exhibited a higher cognitive performance cost when going from the single- to the dual-tasked condition. While placed under a cognitive load, a significant

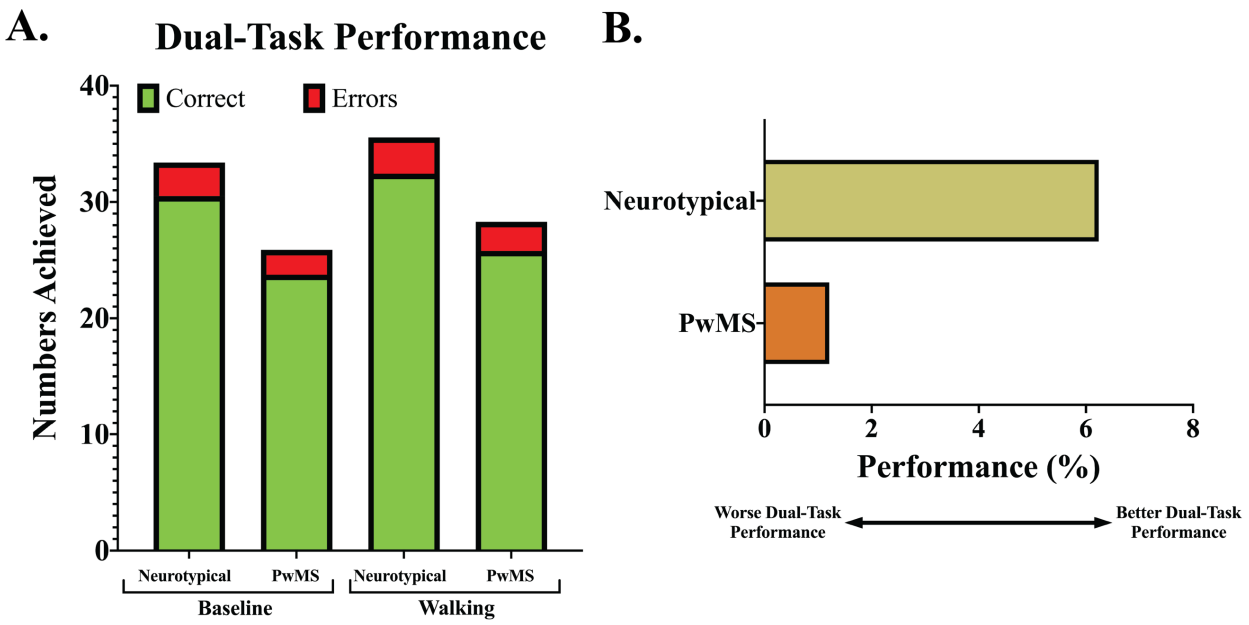

Figure 3 | Dual Task Performances. A.) Averages for the total numbers achieved and the number of errors made by both populations for the single (baseline) and dual-tasked trials. B.) PwMS displayed worst performance (%) over the neurotypical adults when going from the single to dual-tasked condition.

amount of variance in PwMS PCI score was explained by the double support mean, double support CV, and stance CV ($R^2 = 0.683$), F (3, 22) = 15.78, $p = < 0.001$. Alternatively, the neurotypical adults exhibited a significant amount of variance in the PCI score from the stance CV ($R^2 = 0.0102$), F (1, 27) = 3.07, $p = 0.091$ (**Table 2.3A** & **2.3B**).

Fast-Paced: When gait speed was augmented, a significant amount of variance in PwMS PCI score was explained by stance coefficient of variation ($R^2 = 0.343$), F (1, 24) = 12.526, $p =$

0.002. While augmented speed implementation derived no significant modeled predictors in the neurotypical adults (**Table 2.3A** & **2.3B**).

Table 2.3 | Linear "Backwards" Regression Models Across Walking Conditions.

A.) Coefficients for Final Model Outcomes

Neuro-Atypical (PwMS)					Neurotypical				
Predictor Variable % of GCT	β	Intercept	SE	*p*	Predictor Variable % of GCT	β	Intercept	SE	*p*
Self-Selected Pace					**Self-Selected Pace**				
Swing CV	1.685	-1.086	0.284	< .001	Double Support Mean	10.425	1138.923	4.179	0.020
					Stance Mean	-22.441		8.254	0.012
					Double Support CV	-0.274		0.135	0.054
					Stance CV	-24.631		12.182	0.055
					Swing CV	17.862		8.098	0.038
Fast-Pace					**Fast-Pace**				
Stance CV	2.334	-1.189	0.659	0.002	No Significant Predictors				
Dual-Task					**Dual-Task**				
Double Support Mean	-0.172	3.488	0.077	0.036	Stance CV	0.666	1.004	0.380	0.091
Double Support CV	-0.683		0.227	0.006					
Stance CV	4.728		0.911	< .001					

Note. All the listed significant predictors are listed using the stepping criteria of entry: p-value < .05 and Removal: p-value < .10

B.) Model Summary for Final Models

Walking Conditions	r	R^2	Adjusted R^2	RMSE
PwMS				
Self-Selected	0.764	0.584	0.567	1.123
Dual-Task	0.826	0.683	0.639	0.853
Fast	0.586	0.343	0.316	1.227
Neurotypical				
Self-Selected	0.677	0.458	0.340	0.520
Dual-Task	0.320	0.102	0.069	0.546
Fast	0.000	0.000	0.000	0.592

Discussion

This study provides an in-depth look at the constituents of gait phase generation and is the first known study to investigate bilateral coordination via PCI using IMUs in PwMS. Although no interaction was observed between the walking conditions and the group PCI outcomes, a between group effect was present. This lack of interaction with significant group differences suggests that PwMS, regardless of the cognitive load or the augmentation of speed implemented, walk with worse bilateral coordination. By demonstrating poorer bilateral coordination (i.e. a higher PCI) compared to the neurotypical population, our results are in agreement with previous MS [118] and neurodegenerative (e.g. Parkinson Disease (PD)) [112] literature. Furthermore, when speed is augmented (i.e. participants directed to walk faster than their usual self-selected pace) neurotypical adults have historically exhibited no significant PCI interactions [170], coinciding with our absence of significant interactions at the faster pace. Additionally, this absenteeism concurs with traditional gait spatial differentiations exhibited by PwMS, whereby faster walking speeds have yielded an insufficient ability to enable a quantitative synthesis [11].

Deficiency in differentiation may be drawn from a reduced dependence on higher level brain activity during the fast walk and more reliance placed on inferior located anatomical structures. A shift from frontal loop activation of the cortex associated with voluntary or learned activities, will correspond with more automatic control over activities individuals having already acquired familiarization with. This type of shift would imply decreased dependencies on the basal ganglia, supplementary motor area (SMA), or other associated frontal-loop cortical structures and increased utilization curtailed from the brainstem projections including spinal expansions (i.e. central pattern generators) [171]. Like static postural control, dynamic postural

control is not reliant upon a single system but, rather a multitude of activated locations [61], which are weighted pending the demand placed upon them.

When placed under a cognitive load neurotypical adults were able to achieve more numbers and account for less errors while performing both single and dual tasked events verse PwMS. More specifically, the neurotypical adult counting performance cost was less while maintaining a significantly faster gait speed than the PwMS, improving (~ 6%) when transitioning from single tasked counting to dual tasked walking. Whereas PwMS displayed less improvement (~ 2%) during dual tasked walking, presenting conceivable neural points of interest in the frontal loop of the brain. This compilation of cognitive performance cost and bilateral coordination deficits give rise to preliminary neural targets of interest including the SMA, pre-SMA, and other planning/priming areas.

Transitioning to a more biomechanically spatial view of these differentiations, PwMS traditionally present a more protective gait pattern denoted by decreased stride length, step length, and increased step width [11]. These spatial gait changes are accompanied by decreased time spent in the swing phase of the gait cycle and in turn spending significantly more time in both stride and double support phases compared to neurotypical adults, indicative of adapting this more conservative and protective gait strategy [11]. The temporal phase parameters of the gait cycle (i.e. double support, stance, and swing) as components of bilateral coordination presented similar findings, consistently unveiling higher variances in PwMS across all three walking conditions. The priority of the contributions made by these gait phases appear to be dictated by the walking condition.

In neurotypical adults, displayed significantly worse bilateral coordination compared to their self-paced walk, disagreeing with previous neurotypical reports of no significant left-right

stepping impacts stemming from dual task implications [112]. Additionally, these individuals exhibited no significant contributions during faster paced walking, while small contributions were made by a multitude of phases when walking at their self-selected pace. PwMS conversely, demonstrated significant contributors in all three walking conditions with higher variance of the swing (self-selected pace) and stance (fast pace) phases appearing to drive the bilateral coordinated outcomes during speed augmentation. Furthermore, under the cognitive load; double support CV, double support CV, and stance CV were all significant contributors, consistent with attaining a more conservative gait pattern. These results demonstrate that the IMU-based measures are able to quantify bilateral coordination discrepancies in PwMS and furthermore, that the variances in the temporal events should be considered when identifying any deficits or therapeutic approaches for PwMS.

Although the aims purposed in this investigation were fashioned around the nature of basic scientific inquisition, the potential for clinical impacts through therapeutic approaches are evident. Wearable technology provides the ability for clinicians to determine underlying causes of diminutions in functional performance and furthermore, the ability to treat these attenuations [88]. We believe this study has the potential to extend therapeutic capabilities directed at improving gait asymmetries through the reduction of bilateral gait deficiencies. This can potentially be achieved through the development of further therapeutic modalities aimed at the reduction of swing variability in self-selected walking and stance variability when gait speed is increased. To amplify the probability of therapeutic success and direct application, further identification of the underlying neural mechanisms influencing bilateral coordination could aid in determining how the neurological deterioration of these mechanisms predicate bilateral differentiation.

This study was limited to the inclusion of only self-ambulatory relapse-remitting MS participants (i.e. the least severe affected MS population) and it is unknown whether the discoveries demonstrated in this study would be amplified or exemplify a more debilitated population (i.e. secondary or primary progressive MS). Additionally, outcome measures were restricted to temporal quantification of the gait phases, spatial phase measures are unattainable with the Mobility Lab™ analysis software. Future work should be centralized around the gaps in mechanistic knowledge, including neural mechanisms and more in-depth biomechanical mechanisms via motion capture-based kinematic constituents. Although the analysis of this study was directed with intent of a more clinical application, further knowledge could be gleaned from a laboratory-based kinematic and kinetic analyses, allowing for the derivation of specific powers, torques, and spatial measures that constitute these bilateral coordinated phase generated predictors.

In conclusion, PwMS exhibit poorer accuracy and consistency in left-right stepping compared to neurotypical adults irrespective of the augmentation of cognition or speed. The variability within the temporal phases of the gait cycle, point to a more conservative walking patterns and augmented asymmetries indicating potential therapeutic targets. Cognition performance costs when transitioning to dual-tasked walking revealed further deficiencies in PwMS. Together, the concepts established within this research prompts the need to explore the underlying mechanisms of bilateral coordination and address the neural functional performance of these mechanisms.

Chapter 3 | Bridging the Callosal Gap in Gait: A Mechanistic Evaluation of White Matter in Bilateral Coordination

Chapter Summary

Introduction: An essential part of mobility is bilateral coordination of the lower extremities to produce ambulation, coordinated patterns produce locomotive actions, with each leg operating in its own spatial and temporal pattern. The corpus callosum, bridges the two hemispheres of the brain and has proven integral for the coordination of such complex movements. Both coordinated movement and corpus callosum structural integrity are substantially compromised in persons with multiple sclerosis (PwMS). The aim of this project was to assess structural (via MRI-derived diffusion imaging) and functional (via Transcranial Magnetic Stimulation (TMS)) integrity of the transcallosal sensorimotor fiber tract and identify their associations with gait coordination using novel methods of ecologically-valid mobility assessments in both PwMS and age-/gender-matched neurotypical adults. *Methods:* Neurotypical adults (21 female and 8 males; 47 ± 15 years) and PwMS (20 females and 7 males; 48 ± 12 years) underwent a two-minute walk at a self-selected pace. Lower limb asymmetries were quantified via the Phase Coordination Index (PCI), a comprehensive metric to evaluate bipedal coordination by assessing both the accuracy and consistency of phase generation in locomotion. White matter microstructural architecture of transcallosal tracts connecting homologous regions of the sensorimotor cortices were evaluated with diffusion tensor imaging. Radial diffusivity (RD), an indirect marker of myelination, was utilized as the primary outcome. In addition, the ipsilateral silent period (iSP) was used as a functional measure of transcallosal communication quantified with TMS. *Results:* PwMS demonstrated significantly poorer ability to bilaterally coordinate the lower extremities

(PCI: 2.7 ± 1.7 %) during over-ground walking and poorer transcallosal white matter microstructural integrity of sensorimotor fiber tracts (M1a RD: 0.48e-3 ± 0.62e-4 mm^2/s) in comparison to an age and gender matched neurotypical cohort (PCI: 1.8 ± 0.6 and M1a RD: 0.44e-3 ± 0.31e-4 mm^2/s). However, functional connectivity assessments via iSP duration and depth revealed no significant differentiations from neurotypical counterparts. Although, iSP duration in the right hemisphere was discovered to be negatively correlated with poorer bilateral coordination, in PwMS alone. *Discussion:* This analysis has revealed that PwMS walk with poorer consistency and accuracy in a step by step analysis of the gait cycle compared to their neurotypical counterparts. Furthermore, that this increase in asymmetrical gait is associated with microstructural degradation in PwMS. More prominently, these microstructural-bilateral coordination correlations were not exemplified in neurotypical adults emphasizes the importance of transcallosal communication in those with known deficits of this neuroanatomical structure and provides a foundation for future neurorehabilitation approaches.

Introduction

Multiple sclerosis (MS) is an auto-immune based neurodegenerative disease plaguing nearly one million adults in the United States [14] and has evolved into the leading non-traumatic neurodegenerative disease among young adults [15]. This neurological condition on average befalls individuals between 20-40 years of age [17] and is characterized by degradations of the myelin sheath encompassing the white matter tracts throughout the central nervous system [16]. Widespread microstructural quantity and quality concerns accompany disease progression, yielding delays or inhibition of both sensory and motor signal propagation, leading to both mobility and stability impairments [172]. Mobility impairments comprise the majority (93.7 %)

of grievances expressed by people with MS (PwMS) [18] with 85% directed to gait as their chief complaint [173].

To move throughout these multifarious environments, the line between posture and movement becomes blurred whereby movements are defined by the transitions from one posture to another [59]. These transitions are manufactured through complex coordinated ambulatory arrangements to distinguish 'normal walking' [33]. Each movement is fashioned to constrain an undulating center of mass within the confines of a constantly re-establishing (via stepping) base of support through strategically devised foot strikes or placements, completed consciously or unconsciously, in order to prevent a fall [37]. Eventual walking patterns emerge to safely and effectively navigate the highly unpredictable and exceedingly variable environments of daily living. The synchronous complexity of coordinated gait patterns requires effective communication throughout the central nervous system to bilaterally advance body position. Given that each half of the body is controlled by the contralateral brain hemisphere, neurotransmission between brain hemispheres is imperative to gait performance.

The corpus callosum (CC) is the largest recognized white matter fiber bundle in the human body [174], comprised of commissural white matter fiber tracts connecting hemispheres [175] and implicated as the primary site of interhemispheric information transference [74]. Facilitating both excitatory and inhibitory information [73], the microstructural integrity of the CC has been intricately linked to the governing of cognitive functions and signal input for the visual, motor, and somatosensory systems [71]. As a structural component of the central nervous system, the CC displays reductions in microstructural integrity even in the absence of lesions in PwMS [81, 84]. Accompanying CC microstructural reductions are compromised bimanual (i.e. upper extremity) coordinated movements [86]. Although, moving both hands independently in

the same temporal environment is important to an active lifestyle, it does not pose the threat to safety that deficiencies in bilateral (i.e. lower extremity) coordination implicates. PwMS have demonstrated reduced mobility performance [151-156] and endurance [151, 155] accompanied by poorer white matter microstructural integrity. However, a dearth of knowledge exists concerning the neural mechanisms underlying bilateral coordinated movements.

While interlimb coordinated movements have proven germane to mobility and quality of life [175]; cultivating a robust view of the underlying mechanisms of these movements requires going beyond structural grasps and developing a functional understanding of the role that the CC plays in transcallosal communication. During bilateral coordination, each leg must move independently of one another in the same temporal and spatial environment. These lower extremity movements, like bimanual coordinated movements, require precise communication between the two sides of the body (e.g. tying shoelaces, typing, or walking) and compelling the movement of one limb to have an overall inhibitory effect on the ipsilateral motor cortex [176, 177]. Reductions in the inhibitory capability of PwMS have been reported between the primary motor cortices (M1) and are accompanied by poorer manual control and greater motor-related disease severities compared to age-matched controls [85, 178]. However, similar to structural comprehension, literature concerning ipsilateral inhibitory connotations of the lower extremities in PwMS is insufficient and needs to be further identified.

The overarching objective of the present study was directed at providing mechanistic insight into the structural and functional paradigms of bilateral coordination pertaining to both neuro-typical and -atypical (i.e. PwMS) adults. The initial aim was to assess MRI-derived measures of transcallosal sensorimotor fiber tract microstructural quality (via diffusion imaging) in PwMS and neurotypical adults, while identifying their association with bilateral coordination

using novel methods of ecologically-valid mobility assessments. The secondary aim sought to evaluate the functional connections of CC interhemispheric transcallosal inhibition (via ipsilateral silent periods (iSPs)) and the connotations of this functionality reflected within bilateral coordination. We hypothesized that poorer quality of white matter fiber tracts connecting the right and left sensorimotor cortices of the brain (i.e. transcallosal sensorimotor tracts) will be strongly associated with increased lower limb asymmetries and inconsistencies as quantified by the Phase Coordination Index (PCI), specifically within the tracts comprising the primary motor transcallosal fiber bundle. Further postulations instigated from the augmented degradations of the CC microstructure are that poorer interhemispheric inhibition will systemically be associated with reduced bilateral coordination.

Methods

Participants: Thirty participants with a confirmed diagnosis of relapse-remitting MS and thirty additional sex- and age-matched healthy controls were included in this study (demographics and anthropometrics presented in **Table 3.1**). Participants were excluded if they could not safely walk three tenth of a mile (~500 yards) without a walking aid, if they had a joint replacement, musculoskeletal injury, vestibular disorder, or any additional diagnosed neurological condition outside of MS. Further, PwMS were required to have a neurologist confirmed diagnosis of relapsing-remitting MS and excluded if their self-administered Expanded Disability Status Scale (EDSS) was above a 4.0, indicating the ability to independently ambulate and stand/walk on a firm surface for at least 30 non-consecutive minutes. This study was approved by the local Institutional Review Board and all participants gave their informed written consent before beginning any experimental protocols.

Table 3.1 | Demographic, Anthropometrics, and Balance Impairment Summary Means ± Standard Deviations.

	PwMS	**Neurotypical**
Sex	n = 27	n = 29
Female	20	21
Male	7	8
Age (years)	48 ± 12	47 ± 15
Height (m)	1.67 ± 0.08	1.69 ± 0.08
Weight (kg)	68.6 ± 9.2	72.4 ± 14.2
Body Mass index ($kg \cdot m^{-2}$)	24.9 ± 3.8	25.3 ± 4.0
Self-Administered EDSS [median (range)]	3.5 (0.0–4.0)	*Not Applicable*
Mini-BEST		
Overall Impairment Score	21.9 ± 3.8	25.3 ± 2.1
1.Anticipatory	4.9 ± 1.1	5.4 ± 0.8
2.Reactive Postural Control	4.1 ± 1.3	5.4 ± 0.8
3.Sensory Orientation	5.6 ± 0.7	5.9 ± 0.3
4.Dynamic Gait	7.3 ± 1.5	8.6 ± 1.1

Experimental Protocol: Each participant underwent two non-consecutive days of testing consisting of various neuroimaging and mobility assessments. Day one entailed a thirty-six-minute non-contrasted magnetic resonance imaging (MRI) scan protocol comprised of four diffusion weighted imaging sequences (thirteen minutes) to quantify the microstructural structural integrity of CC transcallosal sensorimotor white matter pathways. After the MR procedure, participants underwent an arrangement of mobility and balance impairment assessments encompassed by the Mini Balance Evaluation System Test (Mini-BEST) and culminating with a self-paced continuous two-minute barefoot walk transpiring down a 110-foot hallway. Day two commenced within a two-week span of day one, day two involved the evaluation of the functional performance by assessing interhemispheric inhibition contained within transcallosal communication via transcranial magnetic stimulation (TMS).

Mobility Impairment: Balance impairments were assessed with the Mini-BEST, a comprehensive impairment evaluation designed for the clinical environment and originated from

the BEST. The original BEST was founded on six domains: biomechanical, stability limits/verticality, anticipatory, reactive, sensory orientation, and stability in gait [179]; found to be a valid and reliable comprehensive assessment of balance impairment in neurotypical adults [180, 181], patients with neural injuries (e.g. stroke) [182], and neurodegenerative populations [183-186]. With excellent interrater (ICC $\geq$ 0.91), and test-retest (ICC $\geq$ 0.88) reliability [187], the Mini-BEST is a condensed representation of the BEST, reduced to four domains: anticipatory postural adjustments, reactive postural control, sensory orientation, and balance during gait [188]. Furthermore, the Mini-BEST has revealed comparable accuracy to the BEST in identifying fallers [187].

All participants underwent the fourteen independent assessments comprising the Mini-BEST and were rated upon the accompanied discriminate scale of 0 (unable to perform/requires help), 1 (moderate issues with completing the assessment), or 2 (normal performance) [188, 189]. Detailed explanations of each Mini-BEST assessment and the official examination form can be found at http://www.bestest.us/ [190]. Conclusions drawn about balance impairment were surmised from the overall Mini-BEST score [188, 189] and specified deficits were extracted from the individual domains comprising the overall Mini-BEST score. Scored out of a maximum 28 points, the lower the overall is score is an indication of sufficient balance deficiencies and overall score variations of four or more points signify a minimal clinically important difference (MCID) [191]. Within this examination, PwMS demonstrated increased balance deficits overall and within each of the domains comprising the Mini-BEST however, these scores did not surpass the MCID (scores displayed in **Table 1**).

Bilateral Coordination: A 110-foot hallway was utilized for the continuous two-minute walk to minimize both the amount of turns required and points of deceleration. Each participant

was directed to walk at their own unimpeded self-selected pace, ambulating back and forth down the hallway until they exceeded the two-minute duration (*data was derived from the same population detailed in the chapter 2 study*). A step-by-step stride analyses was derived from six tri-axial Opal™ (sampling frequency 128 Hz, APDM Inc, Portland, OR, USA) body-worn inertial monitoring units placed on the sternum, lumbar, wrists, and feet. All stride outcomes were achieved from the APDM Inc. Mobility Lab™ (http://apdm.com) software and exported to a custom MATLAB (MathWorks, Natick, MA, USA, version R2017a) script for quantification of bilateral coordinated via PCI derived from equations developed by Plotnik and colleagues [106].

Used as the primary outcome of left-right coordinated stepping, PCI ($\varphi\_CV + \mathrm{P}\varphi_{\mathrm{ABS}}$) represents the accuracy ($\varphi\_\mathrm{ABS} = |\varphi - 180°| \rightarrow \mathrm{P}\varphi_{\mathrm{ABS}} = 100 * (\frac{\varphi\_ABS}{180})$) and consistency ($\varphi\_\mathrm{CV} = \frac{SD_{\varphi}}{mean_{\varphi}}$ [%]) of stepping/phase (φ) generation within the gait cycle [106]. By modeling the gait cycle (heel strike to heel strike of the same foot, i.e. one stride) as 360° and each step as a φ within the gait cycle, a phase generation of 180° would epitomize a perfect phase relationship between the step timing of both legs, ergo perfect bilateral coordination [106]. A PCI score closer to zero indicates better bilateral coordination, in other words, that the individual is generating more accurate and/or consistent phases within the gait cycle [106, 166].

Magnetic Resonance Imaging (MRI): MRI Data Acquisition: Diffusion weighted image acquisition was completed with a 3.0 T Siemens MAGNETOM Prisma^{fit} (Siemens Medical Solutions USA, Inc., Malvern, PA) MRI scanner equipped with a 32-channel head coil and parallel imaging. Diffusion weighting was applied in an anterior > posterior orientation with 27 independent non-collinear orientations (b = 2400 s/mm2) including, six unweighted images (b = 0 s/mm2). High-angular resolution diffusion imaging was utilized in conjunction with an echo-

planar imaging sequence (repetition time (TR) = 4000 ms, echo time (TE) = 77.00 ms, field of view (FoV) = 224 mm (224 mm (RL), 216 mm (AP), 144 mm (FH)), 72 (transversal) slices, slice thickness = 2.00 mm, and voxel dimensions= 2.0 x 2.0 x 2.0 mm). Additionally, a high-resolution T1-weighted anatomical scan (TR = 2400 ms, TE = 2.07 ms, flip angle = 8°, FoV = 256 mm (180 mm (RL), 256 mm (AP), 256 mm (FH)), slices = 224 (sagittal), slice thickness = 0.8 mm, and voxel dimensions = 0.8 x 0.8 x 0.8 mm) was collected for post-processing registration. In addition to the thirteen minutes scan duration for diffusion weighted image acquisition, seven minutes were allocated for a T1-weighted image acquisition.

Diffusion Data Processing: Transcallosal sensorimotor fiber bundle microstructural integrity was assessed during post processing analysis via the ExploreDTI (University Medical Center Utrecht, Netherlands, Version 4.8.6; www.exploredti.com) graphical toolbox; utilized for exploratory diffusion (tensor) MRI and fiber tractography in processing, analyzing, and visualizing diffusion MR data [192]. Raw images were visually inspected for evidence of excess motion artifact or instrumental noise via quality assurance tools available within ExploreDTI. Additionally, image data was corrected for the following: signal drift, Gibbs ringing, eddy currents, subject motion, and distortions with both eddy current and subject motion corrective applications being adjusted to each individuals' own high resolution T1-weighted image. The eight transcallosal sensorimotor fiber tract bundles including: the posterior and anterior primary motor cortex (M1a and M1p), dorsal and ventral premotor cortex (PMd and PMv), supplementary motor area proper (SMA proper) and pre-supplementary motor area (pre-SMA), primary sensory cortex (S1), and the cingulate motor area (CMA)) connecting homologous regions for interhemispheric communication comprising the CC were segmented with the Ruddy atlas available within the ExploreDTI template suite [70]. Tensor estimation were performed

using the iteratively reweighted linear least squares approach and fiber trajectories computed with constrained spherical deconvolution (CSD)-based deterministic whole-brain fiber tractography [70, 193]. Voxel by voxel parameters for CSD tractography were as follows: seedpoint resolution = 2 x 2 x 2 mm, step size = 1 mm, angle threshold of >30, and fiber length range = 50–500 mm.

During post-tractography analysis, each of the derived fiber bundle were again visually inspected for any non-transcallosal tractography components incorporated in the atlas architecture outcomes indicated by previous work from Ruddy and colleagues [70]. In the event of unintended tract inclusions, the unintentional tracts were excised with hand drawn NOT regions of interest. Diffusion analytics were configured from the finalized fiber bundles with primary (radial diffusivity (RD) and secondary (fractional anisotropy (FA) outcome measures of homologous transcallosal tracts being derived for each participant. The secondary outcome of FA is a normalized rotationally invariant index that ranges from 0 (*isotropic*) to 1 (*anisotropic*), higher FA values reflect higher microstructural integrity of the white matter tract [194]. Conversely, a higher RD value reflects poorer microstructural integrity, this primary outcome represents an indirect measure of myelination by analytics drawn from diffusion tensor along secondary and tertiary axes ($\lambda_{\perp} = [\lambda_2 + \lambda_3] / 2$) [127]. Collectively, these outcome measures allow for an encompassed view of the transcallosal microstructural alterations between neurotypical adults and PwMS.

Transcranial Magnetic Stimulation (TMS): TMS Ipsilateral Silent Period Data Acquisition: Subjects were seated in a fully adjustable TMS chair with their feet resting on a custom-built adjustable platform. Motor evoked potentials (MEP) were elicited in the tibialis anterior (TA) muscle of each shin with a MagPro X100 stimulator (MagVenture, Farum,

Denmark) using a 2x95mm angled butterfly coil (120-degree, Cool D-B80). In order to be consistent across participants the scalp was mapped using permanent marker. The center of the head was determined by measuring from the nasion to the inion and from the tragus of each ear. Once the center of the scalp was determined, a 2 cm mark was made laterally to each side of center with a 5.5 cm mark made anterior to the lateral points. Upon anterior markings a sagittal line was drawn as a reference for initial coil placement. With participants seated, the 'hot spot' for cortical stimulation of the TA was determined when a TMS stimulus evoked an electromyography (EMG) response from the TA in the contralateral hemisphere. The resting motor threshold (rMT) was determined in each hemisphere and defined as the lowest stimulus intensity that evoked a response $\geq 50\mu V$ on five out of ten stimulations. Muscle activity was recorded via bipolar EMG electrodes (Ag-AgCl, 11mm diameter, $95mm^2$ conductive contact area, with 70mm distance between electrodes, BIOPAC Systems, Inc EL503) sampled at 2000Hz and recorded (BIOPAC Systems, Inc EMG100C).

With each foot (independently) strapped to the platform via one-inch flat nylon webbing connected to a force transducer (BIOPAC Systems, Inc. TSD121C) via carabiner participants were asked to produce a series maximal voluntary contractions (MVC). For each TA participants conducted between two-five dorsiflexion MVC's until force production no longer increased across attempts and the two highest values were within 10% of each other. The same process was replicated for the opposite leg.

The iSP was tested in both cortical hemispheres, the order of testing (i.e. right vs. left) was randomized across participants. To elicit the iSP, participants were asked to maintain isometric dorsiflexion at 15% of their MVC. Participants were given visual biofeedback from a screen directly in front of them, depicting a dial overlaid with a slight transparent visual wedge.

As participants produced force a digital needle pivoted around the center in accordance to the force being produced. The transparent wedge signified where the needle should be maintained during the trial (i.e. 15% of MVC). Participants were asked to maintain the force as steady as possible during the trail. Each trial was three minutes, during which time the researcher gave an ipsilateral cortical stimulation at 120% of the RMT every 7-10 seconds with a total number of stimulations averaging 20 per hemisphere (40 total).

TMS Ipsilateral Silent Period Data Processing: EMG signals were filtered offline using a Comb Band Stop filter in the AcqKnowledge software (BIOPAC Systems, Inc., Santa Barbara, CA). The Comb Band Stop filter removed the 60Hz frequencies and all over harmonics of that frequency (i.e. 60Hz, 120Hz, 180Hz, etc.). Filtered data was then imported into a custom MATLAB script where it was rectified in order to identify and calculate iSP variables for each leg following standard approaches [195]. Briefly, for a given leg, the EMG signal was extracted from 100ms prior to each stimulation to 350ms post stimulation. Duration of the iSP was quantified by identifying the mean consecutive difference (MCD) [196] of the EMG signal for the 100ms prior to each stimulation. Following stimulation, iSP onset was identified as the point when EMG activity dropped below 2.5 standard deviations of the pre-stimulus MCD. Offset off the iSP was defined as the point when the EMG signal raised above the 2.5 standard deviation limit for 50% of the data points in the following 5ms window. This was done to account for natural EMG variability and to limit any false positive silent period offsets [196]. In addition to iSP duration, depth of iSP inhibition was quantified two ways, first the max depth (max-diSP) was calculated by determining the lowest EMG amplitude during the silent period. Second the average EMG depth (diSP) level during the silent period was quantified as a percent of the mean pre-stimulus EMG. Both measures provide an idea of how much the inhibitory activity was able

to reduce the voluntary TA muscle activation [197]. Finally, the presence of an ipsilateral MEP (iMEP) was evaluated [198]. All stimulations were visually inspected for quality with individual iSPs removed if no silent period was captured, the silent period was physiologically too long, or the ipsilateral MEP represented that of a contralateral MEP.

Statistical Analysis: To identify group differences concerning bilateral coordination (i.e. PCI) an independent non-parametric Mann-Whitney t-test was performed. Differentiations between microstructural measures for each of the eight transcallosal sensorimotor fiber bundles were completed using a 2x8 repeated measure analysis of variance (RMANOVA). Multiple RMANOVAs were fulfilled for each of the primary and secondary DTI metrics (FA, RD, and AFD). Where appropriate, Bonferroni post hoc tests were performed to determine which of the conditions differed. Likewise, functional differentiation between hemisphere laterality and iSP depth was identified with a 2x2 RMANOVA and a second 2x2 RMAOVA was fulfilled to examine differences between hemispheres and iSP duration. Product moment correlation coefficients (r) established the relationships between bilateral coordination outcomes and transcallosal sensorimotor fiber bundle integrity metrics diffusion metrics, iSP depths, and iSP durations.

Where appropriate correlations were identified as having no, weak, moderate, strong and very strong relationships by the following correlation coefficient ranges 0.0-0.2, 0.2-0.4, 0.4-0.6, 0.6-0.8, and 0.8-1.0, respectively [199]. Risk of type I error was set at $\alpha = 0.05$ for all statistical analyses. All statistical analyses were computed in JASP (University of Amsterdam, Amsterdam, Netherlands, Version 0.11.1) and graphical representations were derived using GraphPad Prism (GraphPad Software, La Jolla, CA, Version 8.3.0).

Results

At a self-selected walking pace, PwMS walk with significantly poorer bilateral coordination compared to their neurotypical counterparts; generating phases with less accuracy and consistency when deriving left-right stepping patterns (**Figure 3.1**). PwMS also displayed

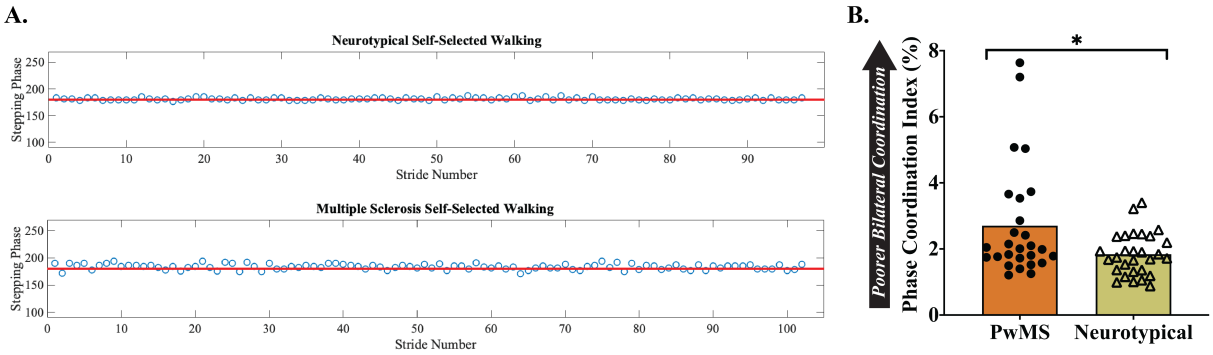

Figure 3.1 | Phase Coordination Index. A.) Displayed are plotted representation of the stride-by-stride coordinated patterns of neurotypical adults (*top*) and PwMS (*bottom*) as quantified by the Phase Coordination Index (PCI). Within the plots, 180° (i.e. a perfectly coordinated phase(s) generation) is indicated by the red line and deviations from this line are indicative of worse bilateral coordination. **B.)** PCI performance during the 2-minute self-selected pace walk between PwMS (1.8 ± 0.6) and neurotypical (2.7 ± 1.7) adults. The mean PCI value for each group represented by the colored bars (PwMS: orange & neurotypical adults: gold) and the shapes denoting the individual values composing the PCI means for each group (PwMS: darkened circles & neurotypical adults: open triangles). The single star indicates significance at the 5% level.

structural differences from the neurotypical adults for the CC transcallosal sensorimotor fiber bundles, displaying significantly higher RD and lower FA (primary) quantifications across bundles (see **Table 3.2**). Additionally, PwMS exhibited significant relationships between bilateral coordination and primary/secondary diffusion metrics across transcallosal sensorimotor white matter fiber bundles. For example, the M1a (RD: $r = 0.473$, $p = 0.006$ (displayed in **Figure 3.3A)**; FA: $r = -0.514$, $p = < 0.001$) showed the strongest relationship to bilateral coordination and displayed this association across both diffusion outcomes. Contrariwise, the neurotypical

adults presented only a single positive correlation between bilateral coordination and RD microstructural integrity of the PMv.

Table 3.2 | Summary of Means (Standard Deviations) for Transcallosal Sensorimotor Fiber Bundle Microstructural Integrity.

Fiber Bundle	PwMS*		Neurotypical*	
	RD (mm^2/s)	**FA**	**RD** (mm^2/s)	**FA**
CMA	0.49e -3 (0.49e -4)	0.40 (0.04)	0.46e -3 (0.30e -4)	0.43 (0.03)
Pre-SMA	0.44e -3 (0.55e -4)	0.48 (0.05)	0.41e -3 (0.27e -4)	0.50 (0.04)
SMA-Proper	0.43e -3 (0.53e -4)	0.48 (0.06)	0.40e -3 (0.29e -4)	0.51 (0.05)
PMd	0.45e -3 (0.48e -4)	0.47 (0.05)	0.42e -3 (0.28e -4)	0.50 (0.04)
PMv	0.49e -3 (0.40e -4)	0.40 (0.04)	0.47e -3 (0.26e -4)	0.41 (0.04)
M1a	0.48e -3 (0.62e -4)	0.44 (0.06)	0.44e -3 (0.31e -4)	0.48 (0.04)
M1p	0.53e -3 (0.52e -4)	0.36 (0.04)	0.49e -3 (0.31e -4)	0.38 (0.04)
S1	0.50e -3 (0.43e -4)	0.39 (0.04)	0.47e -3 (0.43e -4)	0.42 (0.04)

Note. * significance between groups across all transcallosal sensorimotor fiber bundles fiber bundles at p-value < .05.

Table 3.3 | Correlations for Bilateral Coordination and Microstructural Integrity Measures of the Transcallosal Sensorimotor Fiber Tracts.

Fiber Bundle	PwMS		Neurotypical	
	RD	**FA**	**RD**	**FA**
CMA	0.395*	-0.334**	0.104	-0.102
Pre-SMA	0.401*	-0.558***	0.065	-0.002
SMA-Proper	0.439*	-0.401**	0.158	-0.160
PMd	0.434*	-0.504***	0.108	-0.097
PMv	0.355*	-0.238*	0.318*	-0.172
M1a	0.473**	-0.514***	0.122	-0.101
M1p	0.308	-0.355**	0.165	-0.047
S1	0.360*	-0.346**	0.016	-0.100

Note. * significant between fiber bundle microstructural integrity & bilateral coordination at p-value < .05, **p < .01, ***p < .001.

Functionally, both depth and duration of the iSP revealed no significant difference between hemispheres or groups (**Figure 3.3A/3.3B** & **Table 3.4**). Furthermore, the only functional

measure of transcallosal communication significantly correlated to bilateral coordination was the right hemisphere iSP duration, identified only in PwMS (displayed in **Figure 3.2B**).

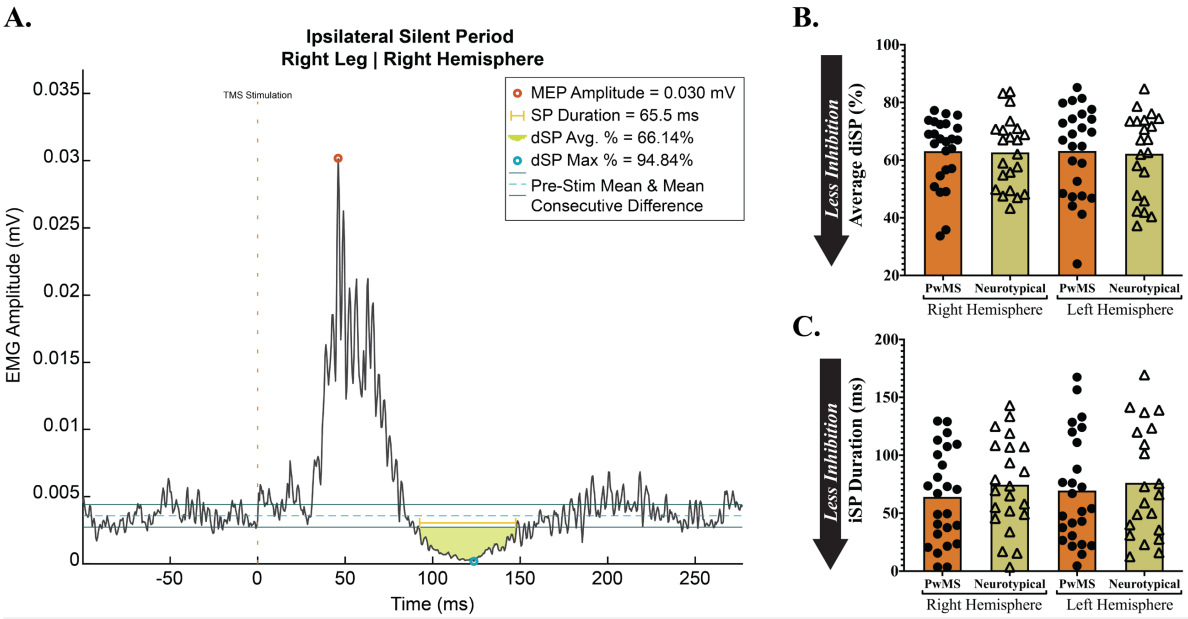

Figure 3.2 | Transcranial Magnetic Stimulation: ipsilateral Silent Period. **A.)** Ipsilateral silent period (iSP) with the depth (*green*) and duration (*yellow measure*) of the inhibitory signal demarked following the TMS stimulation (*red hashed line*) and resulting motor evoked potential (MEP). **B.)** Mean depth of the ipsilateral silent period (diSP) in relation to left and right hemispheres. Shows mean diSP value in both hemispheres for both neurotypical adults and PwMS. **C.)** Mean duration of the ipsilateral silent period (iSP) in relation to left and right hemispheres. Shows mean iSP duration value in both hemispheres for both neurotypical adults and PwMS. In both **B** and **C** bar graphs, the mean values for each group represented by the colored bars (PwMS: orange & neurotypical adults: gold) and the shapes denoting the individual values composing the PCI means for each group (PwMS: darkened circles & neurotypical adults: open triangles). No significance was found between groups or hemispheres.

Table 3.4 | Functional Associations Between Bilateral Coordination and Functional Connectivity of Transcallosal Communication

A. ipsilateral Silent Period Duration

ipsilateral Silent Period Duration				
Brain Hemisphere	PwMS		Neurotypical	
	iSP (ms)	**r**	**iSP (ms)**	**r**
Right	64.0 ± 40.3	-0.347*	74.5 ± 39.5	-0.142
Left	69.5 ± 47.1	-0.081	76.2 ± 48.1	-0.065
ipsilateral Silent Period Depth				
Brain Hemisphere	PwMS		Neurotypical	
	diSP (%)	**r**	**diSP (%)**	**r**
Right	63.1 ± 12.0	-0.086	62.7 ± 12.2	-0.049
Left	63.2 ± 15.5	-0.123	62.2 ± 14.4	-0.126

Note. * significant between fiber bundle microstructural integrity & bilateral coordination at p-value < .05.

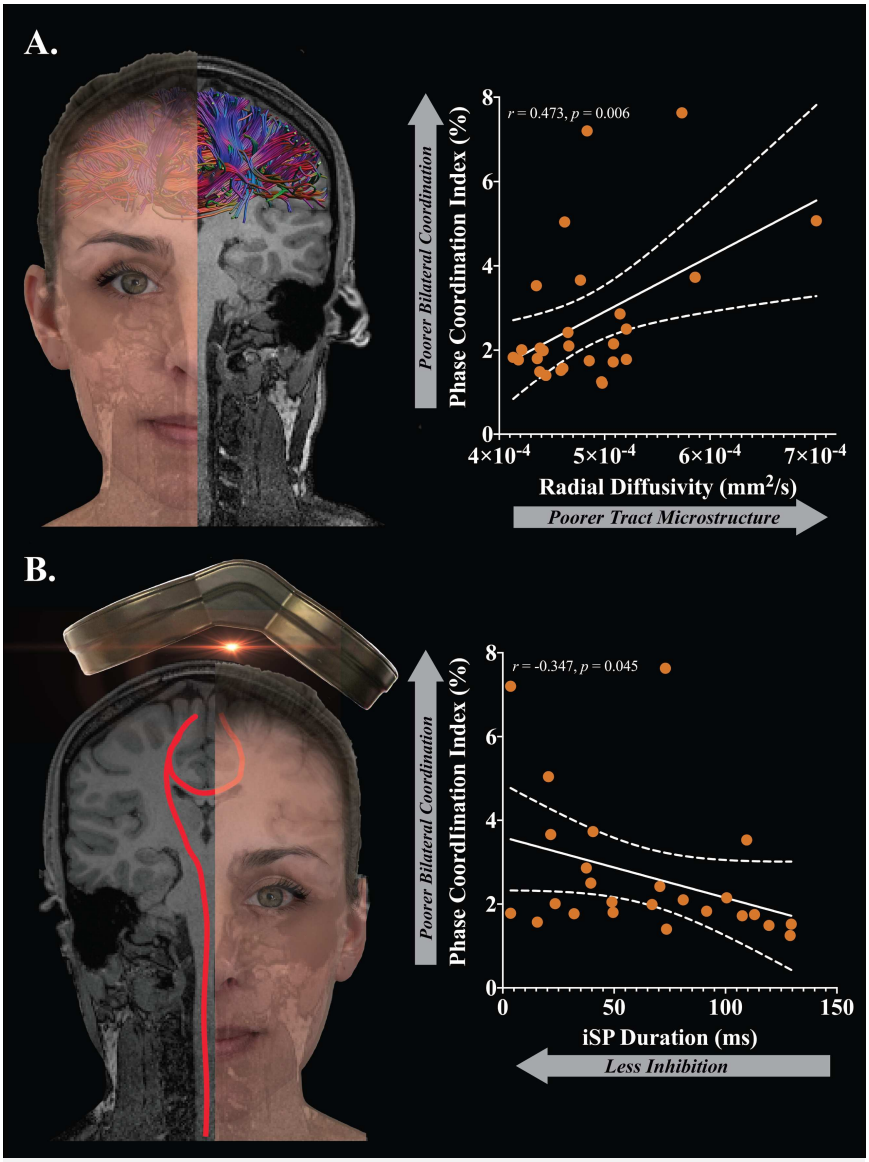

Figure 3.3 | Bridged correlations of bilateral coordination. **A.)** Positive correlation between microstructural integrity of the M1a transcallosal fiber bundle and the phase coordination index across all PwMS (r = 0.473, p = 0.006) and **B)** Negative correlation between right hemisphere ipsilateral silent period duration and the phase coordination index across all PwMS (r = 0.347, p = 0.045).

Discussion

While walking at self-selected pace PwMS displayed overall poorer coordinated left-right stepping compared to neurotypical adults throughout the two-minute walking duration. This

result concurs with preceding spatial and temporal gait characteristics exhibited by PwMS, whereby gait patterns conform to a more fall protective strategy (i.e. increased step width, decreased step length, and other conservative gait adaptations) [11]. The adapted asymmetrical gait patterns (i.e. higher PCI) are comprised inability to generate accurate and consistent phases within the gait cycle compared to the neurotypical population, coinciding with previous outcomes from the neurotypical aging process [110] and alternative neurodegenerative populations (i.e. Parkinson's Disease) [106, 111, 112]. Further identification of the mechanisms driving these bilateral deficits were directed at the initial structural and secondary functional aims of this study. As predicted, PwMS exhibited poorer structural quality of the transcallosal sensorimotor tracts and furthermore, that these tracts were associated with increased lower limb asymmetries, specifically in the primary motor transcallosal bundle. However, these correlating mechanisms were not extended to the age/sex-matched neurotypical adults.

As the first known study to assess the microstructural integrity (via DTI) of the transcallosal sensorimotor white matter fiber bundles in PwMS, the outcomes of this examination parallel gross CC (e.g. rostrum, genu, body, isthmus, and splenium, listed from anterior to posterior, respectively) degradations [200] and reduced structural connectivity observations, occurring in PwMS, even in the absence of lesions [84]. This degradation of connections between right and left sensorimotor cortices of the brain was as hypothesized, to be associated with increased lower limb bilateral coordination. This observation was only exemplified in PwMS, correlations between microstructural integrity and bilateral coordination did not extend into the neurotypical-matched population. This bridged hemispheric sentiment has shown direct properties related to bimanual (i.e. upper extremity) coordination performance including: facilitation, alteration and predictions of movements [74]. In reference to the

orientation of bimanual movements, the anterior portions of the CC have been associated with upper extremity temporal coupling movement [78] and internally guided movements [79]; conversely, the posterior portions of the CC have been associated with spatial coupling [80] and externally-guided movements [79]. These parameters of coordination are essential for the intricate movements and timing associated with bimanually coordinated actions and extend to lower extremity coordinated functionality presented in this evaluation.

When compromised (e.g. degraded), the transcallosal sensorimotor tracts of PwMS display connotations of corrupt coordinated mechanisms of ambulation (i.e. increased asymmetric function), an observation that was not echoed in the neurotypical population. Previous neurotypical age directed research of bimanual movements contradict this bilateral reflection, demonstrating strong associations between CC microstructural degradations and decreased ability to regulate coordinated bimanual movements (e.g. slower/less accurate movements, increased variability, and less synchronous) [81-83]. A uniform response confirmed in PwMS by Bonzano et al. [86], established that PwMS are all together slower in originating in- and anti-phase bimanual upper extremity tasks that are proportional to the decreased integrity of the CC. When extending this notion inferiorly to static/reactive postural control performance, Peterson et al. [161] identified similar interactions which parallel the target conclusions confirmed in the more dynamic task of coordinated ambulation guided by this investigation.

As projected the microstructural quality of the M1a displayed a meaningful association with self-selected coordination in PwMS. These specific cortices (e.g. connecting fiber bundles), along with the supplementary motor cortices and premotor cortices, all play vital roles in the complexity of locomotion and postural stability [72]; a detailed synopsis of the neural circuitry behind gait can be identified in the Gait chapter of the (2018) *Handbook of Clinical Neurology*

[61] . Specifically, the M1a provides the neural system with the aptitude to turn motor plans (via the preSMA/SMA-proper) into firing actions, ultimately aiding the derivation of lower extremity propulsive properties [61]. The M1a provides a target mechanism to move forward in developing therapeutic approaches that could improve asymmetries in the gait of PwMS. Low frequency repetitive TMS (rTMS) offers a non-invasive approach to improve functional connectivity of the motor cortices and thereby motor function [201]. This methodology demonstrates the potential to affect the underlying M1a fiber bundles thus improving gait function however, the aforementioned success has only been concluded in the upper extremities and further investigation is warranted. Alternatively, prior exploration pairing adaptive learning approaches (via split-belt treadmill training paradigms) with non-invasive brain stimulation have yielded enhanced motor learning outcomes [202]. These positive effects could plausibly be translated into the reduction of gait asymmetries and increasing the health span of PwMS. Outside of the M1a connotations, moderate correlations to gait asymmetries were identified concerning both preSMA and SMA-proper fiber tract bundle microstructural integrity, consistent with known mechanisms of neural circuitry in gait. Future investigations should look further into these connections and their roles as functional components in planning initiations, reactions, and pattern generation for ambulation.

Although the surmised rehabilitative treatments previously suggested are largely based around TMS inclusion and reduced interhemispheric inhibition between the M1 cortices compared to age-matched controls have been recognized [85], this sentiment was not sequentially echoed in this examination. Differentiations between groups or hemispheres were absent for both iSP duration and depth. This absence of discrepancy is a reiteration of prior TMS (upper extremity) indications for iSP depth of inhibition however, the duration of inhibition

seems largely consistent in revealing PwMS to have prolonged conduction of the callosal connections [85]. This dearth in differentiation could stem from an insufficient ability to propagate the elicited signal to the target of ongoing EMG activity, in this examination, the lower extremity. Few studies have attempted or accomplished a clear iSP recording at this locality, which could be due to the increased complexity of the neural pathways. Most TMS research applies a more direct approach (e.g. clearer path), recording reflections of inhibitory effects on volitional motor activity at the first dorsal interosseous of the upper extremities. Beyond disoriented signal conductions within the brainstem (i.e. thalamus, basal ganglia, or pedunculopontine nucleus), this must be navigated through the convolution of the spinal cord and spread into the peripherals where at any point signal dissipations are plausible. Although technological advancements like neuro navigation (not enabled in this examination) or the angled figure-eight coil (enabled) increase the likelihood of achieving desired lower extremity quantification (at an increased depth), we could be reaching the extent of our current technological capabilities.

Regardless of the differentiation to the neurotypical adults, PwMS displayed a weak correlation between interhemispheric inhibition duration and bilateral coordination in the right (iSP dominate) hemisphere only. No other correlations were noted by PwMS or the neurotypical population however, this may be a reasonable conclusion on the basis of a recent bimanually coordinated discovery from Bortoletto et al. [203]. Their findings suggest that "the temporal domain is crucial for left hemisphere motor dominance", specifically identifying that bimanually coordinated movements profit from signal transmission in the dominant M1 to nondominant M1 voyage rather than the contrary direction of transmission [203]. The iSP correlation recognized in this lower extremity analysis could stem from similar inferences. By displaying shorter

conduction delays (i.e. inhibition) at the non-dominate M1 (right hemisphere) to the dominate M1 (left hemisphere) a description of shortened signal latency periods could be associated with bilaterally coordinated ambulation. To be conclusive of these hypothesized descriptions, further analyses need to be originated considering transcallosal conduction delays and TMS-evoked potentials at the P15 directed at examinations of the lower extremities.

Although this examination of structural and functional characteristics embarks a significant evaluation of the mechanistic properties underlying bilateral coordinated gait, it was not without some notable limitations. 1.) The number of orientations utilized in the diffusion allocation was limited to 27 independent non-collinear orientations and considering the complexity of the CC structure, accounting for crossing fiber orientations is a concern. However, this was postulated to be remedy by utilizing a multi-tensor model (i.e. CSD) along with the incorporation of higher b-values. By increasing the b-value (2400 s/mm^2; recommended 1000-3000 s/mm^2) and incorporating a higher order diffusion model (HARDI) [127], we believe that sufficient data quality was achieved to perform accurate and reliable tractography of the CC. Future studies may amend concerns directed towards further accountancy of crossing fiber orientations by incorporating more intricate diffusion-based techniques such as non-gaussian based analyses of diffusion kurtosis imaging (DKI). This acquisition, methodology, and application could allow for a better description of the underlying diffusion properties and enhance the detection of microstructural changes [127]. In addition to DKI, a more novel fixel-based analysis (FBA) may be employed, this novel approach incorporates a more comprehensive statistical analyses of white matter quantitative measures involved in various fiber-specific orientations [204]. 2.) As previously declared, neuro navigational technology was not applied to this TMS acquisition thereby conceivably affecting the accuracy and consistency of achieving

the lower extremity target area. This was remediated by applying a scalp mapping acquisition procedure for target locality, in conjunction with an angled figure-eight coil, and the inclusion of EMG recordings to verify muscle outputs. Indubitably, this acquisition technique would benefit from cranial navigational support however, acquisition of the interhemispheric communication for the lower extremities is notoriously difficult to achieve [205], as previously justified. 3.) Lastly, the bilateral coordinated outcomes purposed in this examination were solely derived from temporal aspects of the gait cycle and spatial characteristics were neglected. Future elaborations of asymmetric assessments and therapeutic approaches would benefit from a complete kinematic and kinetic profile to further describe coordinated movements. By developing a more encompassed view of the gait properties (joint angles, torques, powers, and more), more intricate therapeutic techniques can be devised to rehabilitate and hopefully, increase their quality of life.

Navigating the demands imposed by activities of daily living requires precise spatial and temporal movements, dictating not only the quality of the life span but also the health span of both neurotypical and neuro-atypical bipedal human beings. This innovative mechanistic evaluation of bilaterally coordinated movements demonstrated that PwMS walk at their self-selected pace with worse left-right stepping patterns. Furthermore, these coordinated movements appear to be driven more by the microstructural integrity of the transcallosal sensorimotor fiber tracts and less by the functional connectivity of transcallosal connections. Specifically, the sensorimotor fiber bundle connecting the primary motor cortices (M1a) has emerged as a principal target for attenuating asymmetric ambulation and future therapeutic neurorehabilitation evaluations.

Chapter 4 | Advanced Characterization of Static Postural Control Dysfunction and Associated Neural Mechanisms in Persons with Multiple Sclerosis

Chapter Summary

Introduction: Controlling an upright bipedal position is a temporally complex initiative carried out through afferent sensory inputs and efferent postural corrective outputs. The purpose of this investigation was to assess the microstructural architecture of the sensorimotor pathway quality and identify their relation to the multi-dimensional postural control measure of time-to-boundary (TTB) in both neurotypical and -atypical (persons with multiple sclerosis) adults. *Methods:* Postural control was assessed with bi-directional anterior-posterior (AP) and medial-lateral (ML) TTB in four manipulated sensory conditions. While the microstructural integrity of the sensorimotor pathway was established by magnetic resonance-based diffusion imaging outcomes. *Results:* PwMS displayed significantly worse postural control (i.e. shorter TTB) in the AP direction compared to their neurotypical counterparts across each of the four varying sensory testing conditions and poorer microstructural quality of the sensorimotor pathway in comparison to the neurotypical adults. This atypical population displayed a negative correlation (r = -0.431, p = 0.016) between the integrity of the pathway and AP TTB during proprioceptive-based balance. *Discussion:* This is the first known study to establish connections between the microstructural integrity of the sensorimotor pathway and postural control performance via multi-dimensional measures. Observed indications specify that a reduction in sensorimotor pathway microstructural integrity is associated with poorer multi-dimensionally derived postural control in PwMS.

Introduction

Postural control is signified as the act of controlling the position of the body in a given space for the primary purpose of maintaining a stabilized orientation [25] and is regulated by six mechanistic domains including: (1) biomechanical constraints, (2) movement strategies, (3) sensory strategies, (4) orientation in space, (5) control of dynamics, and (6) cognitive processing [9, 45]. Each of these domains are essential for keeping an upright body position as the body continually combats gravitational forces with the objective of constraining the body's center of mass (CoM) within the established base of support (BoS). These aforementioned domains of postural control are complex and involve a multitude of sensory inputs and motor outputs to achieve the desired biomechanical objective, thereby maintaining an upright stabilized postural position [4]. Whether attempting to stand as still as possible or ambulating across the room, our sensory feedback systems (i.e. proprioceptive, vestibular, and visual systems) are constantly relaying information throughout the central nervous system for the construction and execution of motor output corrections [4]. We are continually learning more about the constructs composing these systems and how they are utilized in postural control; given recent evidence that the human brachial plexus is composed of 370,000 axons with a mere 6% of those axons quantified as being motor axons [206], further focus on the role of the sensory systems is warranted. In an optimal environment (i.e. a well-lit room, on a rigid surface) the neurotypical adult has shown to weight the sensory system inputs as 70%, 20%, and 10% for the somatosensory (e.g. proprioceptive), vestibular, and visual respectively [29].

Highlighted by the dominate reliance on proprioceptive sensory feedback, registered afferent information containing postural positioning and surface stability is transported from the peripheral nervous system to the central nervous system. This communication thereby ascends

the spinal cord to the cerebral cortex (somatosensory cortex) via the posterior column-medial lemniscus (PCML) neural pathway [57]. Once organized/processed, a motor plan is relayed for execution from a multitude of motor cortices (primary (M1), premotor, supplementary (SMA)) and the parietal lobe (primary somatosensory cortex (S1)) via the descending efferent corticospinal tracts (CST) [207]. Collectively these ascending and descending fiber tracts can be described as the sensorimotor pathway, constituted of highly conductive white matter tracts and relying upon temporally sensitive informational transference for postural corrections. If the aforementioned sensory inputs are not weighted properly upon the environment or situation, the postural corrections will not be accurately executed in a timely or precise manner thereby deviating the center of gravity (i.e. CoM) beyond the parameters of the BoS, inevitably resulting in instability and a fall [6, 7].

A fall is the involuntarily result of a person coming to rest on the ground and stems from the reduction or loss of postural control, these declines have been found to be ubiquitous with aging, injuries, and disease [208]. Postural control deficiencies plague neurodegenerative disease populations, creating an amplified risk of fall or fall-related injuries. Multiple sclerosis (MS), is an autoimmune-based chorionic-inflammatory neurodegenerative disease characterized by deteriorations of proprioceptive information exerting influence on postural control [209]. Affecting more than 2.1 million people worldwide [2, 3] and approximately 1 million United States citizens [14], MS in a highly unpredictable disease that attacks the central nervous system through demyelination of the axons comprising the white matter, without affecting myelination of the peripheral nervous system [15-17]. Around 75% of people with multiple sclerosis (PwMS) will experience reduced postural control and therefore, incur an increased probability of sustaining a fall [210].

Based on previous work from our laboratory [58], identifiable deficiencies of balance control on proprioceptive-based tasks were associated with reduced white matter microstructural integrity of the cortical proprioceptive tracts in PwMS compared with age-matched neurotypical adults. Although this was an instrumental scientific observation, these associations were established using traditional single-dimensional measures of postural stability (i.e. sway area). These single-dimensional measures are restricted, displaying only spatial explanations of posture and may not accurately reflect true postural control, constructing an over amplification of postural deviations. Innate multi-dimensional (i.e. incorporating both spatial and temporal components) postural stability measures provide alternative quantifications of postural control capabilities with reduced limitations consistent in single-dimensional measures. Time-to-boundary (TTB) is a multi-dimensional measure that provides the amount of time available to make corrective postural adjustments prior to the center of pressure (CoP) or center of gravity traveling outside the BoS established boundary. Precedent discoveries have demonstrated that multi-dimensional postural measures are a more adequate quantification for characterizing postural control in PwMS [211] and various stance conditions [212].

Therefore, the aim of this investigation was to assess the microstructural architecture of the sensorimotor pathway quality and quantity (via diffusion imaging) and identify their relation to the multi-dimensional postural control measure of time-to-boundary in neurotypical adults. Additionally, we sought to identify how the proprioceptive neural underpinnings of this multi-dimensional postural control measure is different between PwMS and neuro-typical adults. We hypothesized that poorer microstructural quality of the sensorimotor pathway will be strongly associated with decreased postural control performance, quantified via a shorter TTB. Furthermore, we theorized that in addition to displaying poorer sensorimotor pathway

microstructural integrity, PwMS will exhibit shorter TTB values (i.e. poorer postural control) compared to their neurotypical counterparts across all postural conditions and emphasized during proprioceptive manipulated conditions.

Methods

Participants: Twenty-seven neuro-atypical (i.e. PwMS) adults with a confirmed diagnosis of relapse-remitting MS (20 females & 7 males; 48 ± 12 years, 1.66 ± 0.08 m, 68.6 ± 9.2 kg, body mass index 24.9 ± 3.8 $kg{\cdot}m^{-2}$) and twenty-nine additional sex- and age-matched neurotypical adults (21 females & 8 males; 47 ± 15 years, 1.69 ± 0.08 m, 72.4 ± 14.2 kg, body mass index 25.3 ± 4.0 $kg{\cdot}m^{-2}$) were included in this study. Participants were excluded from contributing to this investigation if they were unable to stand barefoot on a firm surface, unassisted, for at least 30 non-consecutive minutes (Expanded Disability Systems Scale < 4.0; PwMS median [3.5] and range [0 - 4.0]) or if they had a joint replacement, musculoskeletal or vestibular disorder, or any additional neurological impairment outside of MS. This study was approved by an institutional review board and all participants gave their informed written consent before beginning participation.

Experimental Protocol: Occurring over a single testing session, both groups of participants underwent a mixed battery of neuroimaging and postural control assessments. The assessment began with a thirty-six-minute non-contrasted magnetic resonance imaging (MRI) scan protocol, which included a thirteen-minute diffusion weighted imaging sequence for quantify the microstructural integrity of the white matter sensorimotor pathways (i.e. PCML and CST). Following the MRI, participants performed an instrumented modified Clinical Test of

Sensory Interaction on Balance (imCTSIB), a traditionally clinical assessment of postural control under assorted sensory conditions.

Postural Stability: Time-To-Boundary: Using the standard clinically applicable and widely-popular protocol of the mCTSIB, a subsidized (no conflict dome condition) version of the originated CTSIB [213]. Participants preformed the four separate thirty second trials (1.) eyes open and 2.) eyes closed on a rigid surface; 3.) eyes open and 4.) eyes closed on a compliant surface), whilst standing as still as possible with their hands on the hips and their feet together [214]. Traditionally, this clinical examination has been scored on a semi-quasi pass/fail criterion, if the individual is unable to perform the full 30-second trial, an average duration of the able trials for up to three attempts are computed to differentiate condition performances instigating limited objective conclusions to be drawn. If during the course of the trial, the individual: (1) opens their eyes in an eyes closed condition, (2) raises their arms from the hips, or (3) loses balance and requiring assistance from the spotting examiner to prevent a fall, deeming these actions a failure to maintain postural control and the timing is ceased. The total score represents how well an individual is able to utilize their sensory inputs when one or more sensory systems are manipulated [214]. To draw more objective and conclusive connotations from this clinical exam, the validated instrumented version of the mCTSIB (i.e. imCTSIB) was instituted [215].

A portable force platform, the BTrackS Balance Plate (BBP) (Balance Tracking Systems Inc., San Diego, CA, USA) was utilized in this examination to ascertain validated biomechanical measures capable of quantifying objective laboratory-grade center-of-pressure (CoP) postural stability assessments outside the laboratory in more clinically applicable environments [40]. CoP data was filtered with a second order, low-pass Butterworth filter (cutoff frequency = 4 Hz) using the proprietary software built into the BBP prior to exporting data as text file for further TTB

analyses in MATLAB. The filtered CoP data was applied to a custom MATLAB script, where anterior-posterior (AP) and medial-lateral (ML) TTB measures were derived and applied discretely across each of the four sensory conditions [52]. Both directional components of the derived data were firstly, centered via subtraction of the mean provided by each vector from each data point. Subsequently, velocities for each coordinate data point were computed by exercising finite difference approximations on the CoP coordinate data. The TTB was achieved by dividing the distance between the CoP and the base of support in either direction (AP or ML) by the velocity of the CoP in the same calculated direction. Allowing for a point by point calculation of the time it would take to reach the outer parameter of the BoS at each of the computed velocity and relative CoP position. Each directional TTB score is representative of the smallest windows of time available to make corrective postural changes. In the event that a participant was unable to maintain their postural control or violated any of the previously established clinical mCTSIB errors, the participants were allotted two additional attempts at the trial. In the event that the participant was unable to complete any of the attempts for that trial, the trial (i.e. mCTSIB condition) was deemed a fail. During post-processing, all failed trials were prescribed a 0 (indicative of a fall) for their average TTB outcome in both directions.

Magnetic Resonance Imaging (MRI): MRI Data Acquisition: Diffusion weighted image acquisition was completed with a 3.0 T Siemens MAGNETOM Prisma^{fit} (Siemens Medical Solutions USA, Inc., Malvern, PA) MRI scanner equipped with a 32-channel head coil and parallel imaging. Diffusion weighting was applied in an anterior > posterior orientation with 27 independent non-collinear orientations (b = 2400 s/mm2) including, six unweighted images (b = 0 s/mm2). High-angular resolution diffusion imaging was utilized in conjunction with an echo-planar imaging sequence (repetition time (TR) = 4000 ms, echo time (TE) = 77.00 ms, field of

view (FoV) = 224 mm (224 mm (RL), 216 mm (AP), 144 mm (FH)), 72 (transversal) slices, slice thickness = 2.00 mm, and voxel dimensions= 2.0 x 2.0 x 2.0 mm). Additionally, a high-resolution T1-weighted anatomical scan (TR = 2400 ms, TE = 2.07 ms, flip angle = 8°, FoV = 256 mm (180 mm (RL), 256 mm (AP), 256 mm (FH)), slices = 224 (sagittal), slice thickness = 0.8 mm, and voxel dimensions = 0.8 x 0.8 x 0.8 mm) was collected for post-processing registration. In addition to the thirteen minutes scan duration for diffusion weighted image acquisition, seven minutes were allocated for a T1-weighted image acquisition.

Diffusion Data Processing: Analysis of the sensorimotor pathway microstructural quality and quantity was completed with the using MRI-based diffusion tensor imaging (DTI). The employed with the ExploreDTI (University Medical Center Utrecht, Netherlands, Version 4.8.6; www.exploredti.com) graphical toolbox; utilized for exploratory diffusion (tensor) MRI and fiber tractography in processing, analyzing, and visualizing diffusion MR data [192]. Raw images were visually inspected for evidence of excess motion artifact or instrumental noise via quality assurance tools available within ExploreDTI. Additionally, image data was corrected for the following: signal drift, Gibbs ringing, eddy currents, subject motion, and distortions with both eddy current and subject motion corrective applications being adjusted to each individuals' own high resolution T1-weighted image. Automated anatomical parcellation of the sensorimotor pathway were accomplished by applying the *ICBM_Mori* anatomical template (e.g. atlas) included with the ExploreDTI template suite. The *ICBM_Mori* template is a derivative of the freely available ICBM-152 anatomical template, which incorporates DTI originated fiber orientation and parcellation [216]. From the applied atlas, the indicated regions of interest (ROI) incorporating both the PCML and CST (identified in **Figure 2**) established the ROI-based voxel-view of diffusion metric quantification. The primary neuroimaging analytical outcomes utilized

to objectively quantify the microstructural integrity of the sensorimotor pathway were radial diffusivity (RD) and fractional anisotropy (FA). RD is a quantification of the secondary and tertiary axes ($\lambda_{\perp} = [\lambda_2 + \lambda_3] / 2$) of the diffusion tensor, representing an indirect measure of myelination [127]. A higher RD value is indicative of poorer microstructural integrity, specifically thought to symbolize an indirect reduction of myelination [140, 141]. Alternatively, as a normalized rotationally invariant index that ranges from 0 (isotropic) to 1 (anisotropic), FA is able echo microstructural integrity whereby lower FA values specify poorer white matter tract quality [194]. Post image processing, the primary outcomes (i.e. RD and FA) for both the left and right sensorimotor pathway were averaged together to obtain a gross evaluation of the pathway microstructural integrity.

Statistical Analysis: A 2x4 repeated measures analysis of variance (RMANOVA) was applied to identify differences between groups and average AP TTB measures for the four sensory conditions of the mCTSIB, an analysis that was repeated for the ML direction. In the event that a Mauchly's test of sphericity indicated a violation ($p < 0.05$), a Greenhouse Geisser correction was applied. Where appropriate, Bonferroni post hoc tests were performed to determine which of the sensory conditions differed. Additionally, independent Student t-tests were applied to both of the neuroimaging primary outcomes for the sensorimotor pathway to distinguish differentiation between groups. If a violation of equal variance assumption was indicated via the Levene's test, a Welch correction was implemented to the t-test.

Product moment correlation coefficients (r) were utilized to establish associations between TTB postural outcomes in both directions and sensorimotor pathway integrity diffusion metrics. Where appropriate correlations were identified as having no, weak, moderate, strong and very strong relationships by the following correlation coefficient ranges 0.0-0.2, 0.2-0.4, 0.4-0.6,

0.6-0.8, and 0.8-1.0, respectively [199]. Risk of type I error was set at $\alpha = 0.05$ for all statistical analyses. All statistical analyses were computed in JASP (University of Amsterdam, Amsterdam, Netherlands, Version 0.11.1) and graphical representations were derived using GraphPad Prism 8 (GraphPad Software, La Jolla, CA, Version 8.3.0).

Results

PwMS displayed significantly ($p = 0.018$) worse postural control (i.e. shorter TTB) in the AP direction compared to their neurotypical counterparts across each of the four varying sensory testing conditions (**Figure 4.1**). However, in the ML direction, there were no significant ($p = 0.191$) TTB differentiations between groups (**Table 4.1**).

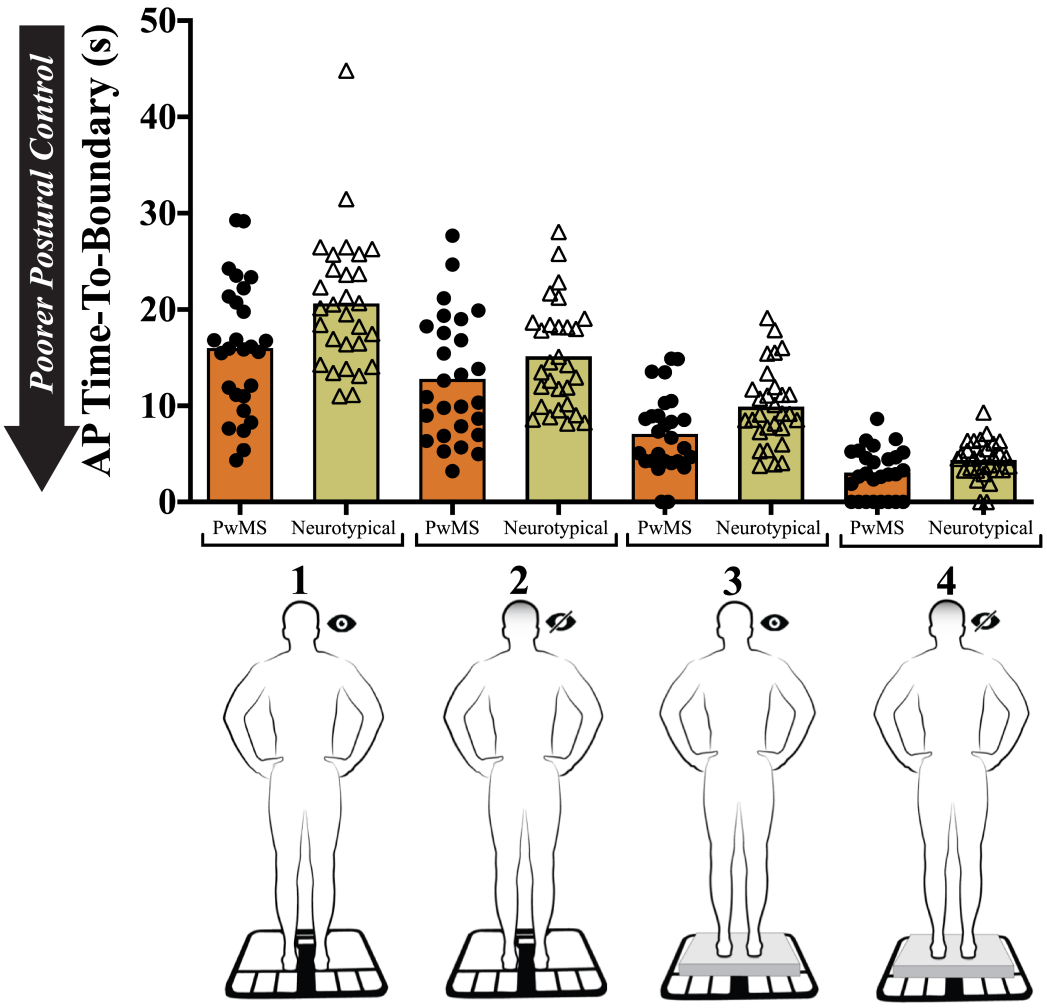

Figure 4.1 | Time-to-boundary for each of the four conditions tested with the imCTSIB in the anterior-posterior direction. A significant main effect of group and condition ($P < 0.05$) was demonstrated, but a group × condition interaction was absent. PwMS presented shorter AP average TTB durations across all four conditions compared to neurotypical, indicating a reduced amount of time to make postural corrections. Plotted data is represented with means (underlying bar plot) and individual values (PwMS: closed circles and neurotypical: open triangles).

Table 4.1 | Summary of Means and Standard Deviations for the Anterior-Posterior and Medial-Lateral mCTSIB Time-To-Boundary Measures (seconds).

mCTSIB Testing Condition	PwMS	Neurotypical
*Anterior-Posterior**		
1. Eyes Open - Rigid Surface	16.00 ± 6.82	20.63 ± 7.02
2. Eyes Closed - Rigid Surface	12.80 ± 6.49	15.15 ± 5.47
3. Eyes Open - Compliant Surface	7.09 ± 4.04	9.93 ± 4.08
4. Eyes Closed - Compliant Surface	3.05 ± 2.49	4.37 ± 2.00
Medial-Lateral		
1. Eyes Open - Rigid Surface	10.55 ± 4.88	12.14 ± 3.26
2. Eyes Closed - Rigid Surface	8.41 ± 4.25	8.81 ± 2.72
3. Eyes Open - Compliant Surface	5.44 ± 3.35	6.33 ± 2.07
4. Eyes Closed - Compliant Surface	2.10 ± 1.76	2.98 ± 1.32

Note. * Significant main effect of group and AP TTB ($p = 0.018$) was demonstrated, but no AP group × condition interaction or ML effects were present.

Besides possessing poorer AP postural control, PwMS presented poorer microstructural quality of the sensorimotor pathway in comparison to the neurotypical adults, exhibiting significantly (Student: $p = 0.006$, Welch: $p = 0.008$) higher RD (PwMS: 0.62e -3 ± 0.66e -4 mm^2/s, neurotypical: 0.58e -3 ± 0.42e -4 mm^2/s) quantification. FA, the normalized measure of microstructural quality (PwMS: 0.33 ± 0.02, neurotypical: 0.34 ± 0.02) failed to reach significance ($p = 0.054$) differentiating the groups (**Figure 4.2C** & **4.2D**).

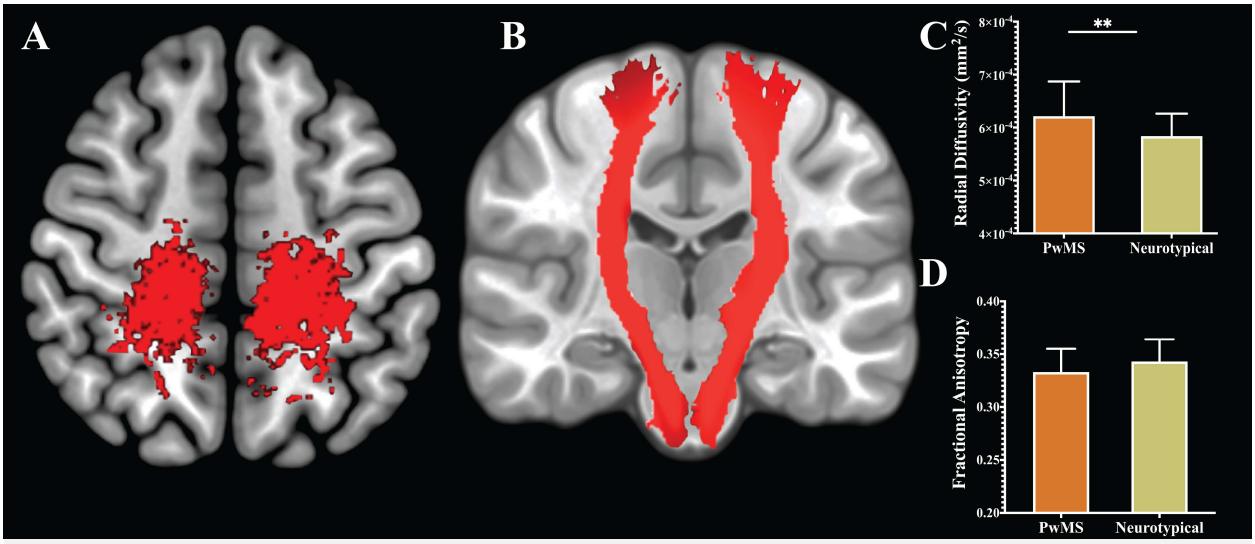

Figure 4.2 | Diminished sensorimotor pathway microstructural integrity in PwMS. (**A**) Axial and (**B**) coronal views of the ICBM-152-based atlas achieved from template suite in *ExploreDTI* (University Medical Center Utrecht, Netherlands, Version 4.8.6; www.exploredti.com). (**C**) PwMS demonstrated significantly greater radial diffusivity (0.62e -3 (0.66e -4)) of the sensorimotor pathway white matter fiber tracts compared to neurotypical adults (0.58e -3 (0.42e -4)). Data are mean (± SD); ** significant group difference at *p-value* < .01. (**D**) PwMS displayed reduced fractional anisotropy (0.33 (0.02)) of the sensorimotor pathway white matter fiber tracts compared to neurotypical adults (0.34 (0.02)) but, failed to achieve a level of significance. Data are mean (± SD); *p-value* = 0.054.

A lone significant negative correlation (r = -0.431, p = 0.016) between the integrity of the pathway via RD and AP TTB in the eyes open, compliant surface condition (mCTSIB condition 2) was discovered in PwMS (**Figure 4.3**). No additional meaningful associations between pathway integrity and TTB postural metrics were identified in the neurotypical population (**Table 4.2**).

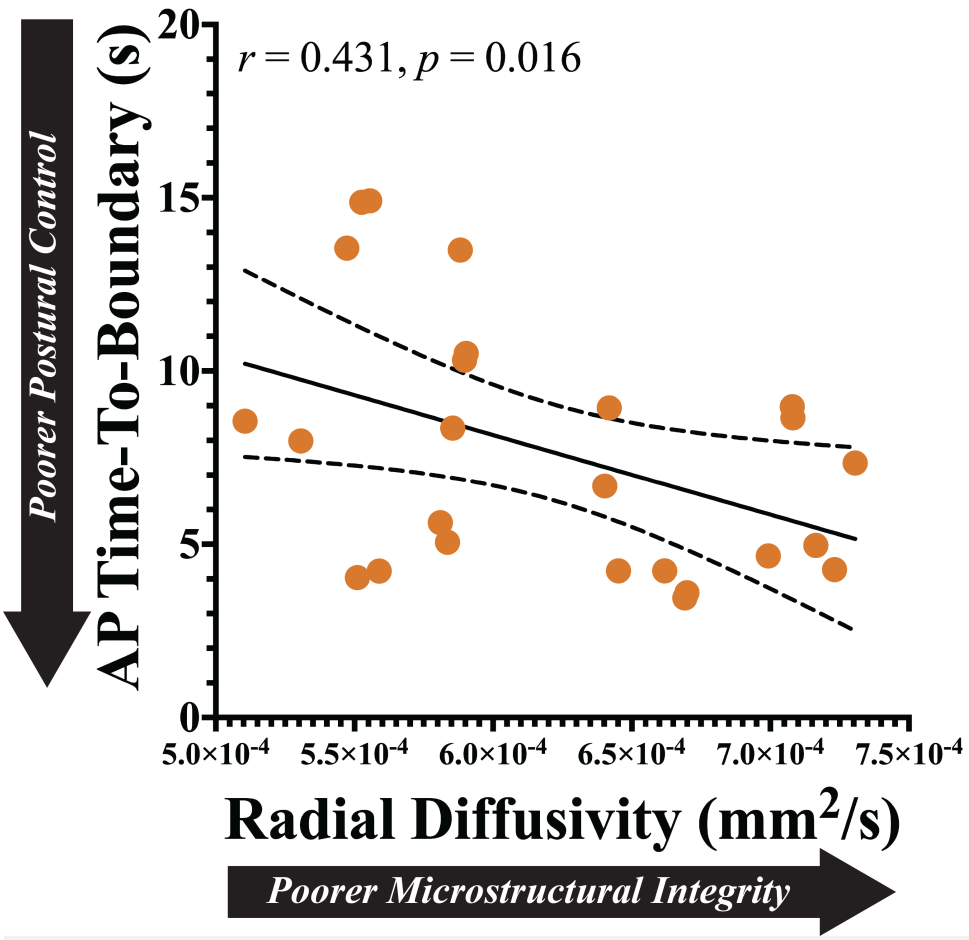

Figure 4.3 | Associations between sensorimotor pathway microstructural integrity and postural control via multi-dimensional quantification in PwMS. Poorer microstructural integrity of the proprioceptive (corticospinal) tracts were associated with poorer postural control. Two PwMS failed to complete the compliant surface/eyes open imCTSIB condition and were negated from the correlation.

Table 4.2 | Correlations for mCTSIB Anterior-Posterior Time-to-Boundary Measures and Radial Diffusivity Measures of Microstructural Integrity for the Sensorimotor Pathway White Matter Tracts.

mCTSIB Testing Condition	PwMS		Neurotypical	
	r	***p***	***r***	***p***
1. Eyes Open - Rigid Surface	-0.316	0.062	-0.247	0.098
2. Eyes Closed - Rigid Surface	-0.327	0.055	-0.276	0.073
3. Eyes Open - Compliant Surface	-0.431*	0.016*	-0.155	0.211
4. Eyes Closed - Compliant Surface	-0.232	0.170	-0.143	0.478

Note. Participants who were unable to complete the trials (i.e. given a TTB of zero) were excluded from the correlation analysis of that trial. No exclusions were recorded for conditions 1 or 2 of the mCTSIB, however two PwMS (n=25) were excluded from condition 3, with eight PwMS (n=19) and two neurotypical adults (n=27) being excluded from the condition 4 analyses. * significant between fiber bundle microstructural integrity & postural control via AP TTB at p-value < .05, **p < .01, ***p < .001.

Discussion

An expansive volume of literature has determined that, PwMS possess a reduced capacity to maintenance postural control and display prominent deficits regardless of the stance condition, detailed in the review *Gait deficits in people with multiple sclerosis* [12]. These surmised discoveries lead to the hypothesis that irrespective of the mCTSIB condition, PwMS would exhibit poorer postural control (i.e. shorter TTB) compared to the neurotypical adults. This theorization supported the AP orientation across testing conditions but disregarded the ML orientation, contradicting copious single-dimensional (e.g. displacement, velocity, and frequency analysis) [217-220] and comparable multi-dimensional (e.g. virtual time to contact) [221] analyses in PwMS.

Explaining the augmented AP deficiencies in the absence of distinct ML dissimilarities from the neurotypical adults could be multifaceted, potentially stemming from an MS demographic factor (e.g. low disability, disease duration, or general active lifestyles). The individuals included in this examination were only clinically moderately (EDSS median of 3.5: a

single functional system showing moderate disability and beyond minimal disability in several other systems [222]) disabled with no functional impairments recognized [223]. Contrasted with the previous multi-dimensional [221] investigations in PwMS which included a severely disabled population (EDSS median of 5.0 (range 2.5–7.5)) with disabilities severe enough to fully impair daily activities and theoretically altering postural control considerably, over the lesser debilitated PwMS.

The geometric BoS is established by the parameters of the foot, anatomically, the foot is designed as a first-class lever in the upright stance position and implicated as a principle component of AP movements during dynamic stability (e.g. six determinants of gait) indicative of daily activity movements [33]. However, when an individual begins to infringe on their limit of stability (exceed the margins of stability), it may be plausible that the individual is required to make alternative ML shifts in an effort to constrain the CoP within the established BoS. This theorization would imply that the limited ML TTB postural control outcomes could stem from PwMS not possessing a level of impairment that approaches the theoretical functional juncture of stability thereby instigating a considerable amplification of a ML postural strategy. Given that the BoS utilized in this analysis was derived from geometric feet parameters, a derived functional BoS parameter (incorporating a limit-of-stability) would ostensibly be a better predictor of stability boundaries, per Slobounov and colleagues outcome endorsement [55]. Regardless of discrepancies in directional discoveries, our multi-dimensional outcome concurs with the inference that with PwMS display poorer postural control compared to neurotypical adults [12, 58, 217, 218].

Preceding explorations in MS have also identified that individuals stricken by this neurodegenerative disease develop substandard proprioceptive tract integrity (higher RD)

compared to healthy controls [58]. This understanding was re-affirmed in the sensorimotor pathway in presented results, verifying the original hypothesis that PwMS would possess inferior microstructural integrity in contrast to their age- and sex-matched counterparts. Although the disparity between groups was substantiated in the RD outcomes, the normalized rotationally invariant index of FA exhibited only trending significance ($p = 0.054$) for group separation upon tract integrity. This inability to reach significance could be stem from unaccounted for partial volume effect-related covariates (crossing-fibers, fiber bundle thickness, fiber orientation, or fiber curvatures) incorporated into the ROI statistical analysis [132]. Nevertheless, evidence suggests that the sensorimotor pathway, a proprioceptive information highway, is degraded in PwMS and as originally speculated.

Although no correlations concerning structure and function were identified in the neurotypical population, our original postulation that the integrity of this postural control mechanism (i.e. sensorimotor pathway) would be associated with postural control performance in PwMS, was accurate. PwMS demonstrated a significant negative correlation between their microstructural integrity and postural control in the AP direction for the third condition of the imCTSIB. A testing condition which specifically manipulates proprioceptive feedback (i.e. compliant surface), while leaving the visual and vestibular system input ostensibly intact. Of the four conditions, this third condition would presumably provide the greatest challenge directly to the proprioceptive system and thereby indicating the microstructural integrity of the sensorimotor pathway as a plausible mechanism for improving proprioceptive-based static postural performance. It is perceivable that the shorten time allotted to PwMS for making postural correction be derived from a temporal competition between the processing of ascending information and descending execution, mimicking upper-extremity paradigms [224]. Although

further affirming depictions of integrative trade-offs are necessary, these conceptual insights are in-line with previous inferences made by Fling and colleagues [58]. Their conclusions deduced that poorer ascending fiber tract integrity of PwMS presented strong correlations to proprioceptive-based balance control, configured using the single-dimensional measure of total sway area. These coinciding associations verify that multi-dimensional measures of proprioceptive-based postural control are a legitimate prognosticator of the sensorimotor pathway microstructural integrity.

The summation of connotations revealed within this examination are not without limitations and future directives: (1) Although, multi-dimensional postural outcomes have been previously established as incorporating increased capacity to detect balance differentiation over single-dimensional measures in PwMS [211], questions still surround more complex multi-dimensional measures. A wider breadth of research centralized around how TTB outcomes are affected by acquisition durations or specifically in MS, disease duration, disease severity (e.g. EDSS), or lesion locality is necessary. (2) As previously detailed, a better understanding of the aspects surrounding functional BoS measures compared to the more geometric BoS derived measures need to be addressed in PwMS. (3) The ROI-based diffusion analysis employed in this examination could be more susceptible to errors derived from crossing-fibers than seen with the employment of tractography-based approaches. Advanced multi-tensor models, constrained spherical deconvolution (with tractography), and diffusion kurtosis tensors all allow for better parcellation of crossing fiber resolution and a more accurate depiction of underlying microarchitectural variances [127]. However, an ROI analysis benefits from reduced dependencies on parameter settings incorporated in tractography approaches. Additionally, the distinct DTI registration and automated parcellations projected by the sensorimotor pathway (i.e.

CST and PCML) make an ROI approach a more consistent approach for this analysis. Although this exam provided a fundamental approach to identifying the mechanism responsible for proprioceptive postural control, further explorations should advance these concepts with more intricate and innovative DTI approaches.

This is the first known study to establish connections between the microstructural integrity of the sensorimotor pathway and postural control performance via multi-dimensional measures. Observed indications specify that a reduction in sensorimotor pathway microstructural integrity (i.e. increased RD) is associated with poorer multi-dimensionally derived postural control in PwMS. These results build upon previous structure-function connotations purposed within MS literature [58] and appoints the microstructural integrity of the sensorimotor pathway as biomarker for postural performance. All observations extracted from this examination support further research into enumerating the sensory integration contributions of postural maintenance.

Chapter 5 | Dissertation Summary

Echoing Aristotle's (in 4th century BC) "movement is life", the time between birth and death is omnipresent with movement [225] and these movements dictate the quality of life lived. Achieving control within movement or stance requires incredibly complex mechanisms that extend from the peripheral nervous system to the central nervous system. These systems that are comprised of trillions of neurons, axons, and synapses to transmit temporally sensitive information for the purposes of functional ambulation and maintenance of an upright stance. This structural and functional conceptualized knowledge drew the overarching aim of this dissertation, to provide mechanistic insight into the gait and balance of both neuro-typical and -atypical (i.e. PwMS) adults. Thereby providing a substantive understanding of the neural underpinnings contributing to reduced locomotor and postural control that proliferate fall and injury risks.

As identified in the initial investigation of this dissertation work, PwMS demonstrated poorer left-right stepping coordination regardless of their speed or cognitive demand compared to neurotypical adults. Additionally, this neuroatypical participant pool accompanied the altered gait pattern with a more conservative overall gait strategy than the neurotypical adults as predicted, spending a greater percentage of gait cycle timing in contact with the ground. These discoveries lay the foundation for a better understanding of "where" in the gait cycle bilateral coordinated deficiencies are located. The outcomes of this investigation were attained using clinically accessible instrumentation and, beyond providing an assessment criterion for bilateral coordinated movements in PwMS, the outcomes could provide clinicians with an enhanced ability to improve the specificity of temporal gait adjustments contained within rehabilitation

programs. Moreover, this investigation set the stage for subsequent studies into the underlying neural mechanisms of bilateral coordination and structure-function affiliations.

The second part of this composition delved further into these mechanisms, identifying the microstructural integrity of the transcallosal sensorimotor white matter fiber tracts comprising the corpus callosum as potential biomarkers of bilateral coordinated performance. PwMS had positive associations between diminished structural integrity across the sensorimotor callosal fiber bundles and poorer self-selected pace bilateral coordination, concurring with initial postulations that an altered corpus callosum structure makes size-able impacts on ambulatory performance. In particular, the primary (M1a) and supplementary (pre-SMA\ SMA-proper) motor fiber bundles appear to be robust targets for future intervention and neurorehabilitation probing. Intervening on gait adaptations and forcing PwMS to walk with a more symmetrical gait pattern (i.e. split-belt intervention paradigm) has the potential to gain acute improvements to gait performance. The neural mechanisms identified herein provides target supraspinal regions (i.e. M1a, pre-SMA, or SMA-proper) to evaluate the efficacy of intervening practices. Symmetrical insufficiencies in gait, generate both mechanical and metabolic debits, thereby increasing the potential for a fall and influencing quality of life.

The final study further detailed structure-function associations in a less dynamic, static postural task, where the base of support stayed constant. Using innovative multi-dimensional measures of postural control during procedures that increasingly challenged the postural control system, inadequacies were identified in PwMS substantiating the original hypotheses. However; uncharacteristically, PwMS only displayed significant deficits (i.e. shorter time-to-boundary) in the anterior-posterior direction compared to their neurotypical counterparts. This contrasting view may be a prospective byproduct of an amplified aptitude for time-to-boundary (a multi-

dimensional measure) to detect balance impairments in PwMS [211] compared to traditional outcomes. Furthermore, these substandard temporal capacities to derive postural corrections during proprioceptive-based balance tasks were associated with poorer sensorimotor pathway (i.e. CST and PCML) microstructural integrity. These outcomes affirm previous laboratory conclusions [58] that static postural control is affected by proprioceptive pathway microstructural integrity in PwMS and revealing a biomarker for impending rehabilitative interventions and supporting the need for alternative assessment metrics to quantify postural control.

With no known cure and such a wide breadth of individuals effected by this auto immune-based neurodegenerative disease, the research efforts deployed in this dissertation have provided a comprehensive view of the neural mechanisms underlying postural control/mobility impairments in PwMS. The procurement of specific biomarkers that contribute to static and dynamic postural control will allow for further therapeutic investigations to be established and optimistically implemented in the near future. My hope is that the impact unveiled within this conceptual knowledge will ultimately influence the MS postural control deficit model established by Luca Prosperini and Letzia Castelli [226] whereby, a reduction of overall postural control deficits (both dynamic and static) will cascade into the diminution of accidental falls and fear of falling, generating an upsurge in mobility. Ultimately, achieving the culminating ambition to influence quality of life by diminishing the number of fall-related injuries experienced by PwMS, and inevitably eradicate the influences of deconditioning.

References

1. Richmond, S.B. and B.W. Fling, *Transcallosal Control of Bilateral Actions.* Exerc Sport Sci Rev, 2019. **47**(4): p. 251-257.
2. *Centers for Disease Control and Prevention, National Center for Injury Prevention and Control*. Web–based Injury Statistics Query and Reporting System (WISQARS) 2016.
3. Florence, C.S., et al., *Medical Costs of Fatal and Nonfatal Falls in Older Adults.* J Am Geriatr Soc, 2018. **66**(4): p. 693-698.
4. Horak, F.B., *Postural Control*, in *Encyclopedia of Neuroscience*. 2009, Springer: Heidelberg, Berlin. p. 3312-3319.
5. Whiting, W. and S. Rugg, *Five factors determine stability and mobility*, in *Dynatomy: Dynamic Human Anatomy*. 2015.
6. Whiting, W. and S. Rugg, *Excerpt: Five factors determine stability and mobility*, in *Dynatomy: Dynamic Human Anatomy*. 2006, Human Kinetics: Champaign, IL.
7. Lockhart, T.E., J.L. Smith, and J.C. Woldstad, *Effects of aging on the biomechanics of slips and falls.* Human Factors, 2005. **47**(4): p. 708-729.
8. Winter, D.A., *Biomechanics and motor control of human movement*. Fourth ed. 2009, Hoboken, NJ: John Wiley & Sons, Inc.
9. Horak, F.B., *Postural orientation and equilibrium: what do we need to know about neural control of balance to prevent falls?* Age Ageing, 2006. **35 Suppl 2**: p. ii7-ii11.

10. Gianni, C., et al., *A systematic review of factors associated with accidental falls in people with multiple sclerosis: a meta-analytic approach.* Clin Rehabil, 2014. **28**(7): p. 704-16.

11. Comber, L., R. Galvin, and S. Coote, *Gait deficits in people with multiple sclerosis: A systematic review and meta-analysis.* Gait Posture, 2017. **51**: p. 25-35.

12. Comber, L., et al., *Postural control deficits in people with Multiple Sclerosis: A systematic review and meta-analysis.* Gait Posture, 2018. **61**: p. 445-452.

13. Zwibel, H.L. and J. Smrtka, *Improving quality of life in multiple sclerosis: an unmet need.* The American Journal of Managed Care, 2011. **17**(5): p. S139-145.

14. Wallin, M.T., et al., *The prevalence of MS in the United States: A population-based estimate using health claims data.* Neurology, 2019.

15. Dilokthornsakul, P., et al., *Multiple sclerosis prevelence in the United States commercially insured population.* Neurology, 2016. **86**: p. 1014-1021.

16. Goldenberg, M.M., *Multiple Sclerosis Review.* P & T: a peer-reviewed journal for formulary management, 2012. **37**(3): p. 175-184.

17. Cohen, J.A. and R. Alexander, *Hankbook of multiple sclerosis*. Second ed. 2012, London, UK: Springer Healthcare.

18. Peterson, E.W., et al., *Injurious falls among middle aged and older adults with multiple sclerosis.* Arch Phys Med Rehabil, 2008. **89**(6): p. 1031-7.

19. Zwibel, H.L., *Contribution of impaired mobility and general symptoms to the burden of multiple sclerosis.* Adv Ther, 2009. **26**(12): p. 1043-57.

20. Sutliff, M.H., *Contribution of impaired mobility to patient burden in multiple sclerosis.* Curr Med Res Opin, 2010. **26**(1): p. 109-19.

21. Scheinberg, L., et al., *Multiple sclerosis: Earning a living.* New York State Journal of Medicine, 1980: p. 1395-1400.

22. LaRocca, N.G., *Impact of walking impairment in multiple sclerosis: perspectives of patients and care partners.* Patient, 2011. **4**(3): p. 189-201.

23. Nilsagård, N., et al., *Falls in people with MS—an individual data meta-analysis from studies from Australia, Sweden, United Kingdom and the United States.* 2015. **21**(1): p. 92-100.

24. Control. (2018). In *Merriam-Webster.com dictionary*. Retrieved from https://www.merriam-webster.com/dictionary/documentation

25. Palmieri, R.M., et al., *Center-of-Pressure Parameters Used in the Assessment of Postural Control.* Journal of Sports Rehabilitation, 2002. **11**: p. 51-66.

26. McGinnis, P.M., *Biomechanics of sport and exercise*. 2005, Champaign, IL: Human Kinetics.

27. Ivanenko, Y. and V.S. Gurfinkel, *Human Postural Control.* Front Neurosci, 2018. **12**: p. 171.

28. Horak, F.B. and J.M. Macpherson, *Postural orientation and equilibrium*, in *Handbook of physiology*. 1996, Oxford University Press: New York. p. 255-292.

29. Peterka, R.J., *Sensorimotor Integration in Human Postural Control.* Journal of Neurophysiology, 2002. **88**: p. 1097-1118.

30. Ting, L.H. and J.M. Macpherson, *A limited set of muscle synergies for force control during a postural task.* J Neurophysiol, 2005. **93**(1): p. 609-13.

31. Horak, F.B. and L.M. Nasher, *Central programming of postural movements: adaptation to altered support surface configurations.* Journal of Neurophysiology, 1986. **55**(6): p. 1369-1381.

32. Chaudhry, H., et al., *Measures of postural stability.* The Journal of Rehabilitation Research and Development, 2004. **41**(5).

33. Levine, D., J. Richards, and M.W. Whittle, *Whittle's Gait Analysis*. Fifth ed. 2012: Elsevier Ltd.

34. Robertson, D.G., et al., *Reasearch methods in biomechanics*. Second ed. 2014, Champaign, IL: Human Kinetics. 428.

35. Goldie, P.A., T.M. Bach, and O.M. Evans, *Force platform measures for evaluating postural control: reliability and validity.* Archives of physical medicine and rehabilitation, 1989. **70**(7): p. 510-517.

36. Browne, J. and N. O''Hare, *A quality control procedure for force platforms.* Physiological Measure, 2000. **21**: p. 515-524.

37. Winter, D.A., A.E. Patla, and J.S. Frank, *Assessment of balance control in humans.* Medical Progress through Technology, 1990. **16**: p. 31-51.

38. Goble, D.J., et al., *An initial evaluation of the btracks balance plate and sports balance software for concussion diagnosis.* International Journal of Sports Physical Therapy, 2016. **11**(2): p. 149-155.

39. Whitney, S.L. and D.M. Wrisley, *The influence of footwear on timed balance scores of the modified clinical test of sensory interaction and balance.* Archives of Physical Medicine and Rehabilitation, 2004. **85**(3): p. 439-443.

40. Richmond, S.B., et al., *Leveling the playing field: Evaluation of a portable instrument for quantifying balance performance.* J Biomech, 2018. **75**: p. 102-107.

41. Goble, D.J., et al., *A Point of Application Study to Determine the Accuracy, Precision and Reliability of a Low-cost Balance Plate for Center of Pressure Measurement.* Journal of Biomechanics, 2018.

42. Paillard, T. and F. Noe, *Techniques and Methods for Testing the Postural Function in Healthy and Pathological Subjects.* Biomed Res Int, 2015. **2015**: p. 891390.

43. Balance Tracking Systems, I., *BTrackS Explore Balance*. 2017.

44. Prieto, T.E., et al., *Measurses of postural steadiness: differences between healthy young and elderly.* IEEE Transactions on Biomedical Engineering, 1996. **43**(9): p. 956-966.

45. Horak, F.B., C.L. Shupert, and A. Mirka, *Components of postural dyscontrol in the elderly: A review.* Neurobiology of Aging, 1989. **10**: p. 727-738.

46. A Hen, S.S.K.T., et al., *Postural control in rheumatoid arthritis patients scheduled for total knee arthroplasty.* Archives of Physical Medicine and Rehabilitation, 2000. **81**(11): p. 1489-1493.

47. Le Clair, K. and C. Riach, *Postural stability measures: what to measure and for how long.* Clinical Biomechanics, 1996. **11**(3): p. 176-178.

48. Braier, M. and T. Hopf, *Ankle orthoses effect on single-limb standing balance in athletes with functional ankle instability.* Archives of Physical Medicine and Rehabilitation, 1998. **79**: p. 939-944.

49. Ekdahl, C., G.B. Jarnlo, and S.I. Andersson, *Standing balance in healthy subjects.* Scandinavian journal of rehabilitation medicine, 1989. **21**(4): p. 187-195.

50. Kirby, R.L., N.A. Price, and D.A. MacLeod, *The influence of foot position on standing balance.* Journal of Biomechanics, 1987. **20**(4): p. 423-427.

51. Uimonen, S., et al., *Effect of positioning of the feet in posturography.* Journal of Vestibular Research, 1992. **2**(4): p. 349-356.

52. Hertel, J., et al., *Time-to-Boundary Measures of Postural Control During Single Quiet Standing.* Journal of Applied Biomechanics, 2006. **22**: p. 67-73.

53. van Wegen, E.E.H., R.E.A. van Emmerik, and G.E. Riccio, *Postural orientation: Age related changes in variability and time-to-boundary.* Human Movement Science, 2002. **21**: p. 61-84.

54. van Wegen, E.E.H., et al., *Stability boundaries and lateral postural control in parkinson's disease.* Motor Control, 2001. **5**(3): p. 254-269.

55. Slobounov, S.M., et al., *Aging and time to instability in posture.* Journal of Gerontology, 1998. **53**(1): p. B71-B78.

56. van Wegan, E.E.H., R.E.A. van Emmerik, and G.E. Ricco, *Postural orientation: Age-related changes in variability and time-to-boundary.* Human Movement Science, 2002. **21**: p. 61-84.

57. Johnson, E.O., et al., *Functional neuroanatomy of propriception.* Journal of surgical orthopaedic advances, 2008. **17**(3): p. 159-164.

58. Fling, B.W., et al., *Associations between Proprioceptive Neural Pathway Structural Connectivity and Balance in People with Multiple Sclerosis.* Front Hum Neurosci, 2014. **8**: p. 814.

59. Brooks, V.B., *The neural basis of motor control*. 1986, New York, NY: Oxford University Press, Inc.

60. Lugade, V., V. Lin, and L.S. Chou, *Center of mass and base of support interaction during gait.* Gait Posture, 2011. **33**(3): p. 406-11.

61. Mirelman, A., et al., *Gait.* Handb Clin Neurol, 2018. **159**: p. 119-134.

62. *Mobility Lab: White Paper*, APDM, Editor. 2015, APDM, Inc.

63. Hausdorff, J.M., et al., *Etiology and modification of gait instability in older adults: a randomized controlled trial of exercise.* Journal of Applied Physiology, 2001. **90**: p. 2117-2129.

64. Armstrong, D.M., *Supraspinal contributions to the initiation and control of locomotion in the cat.* Progressive Neurobiology, 1986. **26**: p. 273-361.

65. Mori, S., *Integration of posture and locomotion in acute decerebrate cats and in awake, freely moving cats* Prgressive Neurobiology, 1987. **28**: p. 161-195.

66. Takakusaki, K., *Neurophysiology of gait: from the spinal cord to the frontal lobe.* Mov Disord, 2013. **28**(11): p. 1483-91.

67. Shik, M.L. and G.N. Orlovsky, *Neurophysiology of locomotor automatism.* Physiology Reviews, 1976. **56**: p. 465-501.

68. Mori, S., et al., *Stimulation of a restricted region in the midline cerebellar white matter evokes coordinated quadrupedal locomotion in the decerebrate cat.* Journal of Neurophysiology, 1999. **82**: p. 290-300.

69. Dietz, V., *Neurophysiology of gait disorders- present and future applications.* Electroencephalography and Clinical Neurophysiology, 1997. **103**: p. 333-355.

70. Ruddy, K.L., A. Leemans, and R.G. Carson, *Transcallosal connectivity of the human cortical motor network.* Brain Struct Funct, 2017. **222**(3): p. 1243-1252.

71. Gazzaniga, M.S., *Cerebral specialization and interhemispheric communication: Does the corpus callosum enable the human condition.* Brain, 2000. **123**: p. 1293-1326.

72. Vanderah, T.W. and D.J. Gould, *Nolte's the human brain: an introduction to its functional anatomy*. 7th ed. 2016, Philadelphia, PA: Elsevier.

73. Boisgontier, M.P., et al., *Complexity of central processing in simple and choice multilimb reaction-time tasks.* PLoS One, 2014. **9**(2): p. e90457.

74. Gooijers, J. and S.P. Swinnen, *Interactions between brain structure and behavior: the corpus callosum and bimanual coordination.* Neurosci Biobehav Rev, 2014. **43**: p. 1-19.

75. Solopova, I.A., et al., *Effects of transcranial magnetic stimulation during voluntary and non-voluntary stepping movements in humans.* Neurosci Lett, 2014. **579**: p. 64-9.

76. Kawashima, R., P.E. Roland, and T. O'Sullivan, *Fields in human motor areas involved in preparation for reaching actual reaching and visuomotor learning: a positron emission tomography study.* Journal of Neuroscience, 1994. **14**(6): p. 3462-3474.

77. Rathelot, J.A. and P.L. Strick, *Subdivisions of primary motor cortex based on cortico-motoneuronal cells.* Proc Natl Acad Sci U S A, 2009. **106**(3): p. 918-23.

78. Preilowski, B.F.B., *Possible contribution of anterior forebrain commissures to bilateral motor coordination.* Neuropsychologia, 1972. **10**: p. 267-277.

79. Eliassen, J.C., K. Baynes, and M.S. Gazzaniga, *Anterior and posterior callosal contributions to simultaneous bimanual movements of the hands and fingers.* Brain, 2000. **123**: p. 2501-2511.

80. Eliassen, J.C., K. Baynes, and M.S. Gazzaniga, *Direction information coordinated via the posterior third of the corpus callosum during bimanual movements.* Experimental Brain Research, 1999. **128**: p. 573-577.

81. Fling, B.W. and R.D. Seidler, *Fundamental differences in callosal structure, neurophysiologic function, and bimanual control in young and older adults.* Cereb Cortex, 2012. **22**(11): p. 2643-52.

82. Fling, B.W., et al., *Differential callosal contributions to bimanual control in young and older adults.* J Cogn Neurosci, 2011. **23**(9): p. 2171-85.

83. Swinnen, S.P., et al., *Age related deficits in motor learning anddifferences in feedback processing during the production of a bimanual coordination pattern.* Cognitive Neurophyschology, 1998. **15**(5): p. 439-466.

84. Wahl, M., et al., *Motor callosal disconnection in early relapsing-remitting multiple sclerosis.* Hum Brain Mapp, 2011. **32**(6): p. 846-55.

85. Boroojerdi, B., et al., *Interhemispheric inhibition in patients with multiple sclerosis.* Electroencephalogr Clin Neurophysiol, 1998. **109**(3): p. 230-7.

86. Bonzano, L., et al., *Callosal contributions to simultaneous bimanual finger movements.* J Neurosci, 2008. **28**(12): p. 3227-33.

87. Lord, S., et al., *Independent domains of gait in older adults and associated motor and nonmotor attributes: validation of a factor analysis approach.* J Gerontol A Biol Sci Med Sci, 2013. **68**(7): p. 820-7.

88. Horak, F., L. King, and M. Mancini, *Role of body-worn movement monitor technology for balance and gait rehabilitation.* Phys Ther, 2015. **95**(3): p. 461-70.

89. Washabaugh, E.P., et al., *Validity and repeatability of inertial measurement units for measuring gait parameters.* Gait Posture, 2017. **55**: p. 87-93.

90. Mancini, M., et al., *Mobility Lab to Assess Balance and Gait with Synchronized Body-worn Sensors.* J Bioeng Biomed Sci, 2011. **Suppl 1**: p. 007.

91. *APDM wearable technologies: Wearable sensors*. 2017 [cited 2019; Available from: https://www.apdm.com/wearable-sensors/.

92. *APDM wearable technologies: Gait and balance*. 2017 [cited 2019; Available from: https://www.apdm.com/mobility/.

93. El-Gohary, M., et al., *Validity of the Instrumented Push and Release Test to Quantify Postural Responses in Persons With Multiple Sclerosis.* Arch Phys Med Rehabil, 2017. **98**(7): p. 1325-1331.

94. Storm, F.A., et al., *Free-living and laboratory gait characteristics in patients with multiple sclerosis.* PLoS One, 2018. **13**(5): p. e0196463.

95. Godinho, C., et al., *A systematic review of the characteristics and validity of monitoring technologies to assess Parkinson's disease.* J Neuroeng Rehabil, 2016. **13**: p. 24.

96. El-Gohary, M., et al., *Continuous monitoring of turning in patients with movement disability.* Sensors (Basel), 2013. **14**(1): p. 356-69.

97. Kirking, B., M. El-Gohary, and Y. Kwon, *The feasibility of shoulder motion tracking during activities of daily living using inertial measurement units.* Gait Posture, 2016. **49**: p. 47-53.

98. Osoba, M.Y., et al., *Balance and gait in the elderly: A contemporary review.* Laryngoscope Investig Otolaryngol, 2019. **4**(1): p. 143-153.

99. Chung, L.H., et al., *Leg power asymmetry and postural control in women with multiple sclerosis.* Med Sci Sports Exerc, 2008. **40**(10): p. 1717-24.

100. Van Emmerik, R.E., et al., *Postural control in women with multiple sclerosis: effects of task, vision and symptomatic fatigue.* Gait Posture, 2010. **32**(4): p. 608-14.

101. Kalron, A., A. Achiron, and Z. Dvir, *Muscular and gait abnormalities in persons with early onset multiple sclerosis.* J Neurol Phys Ther, 2011. **35**(4): p. 164-9.

102. Sandroff, B.M., J.J. Sosnoff, and R.W. Motl, *Physical fitness, walking performance, and gait in multiple sclerosis.* J Neurol Sci, 2013. **328**(1-2): p. 70-6.

103. Rudroff, T., et al., *Asymmetric glucose uptake in leg muscles of patients with Multiple Sclerosis during walking detected by [18F]-FDG PET/CT.* NeuroRehabilitation, 2014. **35**(4): p. 813-23.

104. Adeva-Andany, M., et al., *Comprehensive review on lactate metabolism in human health.* Mitochondrion, 2014. **17**: p. 76-100.

105. Rudroff, T. and F. Proessl, *Effects of Muscle Function and Limb Loading Asymmetries on Gait and Balance in People With Multiple Sclerosis.* Front Physiol, 2018. **9**: p. 531.

106. Plotnik, M., N. Giladi, and J.M. Hausdorff, *A new measure for quantifying the bilateral coordination of human gait: effects of aging and Parkinson's disease.* Exp Brain Res, 2007. **181**(4): p. 561-70.

107. Kribus-Shmiel, L., et al., *How many strides are required for a reliable estimation of temporal gait parameters? Implementation of a new algorithm on the phase coordination index.* PLoS One, 2018. **13**(2): p. e0192049.

108. James, E.G., et al., *Coordination Impairments Are Associated With Falling Among Older Adults.* Exp Aging Res, 2017. **43**(5): p. 430-439.

109. Gimmon, Y., et al., *Gait Coordination Deteriorates in Independent Old-Old Adults.* J Aging Phys Act, 2018. **26**(3): p. 382-389.

110. Swanson, C.W. and B.W. Fling, *Associations between gait coordination, variability and motor cortex inhibition in young and older adults.* Exp Gerontol, 2018. **113**: p. 163-172.

111. Plotnik, M., N. Giladi, and J.M. Hausdorff, *Bilateral coordination of walking and freezing of gait in Parkinson's disease.* Eur J Neurosci, 2008. **27**(8): p. 1999-2006.

112. Plotnik, M., N. Giladi, and J.M. Hausdorff, *Bilateral coordination of gait and Parkinson's disease: the effects of dual tasking.* J Neurol Neurosurg Psychiatry, 2009. **80**(3): p. 347-50.

113. Peterson, D.S., et al., *Evidence for a relationship between bilateral coordination during complex gait tasks and freezing of gait in Parkinson's disease.* Parkinsonism Relat Disord, 2012. **18**(9): p. 1022-6.

114. Williams, A.J., D.S. Peterson, and G.M. Earhart, *Gait coordination in Parkinson disease: effects of step length and cadence manipulations.* Gait Posture, 2013. **38**(2): p. 340-4.

115. Kalron, A., Z. Dvir, and A. Achiron, *Walking while talking--difficulties incurred during the initial stages of multiple sclerosis disease process.* Gait Posture, 2010. **32**(3): p. 332-5.

116. Allali, G., et al., *Walking while talking in patients with multiple sclerosis: the impact of specific cognitive loads.* Neurophysiol Clin, 2014. **44**(1): p. 87-93.

117. Benedetti, M.G., et al., *Gait abnormalities in minimally impaired multiple sclerosis patients.* Multiple Sclerosis, 1999. **5**: p. 363-368.

118. Gianfrancesco, M.A., et al., *Speed- and cane-related alterations in gait parameters in individuals with multiple sclerosis.* Gait Posture, 2011. **33**(1): p. 140-2.

119. Kalron, A., et al., *Quantifying gait impairment using an instrumented treadmill in people with multiple sclerosis.* ISRN Neurol, 2013. **2013**: p. 867575.

120. Kalron, A., et al., *Gait and jogging parameters in people with minimally impaired multiple sclerosis.* Gait Posture, 2014. **39**(1): p. 297-302.

121. Kalron, A., *Association between perceived fatigue and gait parameters measured by an instrumented treadmill in people with multiple sclerosis: a cross-sectional study.* J Neuroeng Rehabil, 2015. **12**: p. 34.

122. Kalron, A., L. Frid, and M. Gurevich, *Concern about falling is associated with step length in persons with multiple sclerosis.* European Journal of Physical and Rehabilitation Medicine, 2015. **51**: p. 197-205.

123. Kelleher, K.J., et al., *The characterisation of gait patterns of people with multiple sclerosis.* Disabil Rehabil, 2010. **32**(15): p. 1242-50.

124. Salter, A.R., et al., *Impact of loss of mobility on instrumental activities of daily living and socioeconomic status in patients with MS.* Curr Med Res Opin, 2010. **26**(2): p. 493-500.

125. Patwardhan, M.B., et al., *Cost of multiple sclerosis by level of disability: a review of literature.* Multiple Sclerosis, 2005. **11**: p. 232-239.

126. *Diffusion*. (2018). In *Merriam-Webster.com dictionary*. Retrieved from https://www.merriam-webster.com/dictionary/documentation

127. Van Hecke, W., L. Emsell, and S. Sunaert, eds. *Diffusion tensor imaging: a practical handbook*. 1st ed. 2016, Springer Science+Buisness Media: New York, NY.

128. Tournier, J.D., S. Mori, and A. Leemans, *Diffusion tensor imaging and beyond.* Magn Reson Med, 2011. **65**(6): p. 1532-56.

129. Noll, D. *MRI Physics 1 and 2: Recap*. in *Training Course in fMRI*. 2018. Ann Arbor, MI.

130. Welsh, R. *Diffusion Tensor Imaging*. in *Training in fMRI Course*. 2018. University of Michigan.

131. Noll, D. *MRI Physics* in *Training Course in fMRI*. 2018. University of Michigan.

132. Jones, D.K., T.R. Knosche, and R. Turner, *White matter integrity, fiber count, and other fallacies: the do's and don'ts of diffusion MRI.* Neuroimage, 2013. **73**: p. 239-54.

133. Moura, L.M., et al., *Diffusion Tensor Imaging Biomarkers to Predict Motor Outcomes in Stroke: A Narrative Review.* Front Neurol, 2019. **10**: p. 445.

134. Alexander, A.L., et al., *Diffusion tensor imaging of the brain.* Neurotherapeutics, 2007. **4**(3): p. 316-329.

135. Soares, J.M., et al., *A hitchhiker's guide to diffusion tensor imaging.* Front Neurosci, 2013. **7**: p. 31.

136. Jeurissen, B., et al., *Diffusion MRI fiber tractography of the brain.* NMR Biomed, 2019. **32**(4): p. e3785.

137. Raffelt, D., et al., *Apparent Fibre Density: A novel measure for the analysis of diffusion-weighted magnetic resonance images.* NeuroImage, 2012. **59**(4): p. 3976-3994.

138. Jones, D.K. and A. Leemans, *Diffusion Tensor Imaging.* Methods in Molecualr Biology, 2011. **711**: p. 127-144.

139. Andersen, O., et al., *Diffusion tensor imaging in multiple sclerosis at different final outcomes.* Acta Neurol Scand, 2018. **137**(2): p. 165-173.

140. Song, S.-K., et al., *Dysmyelination Revealed through MRI as Increased Radial (but Unchanged Axial) Diffusion of Water.* NeuroImage, 2002. **17**(3): p. 1429-1436.

141. Concha, L., *A macroscopic view of microstructure: using diffusion-weighted images to infer damage, repair, and plasticity of white matter.* Neuroscience, 2014. **276**: p. 14-28.

142. Sbardella, E., et al., *Functional connectivity changes and their relationship with clinical disability and white matter integrity in patients with relapsing–remitting multiple sclerosis.* Multiple Sclerosis Journal, 2015. **2**(13): p. 1681-1692.

143. Soyuer, F., M. Mirza, and U. Erkorkmaz, *Balance performance in three forms of multiple sclerosis.* Neurol Res, 2006. **28**(5): p. 555-62.

144. Jackson, R.T., C.M. Epstein, and W.R. Del'Aune, *Abnormalities in posturography and estimations of visual vertical and horizontal in multiple sclerosis.* The American Journal of Otology, 1995. **16**(1): p. 88-93.

145. Beaulieu, C., *What makes diffusion anisotropic in the nervous system?*, in *Diffusion MRI: Theory, Methods, and Applications.* 2011, Oxford University Press: Oxford, UK. p. 92–109.

146. Bronstein, A.M. and M. Pavlou, *Balance.* Handbook of Clinical Neurology, 2013. **110**: p. 189-208.

147. Prosperini, L., et al., *Multiple sclerosis: White and gray matter damage associated with balance deficit detected at static posturography.* Radiology, 2013. **268**(1): p. 181-189.

148. Joseph, R., *The right cerebral hemisphere: emotion, music, visual-spatial skills, body-image, dreams, and awareness.* Journal of clinical psychology, 1988. **44**(5): p. 630-673.

149. Meyer-Moock, S., et al., *Systematic literature review and validity evaluation of the Expanded Disability Status Scale (EDSS) and the Multiple Sclerosis Functional Composite (MSFC) in patients with multiple sclerosis.* BMC Neurol, 2014. **14**: p. 58.

150. Ozturk, A., et al., *MRI of the corpus callosum in multiple sclerosis: association with disability.* Mult Scler, 2010. **16**(2): p. 166-77.

151. Fritz, N.E., et al., *Quantitative measures of walking and strength provide insight into brain corticospinal tract pathology in multiple sclerosis.* Neuroimage Clin, 2017. **14**: p. 490-498.

152. Tovar-Moll, F., et al., *Diffuse and focal corticospinal tract disease and its impact on patient disability in multiple sclerosis.* J Neuroimaging, 2015. **25**(2): p. 200-206.

153. Li, Y., et al., *Diffusion tensor imaging based network analysis detects alterations of neuroconnectivity in patients with clinically early relapsing-remitting multiple sclerosis.* Hum Brain Mapp, 2013. **34**(12): p. 3376-91.

154. Brambilla, L., et al., *Early effect of dalfampridine in patients with MS: A multi-instrumental approach to better investigate responsiveness.* J Neurol Sci, 2016. **368**: p. 402-7.

155. Hubbard, E.A., et al., *Diffusion tensor imaging of the corticospinal tract and walking performance in multiple sclerosis.* J Neurol Sci, 2016. **363**: p. 225-31.

156. Klineova, S., et al., *Relationship between timed 25-foot walk and diffusion tensor imaging in multiple sclerosis.* Mult Scler J Exp Transl Clin, 2016. **2**: p. 2055217316655365.

157. Fritz, N.E., et al., *Distinguishing among multiple sclerosis fallers, near-fallers and non-fallers.* Mult Scler Relat Disord, 2017. **19**: p. 99-104.

158. Peterson, D.S., et al., *Supraspinal control of automatic postural responses in people with multiple sclerosis.* Gait Posture, 2016. **47**: p. 92-5.

159. Wilson, J., et al., *The neural correlates of discrete gait characteristics in ageing: A structured review.* Neurosci Biobehav Rev, 2019. **100**: p. 344-369.

160. Gulani, V., et al., *Apparent diffusion tensor measurements in myelin deficient rat spinal cords.* Magnetic Resounance in Medicine, 2001. **45**: p. 191-195.

161. Peterson, D.S., et al., *Corpus Callosum Structural Integrity Is Associated With Postural Control Improvement in Persons With Multiple Sclerosis Who Have Minimal Disability.* Neurorehabil Neural Repair, 2017. **31**(4): p. 343-353.

162. Prosperini, L., et al., *Multiple sclerosis: Changes in microarchitecture of white matter tracts after training with a video game balance board.* Radiology, 2014. **273**(2): p. 529-538.

163. Cruz-Jimenez, M., *Normal Changes in Gait and Mobility Problems in the Elderly.* Phys Med Rehabil Clin N Am, 2017. **28**(4): p. 713-725.

164. Townsend, M.A., *Biped gait stabilization via foot placement.* Journal of Biomechanics, 1985. **18**(1): p. 21-38.

165. Winter, D.A. and M.W. Rogers, *Foot trajectory in human gait: a precise and multifactorial motor control task.* Physical Therapy, 1992. **72**(1): p. 45-53.

166. Han, S.H., et al., *Quantitative analysis of the bilateral coordination and gait asymmetry using inertial measurement unit-based gait analysis.* PLoS One, 2019. **14**(10): p. e0222913.

167. Swanson, C.W., Z.J. Haigh, and B.W. Fling, *Two-minute walk tests demonstrate similar age-related gait differences as a six-minute walk test.* Gait Posture, 2019. **69**: p. 36-39.

168. Morris, R., et al., *Validity of Mobility Lab (version 2) for gait assessment in young adults, older adults and Parkinson's disease.* Physiol Meas, 2019. **40**(9): p. 095003.

169. Veldkamp, R., et al., *Structured Cognitive-Motor Dual Task Training Compared to Single Mobility Training in Persons with Multiple Sclerosis, a Multicenter RCT.* J Clin Med, 2019. **8**(12).

170. Plotnik, M., et al., *Effects of walking speed on asymmetry and bilateral coordination of gait.* Gait Posture, 2013. **38**(4): p. 864-9.

171. Mancini, M., J.G. Nutt, and F.B. Horak, *How is balance controlled by the nervous system?*, in *Balance Dysfunction in Parkinson's Disease*. 2020. p. 1-24.

172. van Emmerik, R.E., et al., *Enhancing postural stability and adaptability in multiple sclerosis.* Adv Exp Med Biol, 2014. **826**: p. 251-76.

173. Larocca, N., *Impact of walking impairment in multiple sclerosis: perspectives of patients and care partners.* The Patient: Patient-Centered Outcomes Research, 2011. **4**(3): p. 189-201.

174. Serbruyns, L., et al., *Bimanual motor deficits in older adults predicted by diffusion tensor imaging metrics of corpus callosum subregions.* Brain Struct Funct, 2015. **220**(1): p. 273-90.

175. Gooijers, J., et al., *Diffusion tensor imaging metrics of the corpus callosum in relation to bimanual coordination: effect of task complexity and sensory feedback.* Hum Brain Mapp, 2013. **34**(1): p. 241-52.

176. Sohn, Y.H., et al., *Excitability of the ipsilateral motor cortex during phasic voluntary hand movement.* Exp Brain Res, 2003. **148**(2): p. 176-85.

177. Stinear, C.M. and W.D. Byblow, *Role of intracortical inhibition in selective hand muscle activation.* J Neurophysiol, 2003. **89**(4): p. 2014-20.

178. Schmierer, K., et al., *Correlates of disability in multiple sclerosis detected by transcranial magnetic stimulation.* Neurology, 2002. **59**(8): p. 1218-24.

179. King, L.A., et al., *Comparing the Mini-BESTest with the Berg Balance Scale to Evaluate Balance Disorders in Parkinson's Disease.* Parkinsons Dis, 2012. **2012**: p. 375419.

180. Horak, F.B., D.M. Wrisley, and J. Frank, *The Balance Evaluation Systems Test (BESTest) to differentiate balance deficits.* Physical Therapy, 2009. **89**(5): p. 484-498.

181. Padgett, P.K., J.V. Jacobs, and S.L. Kasser, *Is the BESTest at its best? A suggested brief version based on interrater reliability, validity, internal consistency, and theoretical construct.* Phys Ther, 2012. **92**(9): p. 1197-207.

182. Chinsongkram, B., et al., *Reliability and Validity of the Balance Evaluation Systems Test (BESTest) in People With Subacute Stroke.* Physical Therapy, 2014. **94**(11): p. 1632-1643.

183. Leddy, A.L., B.E. Crowner, and G.M. Earhart, *Functional Gait Assessment and Balance Evaluation System Test: Reliability, Validity, Sensitivity, and Specificity for Identifying Individuals With Parkinson Disease Who Fall.* Physical Therapy, 2011. **91**(1): p. 102-113.

184. Duncan, R.P., et al., *Comparative Utility of the BESTest, Mini-BESTest, and Brief-BESTest for Predicting Falls in Individuals With Parkinson Disease: A Cohort Study.* Physical Therapy, 2013. **93**(4): p. 542-550.

185. Potter, K., et al., *Reliability, validity, and responsiveness of the Balance Evaluation Systems Test (BESTest) in individuals with multiple sclerosis.* Physiotherapy, 2017.

186. Jacobs, J.V. and S.L. Kasser, *Balance impairment in people with multiple sclerosis: preliminary evidence for the Balance Evaluation Systems Test.* Gait Posture, 2012. **36**(3): p. 414-8.

187. Leddy, A.L., B.E. Crowner, and G.M. Earhart, *Utility of the Mini-BESTest, BESTest, and BESTest sections for balance assessments in individuals with Parkinson disease.* J Neurol Phys Ther, 2011. **35**(2): p. 90-7.

188. Franchignoni, F., et al., *Using psychometric techniques to improve the Balance Evaluation Systems Test: the mini-BESTest.* J Rehabil Med, 2010. **42**(4): p. 323-31.

189. Franchignoni, F., et al., *Enhancing the usefulness of the Mini-BESTest for measuring dynamic balance: a Rasch validation study.* European Journal of Physical and Rehabilitation Medicine, 2015. **51**(4): p. 429-437.

190. *Mini-BESTest: Balance Evaluation Systems Test*. 2005-2013; Available from: http://www.bestest.us/test_copies/.

191. Godi, M., et al., *Comparison of reliability, validity, and responsiveness of the mini-BESTest and Berg Balance Scale in patients with balance disorders.* Phys Ther, 2013. **93**(2): p. 158-67.

192. Leemans, A., B. Jeurissen, and J. Sijbers, *ExploreDTI: a graphical toolbox for processing, analyzing, and visualizing diffusion MR*, in *17th Annual Meeting of Intl Soc Mag Reson Med.* 2009: Hawaii, USA.

193. Tournier, J.D., F. Calamante, and A. Connelly, *Robust determination of the fibre orientation distribution in diffusion MRI: non-negativity constrained super-resolved spherical deconvolution.* Neuroimage, 2007. **35**(4): p. 1459-72.

194. Basser, P.J. and C. Pierpaoli, *Microstructural and physiological features of tissues elucidated by quantitative-diffusion-tensor MRI.* J Magn Reson B, 1996. **111**(3): p. 209-19.

195. Fling, B.W. and R.D. Seidler, *Task-dependent effects of interhemispheric inhibition on motor control.* Behav Brain Res, 2012. **226**(1): p. 211-7.

196. Garvey, M.A., et al., *New graphical method to measure silent periods evoked by transcranial magnetic stimulation.* Clinical Neurophysiology, 2001. **112**(8): p. 1451-1460.

197. Jung, P. and U. Ziemann, *Differences of the ipsilateral silent period in small hand muscles.* Muscle Nerve, 2006. **34**(4): p. 431-6.

198. Ziemann, U., et al., *Dissociation of the pathways mediating ipsilateral and contralateral motor-evoked potentials in human hand and arm muscles.* Journal of Physiology, 1999(518): p. 895-906.

199. Salkind, N.J., *Statistics for people who (think they) hate statistics*. 6th ed. 2017, Thousand Oaks, CA: SAGE Publications.

200. Pokryszko-Dragan, A., et al., *Diffusion tensor imaging findings in the multiple sclerosis patients and their relationships to various aspects of disability.* Journal of Neuroscience, 2018. **391**: p. 127-133.

201. Udea, R., et al., *MRI evaluation of motor function recovery by rTMS and intensive occupational therapy and changes in the activity of motor cortex.* International Journal of Neuroscience, 2019(3): p. 309-317.

202. Jayaram, G., et al., *Human locomotor adaptive learning is proportional to depression of cerebellar excitability.* Cereb Cortex, 2011. **21**(8): p. 1901-9.

203. Bortoletto, M., et al., *Asymmetric transcallosal conduction delay leads to finer bimanual coordination.* Cerebral Cortex, 2020. **8**: p. 1901-1909.

204. Zivari Adab, H., et al., *Fiber-specific variations in anterior transcallosal white matter structure contribute to age-related differences in motor performance.* Neuroimage, 2020. **209**: p. 116530.

205. Kesar, T.M., J.W. Stinear, and S.L. Wolf, *The use of transcranial magnetic stimulation to evaluate cortical excitability of lower limb musculature: Challenges and opportunities.* Restor Neurol Neurosci, 2018. **36**(3): p. 333-348.

206. Gesslbauer, B., et al., *Axonal components of nerves innervating the human arm.* Ann Neurol, 2017. **82**(3): p. 396-408.

207. Lemon, R.N., *Descending pathways in motor control.* Annu Rev Neurosci, 2008. **31**: p. 195-218.

208. Stolze, H., et al., *Falls in frequent neurological diseases--prevalence, risk factors and aetiology.* J Neurol, 2004. **251**(1): p. 79-84.

209. Cameron, M.H. and S. Lord, *Postural control in multiple sclerosis: implications for fall prevention.* Curr Neurol Neurosci Rep, 2010. **10**(5): p. 407-12.

210. Martyn, C., *Symptoms and signs in the course of the disease*, in *McAlpine's Multiple Sclerosis*. 2005, Churchill Livingstone Elesevier. p. 298-300.

211. Whittier, T.T., et al., *Virtual time-to-contact identifies balance deficits better than traditional metrics in people with multiple sclerosis.* Exp Brain Res, 2020. **238**(1): p. 93-99.

212. Richmond, S.B., et al., *Setting boundaries: Utilization of time to boundary for objective evaluation of the balance error scoring system.* J Sports Sci, 2020. **38**(1): p. 21-28.

213. Shumway-Cook, A. and F. Horak, *Assessing the influence of sensory interaction on balance.* Journal of Physical Therapy, 1986. **66**(10): p. 1548-1550.

214. *Modified Clinical Test of Sensory Interaction in Balance (CTSIB -M)*. Fall Proof Program: Center For Successful Aging, Cal State Fullerton [cited 2020; Available from: https://www.sralab.org/sites/default/files/2017-06/204Lmctsib.pdf.

215. Freeman, L., et al., *Instrumented Test of Sensory Integration for Balance: A Validation Study.* J Geriatr Phys Ther, 2018. **41**(2): p. 77-84.

216. Mori, S., et al., *Stereotaxic White Matter Atlas Based on Diffusion Tensor Imaging in an ICBM Template.* Neuroimage, 2008. **40**(2): p. 570-582.

217. Sosnoff, J.J., S. Shin, and R.W. Motl, *Multiple sclerosis and postural control: the role of spasticity.* Arch Phys Med Rehabil, 2010. **91**(1): p. 93-9.

218. Sosnoff, J.J., et al., *Mobility, balance and falls in persons with multiple sclerosis.* PLoS One, 2011. **6**(11): p. e28021.

219. Kanekar, N., Y.J. Lee, and A.S. Aruin, *Frequency analysis approach to study balance control in individuals with multiple sclerosis.* J Neurosci Methods, 2014. **222**: p. 91-6.

220. Prosperini, L., et al., *The diagnostic accuracy of static posturography in predicting accidental falls in people with multiple sclerosis.* Neurorehabil Neural Repair, 2013. **27**(1): p. 45-52.

221. Cattaneo, D., et al., *The virtual time to contact in the evaluation of balance disorders and prediction of falls in people with multiple sclerosis.* Disabil Rehabil, 2012. **34**(6): p. 470-7.

222. Kurtzke, J.F., *Rating neurologic impairment in multiple sclerosis: An expanded disability status scale (EDSS).* Neurology, 1983. **33**: p. 1444-1452.

223. van Munster, C.E. and B.M. Uitdehaag, *Outcome Measures in Clinical Trials for Multiple Sclerosis.* CNS Drugs, 2017. **31**(3): p. 217-236.

224. Sengupta, S., et al., *Uncertainty modulated exploration in the trade-off between sensing and acting.* PLoS One, 2018. **13**(7): p. e0199544.

225. Starosta, W., *Science of human movments – meaning, name, directions of development.* Jounal of Human Kinetics, 2001. **6**: p. 3-22.

226. Prosperini, L. and L. Castelli, *Spotlight on postural control in patients with multiple sclerosis.* Degener Neurol Neuromuscul Dis, 2018. **8**: p. 25-34.

Mini-BESTest: Balance Evaluation Systems Test

ANTICIPATORY ***SUB SCORE:*** /6

1. SIT TO STAND

Instruction: "Cross your arms across your chest. Try not to use your hands unless you must. Do not let your legs lean against the back of the chair when you stand. Please stand up now."

(2) Normal: Comes to stand without use of hands and stabilizes independently.
(1) Moderate: Comes to stand WITH use of hands on first attempt.
(0) Severe: Unable to stand up from chair without assistance, OR needs several attempts with use of hands.

2. RISE TO TOES

Instruction: "Place your feet shoulder width apart. Place your hands on your hips. Try to rise as high as you can onto your toes. I will count out loud to 3 seconds. Try to hold this pose for at least 3 seconds. Look straight ahead. Rise now."

(2) Normal: Stable for 3 s with maximum height.
(1) Moderate: Heels up, but not full range (smaller than when holding hands), OR noticeable instability for 3 s.
(0) Severe: ≤ 3 s.

3. STAND ON ONE LEG

Instruction: "Look straight ahead. Keep your hands on your hips. Lift your leg off of the ground behind you without touching or resting your raised leg upon your other standing leg. Stay standing on one leg as long as you can. Look straight ahead. Lift now."

Left: *Time in Seconds Trial 1:_____ Trial 2:_____*
(2) Normal: 20 s.
(1) Moderate: < 20 s.
(0) Severe: Unable.

Right: *Time in Seconds Trial 1:_____ Trial 2:_____*
(2) Normal: 20 s.
(1) Moderate: < 20 s.
(0) Severe: Unable

To score each side separately use the trial with the longest time.
To calculate the sub-score and total score use the side [left or right] with the lowest numerical score [i.e. the worse side].

REACTIVE POSTURAL CONTROL ***SUB SCORE:*** /6

4. COMPENSATORY STEPPING CORRECTION- FORWARD

Instruction: "Stand with your feet shoulder width apart, arms at your sides. Lean forward against my hands beyond your forward limits. When I let go, do whatever is necessary, including taking a step, to avoid a fall."

(2) Normal: Recovers independently with a single, large step (second realignment step is allowed).
(1) Moderate: More than one step used to recover equilibrium.
(0) Severe: No step, OR would fall if not caught, OR falls spontaneously.

5. COMPENSATORY STEPPING CORRECTION- BACKWARD

Instruction: "Stand with your feet shoulder width apart, arms at your sides. Lean backward against my hands beyond your backward limits. When I let go, do whatever is necessary, including taking a step, to avoid a fall."

(2) Normal: Recovers independently with a single, large step.
(1) Moderate: More than one step used to recover equilibrium.
(0) Severe: No step, OR would fall if not caught, OR falls spontaneously.

6. COMPENSATORY STEPPING CORRECTION- LATERAL

Instruction: "Stand with your feet together, arms down at your sides. Lean into my hand beyond your sideways limit. When I let go, do whatever is necessary, including taking a step, to avoid a fall."

Left
(2) Normal: Recovers independently with 1 step (crossover or lateral OK).
(1) Moderate: Several steps to recover equilibrium.
(0) Severe: Falls, or cannot step.

Right
(2) Normal: Recovers independently with 1 step (crossover or lateral OK).
(1) Moderate: Several steps to recover equilibrium.
(0) Severe: Falls, or cannot step.

Use the side with the lowest score to calculate sub-score and total score.

SENSORY ORIENTATION ***SUB SCORE:*** /6

7. STANCE (FEET TOGETHER); EYES OPEN, FIRM SURFACE

Instruction: "Place your hands on your hips. Place your feet together until almost touching. Look straight ahead. Be as stable and still as possible, until I say stop."

Time in seconds:_____
(2) Normal: 30 s.
(1) Moderate: < 30 s.
(0) Severe: Unable.

8. STANCE (FEET TOGETHER); EYES CLOSED, FOAM SURFACE

Instruction: "Step onto the foam. Place your hands on your hips. Place your feet together until almost touching. Be as stable and still as possible, until I say stop. I will start timing when you close your eyes."

Time in seconds:_____

(2) Normal: 30 s.
(1) Moderate: < 30 s.
(0) Severe: Unable.

9. INCLINE- EYES CLOSED

Instruction: "Step onto the incline ramp. Please stand on the incline ramp with your toes toward the top. Place your feet shoulder width apart and have your arms down at your sides. I will start timing when you close your eyes."

Time in seconds:_____

(2) Normal: Stands independently 30 s and aligns with gravity.
(1) Moderate: Stands independently <30 s OR aligns with surface.
(0) Severe: Unable.

DYNAMIC GAIT ***SUB SCORE:*** **/10**

10. CHANGE IN GAIT SPEED

Instruction: "Begin walking at your normal speed, when I tell you 'fast', walk as fast as you can. When I say 'slow', walk very slowly."

(2) Normal: Significantly changes walking speed without imbalance.
(1) Moderate: Unable to change walking speed or signs of imbalance.
(0) Severe: Unable to achieve significant change in walking speed AND signs of imbalance.

11. WALK WITH HEAD TURNS – HORIZONTAL

Instruction: "Begin walking at your normal speed, when I say "right", turn your head and look to the right. When I say "left" turn your head and look to the left. Try to keep yourself walking in a straight line."

(2) Normal: performs head turns with no change in gait speed and good balance.
(1) Moderate: performs head turns with reduction in gait speed.
(0) Severe: performs head turns with imbalance.

12. WALK WITH PIVOT TURNS

Instruction: "Begin walking at your normal speed. When I tell you to 'turn and stop', turn as quickly as you can, face the opposite direction, and stop. After the turn, your feet should be close together."

(2) Normal: Turns with feet close FAST (≤ 3 steps) with good balance.
(1) Moderate: Turns with feet close SLOW (≥4 steps) with good balance.
(0) Severe: Cannot turn with feet close at any speed without imbalance.

13. STEP OVER OBSTACLES

Instruction: "Begin walking at your normal speed. When you get to the box, step over it, not around it and keep walking."

(2) Normal: Able to step over box with minimal change of gait speed and with good balance.
(1) Moderate: Steps over box but touches box OR displays cautious behavior by slowing gait.
(0) Severe: Unable to step over box OR steps around box.

14. TIMED UP & GO WITH DUAL TASK ***[3 METER WALK]***

Instruction TUG: "When I say 'Go', stand up from chair, walk at your normal speed across the tape on the floor, turn around, and come back to sit in the chair."

Instruction TUG with Dual Task: "Count backwards by threes starting at ___. When I say 'Go', stand up from chair, walk at your normal speed across the tape on the floor, turn around, and come back to sit in the chair. Continue counting backwards the entire time."

TUG:_____seconds; Dual Task TUG:_____seconds

(2) Normal: No noticeable change in sitting, standing or walking while backward counting when compared to TUG without Dual Task.
(1) Moderate: Dual Task affects either counting OR walking (>10%) when compared to the TUG without Dual Task.
(0) Severe: Stops counting while walking OR stops walking while counting.

When scoring item 14, if subject's gait speed slows more than 10% between the TUG without and with a Dual Task the score should be decreased by a point.

TOTAL SCORE:_____/28

Mini-BESTest Instructions

Subject Conditions: Subject should be tested with flat-heeled shoes OR shoes and socks off.
Equipment: Temper® foam (also called T-foam™ 4 inches thick, medium density T41 firmness rating), chair without arm rests or wheels, incline ramp, stopwatch, a box (9" height) and a 3 meter distance measured out and marked on the floor with tape [from chair].
Scoring: The test has a maximum score of **28** points from **14 items** that are each scored from 0-2.
"0" indicates the lowest level of function and "2" the highest level of function.
If a subject must use an assistive device for an item, score that item one category lower.
If a subject requires physical assistance to perform an item, score "0" for that item.
For **Item 3** (stand on one leg) and **Item 6** (compensatory stepping-lateral) only include the score for one side (the worse score).
For **Item 3** (stand on one leg) select the best time of the 2 trials [from a given side] for the score.
For **Item 14** (timed up & go with dual task) if a person's gait slows greater than 10% between the TUG without and with a dual task then the score should be decreased by a point.

1. SIT TO STAND	Note the initiation of the movement, and the use of the subject's hands on the seat of the chair, the thighs, or the thrusting of the arms forward.
2. RISE TO TOES	Allow the subject two attempts. Score the best attempt. (If you suspect that subject is using less than full height, ask the subject to rise up while holding the examiners' hands.) Make sure the subject looks at a non-moving target 4-12 feet away.
3. STAND ON ONE LEG	Allow the subject two attempts and record the times. Record the number of seconds the subject can hold up to a maximum of 20 seconds. Stop timing when the subject moves hands off of hips or puts a foot down. Make sure the subject looks at a non-moving target 4-12 feet ahead. Repeat on other side.
4. COMPENSATORY STEPPING CORRECTION-FORWARD	Stand in front of the subject with one hand on each shoulder and ask the subject to lean forward (Make sure there is room for them to step forward). Require the subject to lean until the subject's shoulders and hips are in front of toes. After you feel the subject's body weight in your hands, very suddenly release your support. The test must elicit a step. NOTE: Be prepared to catch subject.
5. COMPENSATORY STEPPING CORRECTION - BACKWARD	Stand behind the subject with one hand on each scapula and ask the subject to lean backward (Make sure there is room for the subject to step backward.) Require the subject to lean until their shoulders and hips are in back of their heels. After you feel the subject's body weight in your hands, very suddenly release your support. Test must elicit a step. NOTE: Be prepared to catch subject.
6. COMPENSATORY STEPPING CORRECTION- LATERAL	Stand to the side of the subject, place one hand on the side of the subject's pelvis, and have the subject lean their whole body into your hands. Require the subject to lean until the midline of the pelvis is over the right (or left) foot and then suddenly release your hold. NOTE: Be prepared to catch subject.
7. STANCE (FEET TOGETHER); EYES OPEN, FIRM SURFACE	Record the time the subject was able to stand with feet together up to a maximum of 30 seconds. Make sure subject looks at a non-moving target 4-12 feet away.
8. STANCE (FEET TOGETHER); EYES CLOSED, FOAM SURFACE	Use medium density Temper® foam, 4 inches thick. Assist subject in stepping onto foam. Record the time the subject was able to stand in each condition to a maximum of 30 seconds. Have the subject step off of the foam between trials. Flip the foam over between each trial to ensure the foam has retained its shape.
9. INCLINE EYES CLOSED	Aid the subject onto the ramp. Once the subject closes eyes, begin timing and record time. Note if there is excessive sway.
10. CHANGE IN SPEED	Allow the subject to take 3-5 steps at normal speed, and then say "fast". After 3-5 fast steps, say "slow". Allow 3-5 slow steps before the subject stops walking.
11. WALK WITH HEAD TURNS-HORIZONTAL	Allow the subject to reach normal speed, and give the commands "right, left" every 3-5 steps. Score if you see a problem in either direction. If subject has severe cervical restrictions allow combined head and trunk movements.
12. WALK WITH PIVOT TURNS	Demonstrate a pivot turn. Once the subject is walking at normal speed, say "turn and stop." Count the number of steps from "turn" until the subject is stable. Imbalance may be indicated by wide stance, extra stepping or trunk motion.
13. STEP OVER OBSTACLES	Place the box (9 inches or 23 cm height) 10 feet away from where the subject will begin walking. Two shoeboxes taped together works well to create this apparatus.
14. TIMED UP & GO WITH DUAL TASK	*Use the TUG time to determine the effects of dual tasking. The subject should walk a 3 meter distance. TUG:* Have the subject sitting with the subject's back against the chair. The subject will be timed from the moment you say "Go" until the subject returns to sitting. Stop timing when the subject's buttocks hit the chair bottom and the subject's back is against the chair. The chair should be firm without arms. *TUG With Dual Task*: While sitting determine how fast and accurately the subject can count backwards by threes starting from a number between 100-90. Then, ask the subject to count from a different number and after a few numbers say "Go". Time the subject from the moment you say "Go" until the subject returns to the sitting position. Score dual task as affecting counting or walking if speed slows (>10%) from TUG and or new signs of imbalance.

FALL PROOF PROGRAM: CENTER FOR SUCCESSFUL AGING, CAL STATE FULLERTON

Modified Clinical Test of Sensory Interaction in Balance (CTSIB-M)

***Administer only one trial per condition if participant able to complete first trial without loss of balance.**

Condition One:	***Eyes Open, Firm Surface***			
	Trial One	Total Time:	_____ /	30 sec
	Trial Two	Total Time:	_____ /	30 sec
	Trial Three	Total Time:	_____ /	30 sec
Condition Two:	***Eyes Closed, Firm Surface***			
	Trial One	Total Time:	_____ /	30 sec
	Trial Two	Total Time:	_____ /	30 sec
	Trial Three	Total Time:	_____ /	30 sec
Condition Three:	***Eyes Open, Foam Surface***			
	Trial One	Total Time:	_____ /	30 sec
	Trial Two	Total Time:	_____ /	30 sec
	Trial Three	Total Time:	_____ /	30 sec
Condition Four:	***Eyes Closed, Foam Surface***			
	Trial One	Total Time:	_____ /	30 sec
	Trial Two	Total Time:	_____ /	30 sec
	Trial Three	Total Time:	_____ /	30 sec
		TOTAL:	**_____ /**	**120 sec**

Purpose of Test:

This test is designed to assess how well an older adult is using sensory inputs when one or more sensory systems are compromised. In condition one, all sensory systems (i.e., vision, somatosensory, and vestibular) are available for maintaining balance. In condition two, vision has been removed and the older adult must rely on the somatosensory and vestibular systems to balance. In condition three, the somatosensory system has been compromised and the older adults must use vision and the vestibular system to balance. In condition four, vision has been removed and the somatosensory system has been compromised. The older adults must not rely primarily on the vestibular inputs to balance.

Begin timing each trial using a stopwatch. The trial is over when (a) the participant opens his/her eyes in an eyes closed condition, (b) raises arms from sides, (c) loses balance and requires manual assistance to prevent a fall.

This test provides some insight into whether each of the sensory system available for balance are being used effectively. Failure to maintain balance in condition two indicates that the older adults is visually dependent. They are not using somatosensory inputs to maintain balance when eyes are closed. Failure to maintain balance in conditions 3 and 4 indicate that the visual and/or vestibular system is not being used to maintain balance. Poor performance on this test would suggest the need for multisensory training if the medial history does not indicate that

Appendix 3 | Statistical Analysis: A Temporal Analysis of Bilateral Coordination in Neurotypical and Atypical Adults

Phase Coordination Index (PCI)

PCI Repeated Measures ANOVA

Within Subjects Effects

	Sum of Squares	df	Mean Square	F	p
PCI	0.477	2	0.238	1.209	0.302
PCI ✻ Group	0.620	2	0.310	1.574	0.212
Residual	20.891	106	0.197		

Note. Type III Sum of Squares

Between Subjects Effects

	Sum of Squares	df	Mean Square	F	p
Group	19.273	1	19.273	5.766	0.020
Residual	177.153	53	3.343		

Note. Type III Sum of Squares

PCI Descriptive Statistics

Descriptive Statistics

	Normal PCI		Dual Task PCI		Fast PCI	
	Neurotypical	PwMS	Neurotypical	PwMS	Neurotypical	PwMS
Valid	29	27	29	26	29	27
Missing	0	0	0	1	0	0
Mean	1.840	2.704	1.759	2.528	2.018	2.636
Std. Deviation	0.640	1.708	0.566	1.421	0.582	1.464
Minimum	0.880	1.207	0.798	1.020	0.897	1.120
Maximum	3.400	7.630	2.945	7.010	3.150	7.710

Gait Speed

Gait Speed Repeated Measures ANOVA

Within Subjects Effects

	Sphericity Correction	Sum of Squares	df	Mean Square	F	p
Condition	None	5.833[a]	2.000[a]	2.917[a]	299.061[a]	< .001[a]
	Greenhouse-Geisser	5.833[a]	1.295[a]	4.504[a]	299.061[a]	< .001[a]
Condition ✻ Group	None	0.095[a]	2.000[a]	0.048[a]	4.871[a]	0.010[a]
	Greenhouse-Geisser	0.095[a]	1.295[a]	0.073[a]	4.871[a]	0.022[a]
Residual	None	0.956	98.000	0.010		
	Greenhouse-Geisser	0.956	63.464	0.015		

Note. Type III Sum of Squares

[a] Mauchly's test of sphericity indicates that the assumption of sphericity is violated ($p < .05$).

Between Subjects Effects

	Sum of Squares	df	Mean Square	F	p
Group	1.021	1	1.021	10.249	0.002
Residual	4.883	49	0.100		

Note. Type III Sum of Squares

Post Hoc Tests

Post Hoc Comparisons - Condition

		Mean Difference	SE	t	p_{bonf}
Dual	Fast	-0.459	0.025	-18.670	< .001
	Self	-0.101	0.010	-9.853	< .001
Fast	Self	0.358	0.023	15.608	< .001

Note. Bonferroni adjusted confidence intervals.

Descriptive Statistics

	Self Selected		Fast		Dual	
	Neurotypical	PwMS	Neurotypical	PwMS	Neurotypical	PwMS
Valid	29	27	29	27	27	24
Missing	0	0	0	0	2	3
Mean	1.249	1.122	1.671	1.415	1.156	1.019
Std. Deviation	0.113	0.204	0.178	0.294	0.129	0.212
Minimum	1.100	0.625	1.405	0.845	0.945	0.525
Maximum	1.500	1.535	2.050	2.010	1.385	1.350

Self-Selected Walking

PwMS: Backward Linear Regression

Model Summary

Model	R	R^2	Adjusted R^2	RMSE	Durbin-Watson Autocorrelation	Durbin-Watson Statistic	Durbin-Watson p
1	0.799	0.639	0.530	1.170	-0.155	2.289	0.479
2	0.796	0.634	0.546	1.150	-0.167	2.313	0.395
3	0.792	0.628	0.560	1.133	-0.170	2.322	0.355
4	0.782	0.611	0.561	1.132	-0.104	2.192	0.572
5	0.768	0.590	0.556	1.138	-0.140	2.259	0.459
6	0.764	0.584	0.567	1.123	-0.155	2.292	0.418

ANOVA

Model		Sum of Squares	df	Mean Square	F	p
1	Regression	48.413	6	8.069	5.889	0.001
	Residual	27.401	20	1.370		
	Total	75.814	26			
2	Regression	48.032	5	9.606	7.261	< .001
	Residual	27.782	21	1.323		
	Total	75.814	26			
3	Regression	47.577	4	11.894	9.267	< .001
	Residual	28.237	22	1.284		
	Total	75.814	26			
4	Regression	46.345	3	15.448	12.057	< .001
	Residual	29.470	23	1.281		
	Total	75.814	26			
5	Regression	44.754	2	22.377	17.290	< .001
	Residual	31.061	24	1.294		
	Total	75.814	26			
6	Regression	44.271	1	44.271	35.087	< .001
	Residual	31.543	25	1.262		
	Total	75.814	26			

Coefficients

Model		Unstandardized	Standard Error	Standardized	t	p	Collinearity Statistics	
							Tolerance	VIF
1	(Intercept)	-4625.536	4640.719		-0.997	0.331		
	Double Support Mean	2.171	3.612	4.798	0.601	0.555	0.000	3526.849
	Stance Mean	43.918	45.927	48.762	0.956	0.350	0.000	143891.498
	Swing Mean	48.653	47.118	54.020	1.033	0.314	0.000	151450.072
	Double Support CV	-0.127	0.240	-0.146	-0.527	0.604	0.236	4.242
	Stance CV	-5.135	8.148	-1.378	-0.630	0.536	0.004	264.454
	Swing CV	5.271	5.305	2.391	0.993	0.332	0.003	320.500
2	(Intercept)	-4826.552	4544.863		-1.062	0.300		
	Double Support Mean	2.079	3.546	4.595	0.586	0.564	0.000	3518.727
	Stance Mean	46.031	44.959	51.109	1.024	0.318	0.000	142796.525
	Swing Mean	50.551	46.166	56.126	1.095	0.286	0.000	150567.375
	Stance CV	-6.118	7.795	-1.641	-0.785	0.441	0.004	250.616
	Swing CV	5.614	5.174	2.547	1.085	0.290	0.003	315.667
3	(Intercept)	-4335.391	4399.920		-0.985	0.335		
	Stance Mean	43.133	44.015	47.891	0.980	0.338	0.000	141071.745
	Swing Mean	43.657	43.974	48.472	0.993	0.332	0.000	140806.120
	Stance CV	-8.064	6.948	-2.163	-1.161	0.258	0.005	205.222
	Swing CV	6.920	4.600	3.139	1.504	0.147	0.004	257.191
4	(Intercept)	-23.646	20.461		-1.156	0.260		
	Swing Mean	0.567	0.509	0.629	1.114	0.277	0.053	18.866
	Stance CV	-8.571	6.922	-2.299	-1.238	0.228	0.005	204.084
	Swing CV	7.291	4.581	3.307	1.592	0.125	0.004	255.456
5	(Intercept)	-0.863	0.776		-1.112	0.277		
	Stance CV	-1.140	1.867	-0.306	-0.611	0.547	0.068	14.695
	Swing CV	2.336	1.104	1.059	2.115	0.045	0.068	14.695
6	(Intercept)	-1.086	0.676		-1.608	0.120		
	Swing CV	1.685	0.284	0.764	5.923	< .001	1.000	1.000

Descriptives

	N	Mean	SD	SE
PCI	27	2.705	1.708	0.329
Double Support Mean	27	20.111	3.774	0.726
Stance Mean	27	60.061	1.896	0.365
Swing Mean	27	39.944	1.896	0.365
Double Support CV	27	6.599	1.971	0.379
Stance CV	27	1.481	0.458	0.088
Swing CV	27	2.250	0.775	0.149

Collinearity Diagnostics

				Variance Proportions	
Model	Dimension	Eigenvalue	Condition Index	intercept	Swing CV
1	1	6.801	1.000	0.000	0.000
	2	0.125	7.380	0.000	0.001
	3	0.067	10.038	0.000	0.001
	4	0.007	31.880	0.000	0.000
	5	1.684e -4	200.932	0.000	0.851
	6	7.940e -7	2926.583	0.000	0.130
	7	1.554e -9	66144.506	1.000	0.018
2	1	5.854	1.000	0.000	0.000
	2	0.117	7.082	0.000	0.001
	3	0.029	14.174	0.000	0.000
	4	1.719e -4	184.555	0.000	0.853
	5	7.982e -7	2708.155	0.000	0.125
	6	1.565e -9	61157.116	1.000	0.021
3	1	4.879	1.000	0.000	0.000
	2	0.115	6.511	0.000	0.001
	3	0.006	29.688	0.000	0.016
	4	9.138e -5	231.080	0.000	0.977
	5	1.614e -9	54976.090	1.000	0.006
4	1	3.895	1.000	0.000	0.000
	2	0.101	6.211	0.000	0.001
	3	0.004	31.995	0.004	0.035
	4	4.509e -5	293.909	0.996	0.964
5	1	2.934	1.000	0.009	0.001
	2	0.063	6.828	0.845	0.024
	3	0.003	30.349	0.146	0.975
6	1	1.947	1.000	0.026	0.026
	2	0.053	6.085	0.974	0.974

Neurotypical: Backward Linear Regression

Model Summary

Model	R	R^2	Adjusted R^2	RMSE	Durbin-Watson
1	0.677	0.459	0.311	0.531	
2	0.677	0.458	0.340	0.520	1.484

ANOVA

Model		Sum of Squares	df	Mean Square	F	p
1	Regression	5.259	6	0.877	3.107	0.023
	Residual	6.207	22	0.282		
	Total	11.467	28			
2	Regression	5.254	5	1.051	3.890	0.011
	Residual	6.213	23	0.270		
	Total	11.467	28			

Coefficients

Model		Unstandardized	Standard Error	Standardized	t	p	Collinearity Statistics: Tolerance	Collinearity Statistics: VIF
1	(Intercept)	1446.635	2203.037		0.657	0.518		
	Double Support Mean	10.432	4.272	36.256	2.442	0.023	0.000	8957.107
	Stance Mean	-25.534	23.316	-44.398	-1.095	0.285	0.000	66791.867
	Swing Mean	-3.056	21.479	-5.309	-0.142	0.888	0.000	56568.098
	Double Support CV	-0.274	0.138	-0.643	-1.983	0.060	0.234	4.277
	Stance CV	-25.179	13.033	-8.276	-1.932	0.066	0.001	745.766
	Swing CV	18.234	8.678	9.173	2.101	0.047	0.001	774.514
2	(Intercept)	1138.923	411.887		2.765	0.011		
	Double Support Mean	10.425	4.179	36.233	2.494	0.020	0.000	8956.128
	Stance Mean	-22.441	8.254	-39.020	-2.719	0.012	0.000	8743.202
	Double Support CV	-0.274	0.135	-0.645	-2.032	0.054	0.234	4.273
	Stance CV	-24.631	12.182	-8.096	-2.022	0.055	0.001	680.511
	Swing CV	17.862	8.098	8.986	2.206	0.038	0.001	704.408

Descriptives

	N	Mean	SD	SE
PCI	29	1.839	0.640	0.119
Double Support Mean	29	19.063	2.224	0.413
Stance Mean	29	59.543	1.113	0.207
Swing Mean	29	40.462	1.112	0.206
Double Support CV	29	5.641	1.505	0.279
Stance CV	29	1.162	0.210	0.039
Swing CV	29	1.711	0.322	0.060

Part And Partial Correlations

Model		Partial	Part
1	Double Support Mean	0.462	0.383
	Stance Mean	-0.227	-0.172
	Swing Mean	-0.030	-0.022
	Double Support CV	-0.389	-0.311
	Stance CV	-0.381	-0.303
	Swing CV	0.409	0.330
2	Double Support Mean	0.461	0.383
	Stance Mean	-0.493	-0.417
	Double Support CV	-0.390	-0.312
	Stance CV	-0.388	-0.310
	Swing CV	0.418	0.339

Collinearity Diagnostics

Model	Dimension	Eigenvalue	Condition Index	Variance Proportions					
				intercept	Double Support Mean	Stance Mean	Double Support CV	Stance CV	Swing CV
1	1	6.897	1.000	0.000	0.000	0.000	0.000	0.000	0.000
	2	0.067	10.162	0.000	0.000	0.000	0.123	0.000	0.000
	3	0.031	14.940	0.000	0.000	0.000	0.084	0.000	0.001
	4	0.005	36.978	0.000	0.000	0.000	0.423	0.001	0.000
	5	2.264e -5	551.988	0.000	0.003	0.000	0.072	0.845	0.858
	6	1.090e -7	7955.621	0.001	0.945	0.023	0.289	0.098	0.079
	7	1.305e -9	72696.129	0.999	0.051	0.977	0.008	0.056	0.062
2	1	5.905	1.000	0.000	0.000	0.000	0.000	0.000	0.000
	2	0.065	9.548	0.000	0.000	0.000	0.128	0.000	0.000
	3	0.026	14.956	0.000	0.000	0.000	0.107	0.000	0.001
	4	0.004	39.982	0.000	0.000	0.000	0.397	0.002	0.000
	5	2.159e -5	522.954	0.000	0.005	0.000	0.073	0.934	0.951
	6	2.230e -8	16272.261	1.000	0.995	1.000	0.294	0.064	0.048

Dual-Task Walking

PwMS: Backward Linear Regression

Model Summary

Model	R	R^2	Adjusted R^2	RMSE	Durbin-Watson Autocorrelation	Durbin-Watson Statistic	Durbin-Watson p
1	0.828	0.686	0.586	0.914	0.070	1.822	0.640
2	0.828	0.685	0.607	0.891	0.067	1.828	0.673
3	0.827	0.684	0.624	0.872	0.064	1.833	0.626
4	0.826	0.683	0.639	0.853	0.069	1.827	0.654

ANOVA

Model		Sum of Squares	df	Mean Square	F	p
1	Regression	34.619	6	5.770	6.904	< .001
	Residual	15.879	19	0.836		
	Total	50.498	25			
2	Regression	34.614	5	6.923	8.716	< .001
	Residual	15.884	20	0.794		
	Total	50.498	25			
3	Regression	34.534	4	8.634	11.357	< .001
	Residual	15.964	21	0.760		
	Total	50.498	25			
4	Regression	34.473	3	11.491	15.776	< .001
	Residual	16.025	22	0.728		
	Total	50.498	25			

Coefficients

Model		Unstandardized	Standard Error	Standardized	t	p	Collinearity Statistics Tolerance	Collinearity Statistics VIF
1	(Intercept)	-646.768	4196.917		-0.154	0.879		
	Double Support Mean	-3.409	9.463	-9.851	-0.360	0.723	0.000	45177.504
	Stance Mean	9.707	44.781	14.044	0.217	0.831	0.000	253664.905
	Swing Mean	3.316	41.143	4.795	0.081	0.937	0.000	213918.648
	Double Support CV	-0.684	0.260	-0.745	-2.630	0.016	0.207	4.842
	Stance CV	3.650	3.966	1.137	0.920	0.369	0.011	92.286
	Swing CV	0.668	2.421	0.397	0.276	0.786	0.008	125.447
2	(Intercept)	-317.117	915.212		-0.346	0.733		
	Double Support Mean	-3.433	9.220	-9.921	-0.372	0.714	0.000	45131.533
	Stance Mean	6.431	18.327	9.305	0.351	0.729	0.000	44708.143
	Double Support CV	-0.689	0.244	-0.751	-2.830	0.010	0.224	4.474
	Stance CV	3.599	3.816	1.121	0.943	0.357	0.011	89.913
	Swing CV	0.719	2.276	0.428	0.316	0.755	0.009	116.661

Coefficients

Model		Unstandardized	Standard Error	Standardized	t	p	Collinearity Statistics	
							Tolerance	VIF
3	(Intercept)	-241.366	864.122		-0.279	0.783		
	Double Support Mean	-2.629	8.669	-7.595	-0.303	0.765	0.000	41687.196
	Stance Mean	4.900	17.292	7.089	0.283	0.780	0.000	41580.909
	Double Support CV	-0.697	0.237	-0.759	-2.940	0.008	0.226	4.430
	Stance CV	4.766	0.940	1.485	5.068	< .001	0.175	5.705
4	(Intercept)	3.488	1.774		1.966	0.062		
	Double Support Mean	-0.172	0.077	-0.497	-2.232	0.036	0.291	3.440
	Double Support CV	-0.683	0.227	-0.744	-3.007	0.006	0.236	4.246
	Stance CV	4.728	0.911	1.473	5.189	< .001	0.179	5.590

Descriptives

	N	Mean	SD	SE
PCI	26	2.528	1.421	0.279
Double Support Mean	26	21.884	4.107	0.805
Stance Mean	26	60.950	2.056	0.403
Swing Mean	26	39.055	2.055	0.403
Double Support CV	26	5.939	1.548	0.304
Stance CV	26	1.452	0.443	0.087
Swing CV	26	2.305	0.846	0.166

Part And Partial Correlations

Model		Partial	Part
1	Double Support Mean	-0.082	-0.046
	Stance Mean	0.050	0.028
	Swing Mean	0.018	0.010
	Double Support CV	-0.517	-0.338
	Stance CV	0.207	0.118
	Swing CV	0.063	0.035
2	Double Support Mean	-0.083	-0.047
	Stance Mean	0.078	0.044
	Double Support CV	-0.535	-0.355
	Stance CV	0.206	0.118
	Swing CV	0.070	0.040
3	Double Support Mean	-0.066	-0.037
	Stance Mean	0.062	0.035

Part And Partial Correlations

Model		Partial	Part
4	Double Support CV	-0.540	-0.361
	Stance CV	0.742	0.622
	Double Support Mean	-0.430	-0.268
	Double Support CV	-0.540	-0.361
	Stance CV	0.742	0.623

Collinearity Diagnostics

Model	Dimension	Eigenvalue	Condition Index	Variance Proportions			
				intercept	Double Support Mean	Double Support CV	Stance CV
1	1	6.810	1.000	0.000	0.000	0.000	0.000
	2	0.124	7.402	0.000	0.000	0.000	0.002
	3	0.061	10.579	0.000	0.000	0.122	0.000
	4	0.005	38.496	0.000	0.000	0.736	0.033
	5	4.642e -4	121.119	0.000	0.000	0.038	0.891
	6	7.056e -8	9824.337	0.001	0.948	0.053	0.065
	7	1.180e -9	75979.866	0.999	0.052	0.050	0.010
2	1	5.840	1.000	0.000	0.000	0.000	0.000
	2	0.097	7.774	0.000	0.000	0.000	0.002
	3	0.060	9.890	0.000	0.000	0.145	0.000
	4	0.003	40.941	0.000	0.000	0.801	0.052
	5	4.372e -4	115.577	0.000	0.000	0.025	0.897
	6	1.435e -8	20173.617	1.000	1.000	0.029	0.049
3	1	4.886	1.000	0.000	0.000	0.001	0.001
	2	0.069	8.414	0.000	0.000	0.075	0.048
	3	0.041	10.865	0.000	0.000	0.075	0.132
	4	0.003	37.450	0.000	0.000	0.808	0.800
	5	1.542e -8	17799.882	1.000	1.000	0.041	0.020
4	1	3.899	1.000	0.001	0.001	0.001	0.001
	2	0.060	8.035	0.017	0.060	0.099	0.023
	3	0.038	10.169	0.073	0.015	0.057	0.188
	4	0.003	34.837	0.910	0.925	0.843	0.788

Neurotypical: Backward Linear Regression

Model Summary

Model	R	R^2	Adjusted R^2	RMSE	Durbin-Watson Autocorrelation	Durbin-Watson Statistic	Durbin-Watson p
1	0.397	0.158	-0.072	0.585	0.084	1.747	0.521
2	0.397	0.157	-0.026	0.573	0.079	1.762	0.542
3	0.387	0.150	0.008	0.563	0.088	1.726	0.469
4	0.376	0.142	0.039	0.554	0.083	1.731	0.440
5	0.349	0.122	0.055	0.550	0.089	1.751	0.509
6	0.320	0.102	0.069	0.546	0.071	1.806	0.600

ANOVA

Model		Sum of Squares	df	Mean Square	F	p
1	Regression	1.411	6	0.235	0.686	0.663
	Residual	7.538	22	0.343		
	Total	8.950	28			
2	Regression	1.408	5	0.282	0.859	0.523
	Residual	7.541	23	0.328		
	Total	8.950	28			
3	Regression	1.340	4	0.335	1.057	0.399
	Residual	7.610	24	0.317		
	Total	8.950	28			
4	Regression	1.267	3	0.422	1.374	0.273
	Residual	7.682	25	0.307		
	Total	8.950	28			
5	Regression	1.093	2	0.546	1.808	0.184
	Residual	7.857	26	0.302		
	Total	8.950	28			
6	Regression	0.915	1	0.915	3.073	0.091
	Residual	8.035	27	0.298		
	Total	8.950	28			

Coefficients

Model		Unstandardized	Standard Error	Standardized	t	p	Collinearity Statistics	
							Tolerance	VIF
1	(Intercept)	-1158.078	2293.688		-0.505	0.619		
	Double Support Mean	2.275	4.796	9.511	0.474	0.640	0.000	10498.091
	Stance Mean	9.397	23.830	19.716	0.394	0.697	0.000	65289.917
	Swing Mean	13.742	23.036	28.849	0.597	0.557	0.000	61087.903
	Double Support CV	-0.020	0.210	-0.036	-0.094	0.926	0.261	3.831
	Stance CV	3.021	5.004	1.450	0.604	0.552	0.007	150.695
	Swing CV	-1.479	3.188	-1.197	-0.464	0.647	0.006	173.848
2	(Intercept)	-1213.877	2166.707		-0.560	0.581		
	Double Support Mean	2.136	4.461	8.929	0.479	0.637	0.000	9490.187
	Stance Mean	10.096	22.137	21.183	0.456	0.653	0.000	58879.803
	Swing Mean	14.157	22.114	29.720	0.640	0.528	0.000	58829.376
	Stance CV	2.915	4.767	1.399	0.611	0.547	0.007	142.959
	Swing CV	-1.451	3.105	-1.174	-0.467	0.645	0.006	172.291
3	(Intercept)	-246.101	431.076		-0.571	0.573		
	Double Support Mean	2.555	4.293	10.679	0.595	0.557	0.000	9088.168
	Swing Mean	4.899	8.629	10.284	0.568	0.575	0.000	9262.264
	Stance CV	2.929	4.688	1.406	0.625	0.538	0.007	142.953
	Swing CV	-1.464	3.053	-1.185	-0.480	0.636	0.006	172.276
4	(Intercept)	-305.626	406.410		-0.752	0.459		
	Double Support Mean	3.102	4.074	12.968	0.762	0.453	0.000	8445.262
	Swing Mean	6.114	8.120	12.836	0.753	0.459	0.000	8463.176
	Stance CV	0.690	0.424	0.331	1.627	0.116	0.827	1.209
5	(Intercept)	0.386	0.920		0.419	0.679		
	Double Support Mean	0.035	0.046	0.146	0.768	0.449	0.929	1.077
	Stance CV	0.585	0.397	0.281	1.472	0.153	0.929	1.077
6	(Intercept)	1.004	0.442		2.274	0.031		
	Stance CV	0.666	0.380	0.320	1.753	0.091	1.000	1.000

Descriptives

	N	Mean	SD	SE
PCI	29	1.758	0.565	0.105
Double Support Mean	29	20.291	2.363	0.439
Stance Mean	29	60.153	1.186	0.220
Swing Mean	29	39.852	1.187	0.220
Double Support CV	29	4.941	1.033	0.192
Stance CV	29	1.132	0.271	0.050
Swing CV	29	1.718	0.457	0.085

Collinearity Diagnostics

				Variance Proportions	
Model	Dimension	Eigenvalue	Condition Index	intercept	Stance CV
1	1	6.887	1.000	0.000	0.000
	2	0.076	9.550	0.000	0.001
	3	0.033	14.397	0.000	0.000
	4	0.004	42.394	0.000	0.013
	5	1.711e -4	200.629	0.000	0.943
	6	9.606e -8	8467.499	0.001	0.031
	7	1.468e -9	68485.745	0.999	0.012
2	1	5.914	1.000	0.000	0.000
	2	0.074	8.970	0.000	0.001
	3	0.012	22.353	0.000	0.003
	4	1.765e -4	183.072	0.000	0.928
	5	1.053e -7	7494.595	0.001	0.065
	6	1.582e -9	61142.986	0.999	0.003
3	1	4.922	1.000	0.000	0.000
	2	0.066	8.639	0.000	0.001
	3	0.012	20.395	0.000	0.003
	4	1.763e -4	167.103	0.000	0.928
	5	3.506e -8	11848.738	1.000	0.067
4	1	3.951	1.000	0.000	0.003
	2	0.038	10.172	0.000	0.847
	3	0.011	18.902	0.000	0.040
	4	3.827e -8	10160.502	1.000	0.110
5	1	2.961	1.000	0.001	0.005
	2	0.033	9.484	0.065	0.994
	3	0.006	21.375	0.934	0.001
6	1	1.973	1.000	0.013	0.013
	2	0.027	8.606	0.987	0.987

Fast-Pace Walking

PwMS: Backward Linear Regression

Model Summary

Model	R	R^2	Adjusted R^2	RMSE	Durbin-Watson Autocorrelation	Durbin-Watson Statistic	Durbin-Watson p
1	0.659	0.434	0.255	1.280	-0.022	1.996	0.986
2	0.658	0.433	0.292	1.249	-0.013	1.979	0.959
3	0.647	0.419	0.308	1.234	0.027	1.891	0.764
4	0.615	0.378	0.293	1.247	0.012	1.944	0.868
5	0.613	0.376	0.322	1.222	0.001	1.967	0.912
6	0.586	0.343	0.316	1.227	-0.066	2.106	0.758

ANOVA

Model		Sum of Squares	df	Mean Square	F	p
1	Regression	23.880	6	3.980	2.427	0.065
	Residual	31.151	19	1.640		
	Total	55.031	25			
2	Regression	23.840	5	4.768	3.057	0.033
	Residual	31.190	20	1.560		
	Total	55.031	25			
3	Regression	23.034	4	5.759	3.779	0.018
	Residual	31.997	21	1.524		
	Total	55.031	25			
4	Regression	20.812	3	6.937	4.460	0.014
	Residual	34.219	22	1.555		
	Total	55.031	25			
5	Regression	20.681	2	10.340	6.924	0.004
	Residual	34.350	23	1.493		
	Total	55.031	25			
6	Regression	18.872	1	18.872	12.526	0.002
	Residual	36.159	24	1.507		
	Total	55.031	25			

Coefficients

Model		Unstandardized	Standard Error	Standardized	t	p	Collinearity Statistics: Tolerance	Collinearity Statistics: VIF
1	(Intercept)	150.475	150.816		0.998	0.331		
	Double Support Mean	-1.425	1.662	-3.535	-0.857	0.402	0.002	570.810
	Stance Mean	-0.139	0.503	-0.175	-0.276	0.786	0.074	13.478
	Swing Mean	-2.870	2.850	-3.794	-1.007	0.327	0.002	476.542
	Double Support CV	-0.364	0.313	-0.527	-1.162	0.260	0.145	6.910
	Stance CV	6.090	12.370	1.528	0.492	0.628	0.003	323.289
	Swing CV	-1.352	8.746	-0.549	-0.155	0.879	0.002	422.528

Coefficients

Model		Unstandardized	Standard Error	Standardized	t	p	Collinearity Statistics	
							Tolerance	VIF
2	(Intercept)	158.687	137.669		1.153	0.263		
	Double Support Mean	-1.508	1.534	-3.742	-0.983	0.337	0.002	510.868
	Stance Mean	-0.202	0.281	-0.255	-0.719	0.480	0.225	4.436
	Swing Mean	-2.946	2.738	-3.895	-1.076	0.295	0.002	462.163
	Double Support CV	-0.357	0.302	-0.516	-1.181	0.251	0.148	6.741
	Stance CV	4.195	1.681	1.053	2.496	0.021	0.159	6.275
3	(Intercept)	164.779	135.819		1.213	0.239		
	Double Support Mean	-1.776	1.471	-4.406	-1.208	0.241	0.002	480.745
	Swing Mean	-3.262	2.671	-4.313	-1.222	0.235	0.002	450.240
	Double Support CV	-0.423	0.284	-0.612	-1.488	0.152	0.164	6.113
	Stance CV	4.426	1.631	1.110	2.714	0.013	0.165	6.047
4	(Intercept)	0.918	6.243		0.147	0.884		
	Swing Mean	-0.042	0.143	-0.055	-0.290	0.775	0.787	1.271
	Double Support CV	-0.154	0.179	-0.224	-0.863	0.397	0.421	2.376
	Stance CV	2.910	1.052	0.730	2.765	0.011	0.406	2.466
5	(Intercept)	-0.860	1.151		-0.748	0.462		
	Double Support CV	-0.176	0.160	-0.255	-1.101	0.282	0.507	1.972
	Stance CV	3.046	0.922	0.764	3.304	0.003	0.507	1.972
6	(Intercept)	-1.189	1.116		-1.066	0.297		
	Stance CV	2.334	0.659	0.586	3.539	0.002	1.000	1.000

Descriptives

	N	Mean	SD	SE
PCI	26	2.667	1.484	0.291
Double Support Mean	26	16.661	3.681	0.722
Stance Mean	26	58.147	1.871	0.367
Swing Mean	26	41.751	1.961	0.385
Double Support CV	26	8.563	2.147	0.421
Stance CV	26	1.652	0.372	0.073
Swing CV	26	2.321	0.602	0.118

Collinearity Diagnostics

				Variance Proportions	
Model	**Dimension**	**Eigenvalue**	**Condition Index**	**intercept**	**Stance CV**
1	1	6.859	1.000	0.000	0.000
	2	0.073	9.710	0.000	0.000
	3	0.057	11.006	0.000	0.000
	4	0.012	24.338	0.000	0.003
	5	3.629e -4	137.476	0.000	0.106
	6	3.369e -5	451.205	0.005	0.855
	7	1.685e -6	2017.565	0.995	0.037
2	1	5.885	1.000	0.000	0.000
	2	0.066	9.423	0.000	0.014
	3	0.038	12.384	0.000	0.042
	4	0.010	24.127	0.000	0.358
	5	1.686e -4	186.848	0.002	0.014
	6	1.837e -6	1789.693	0.998	0.572
3	1	4.891	1.000	0.000	0.000
	2	0.063	8.799	0.000	0.010
	3	0.036	11.648	0.000	0.049
	4	0.010	21.998	0.000	0.373
	5	1.858e -6	1622.413	1.000	0.568
4	1	3.938	1.000	0.000	0.001
	2	0.046	9.271	0.008	0.080
	3	0.016	15.853	0.000	0.656
	4	7.934e -4	70.448	0.992	0.263
5	1	2.955	1.000	0.005	0.003
	2	0.030	9.855	0.912	0.050
	3	0.015	14.047	0.083	0.948
6	1	1.976	1.000	0.012	0.012
	2	0.024	9.163	0.988	0.988

Neurotypical: Backward Linear Regression

Model Summary

Model	R	R^2	Adjusted R^2	RMSE	Durbin-Watson
1	0.376	0.142	-0.104	0.622	
2	0.376	0.142	-0.054	0.608	
3	0.374	0.140	-0.010	0.595	
4	0.371	0.137	0.030	0.583	
5	0.330	0.109	0.038	0.581	
6	0.273	0.074	0.039	0.581	
7	0.000	0.000	0.000	0.592	1.716

ANOVA

Model		Sum of Squares	df	Mean Square	F	p
1	Regression	1.341	6	0.224	0.578	0.744
	Residual	8.127	21	0.387		
	Total	9.468	27			
2	Regression	1.340	5	0.268	0.725	0.612
	Residual	8.128	22	0.369		
	Total	9.468	27			
3	Regression	1.323	4	0.331	0.934	0.462
	Residual	8.145	23	0.354		
	Total	9.468	27			
4	Regression	1.301	3	0.434	1.274	0.306
	Residual	8.167	24	0.340		
	Total	9.468	27			
5	Regression	1.031	2	0.516	1.528	0.237
	Residual	8.437	25	0.337		
	Total	9.468	27			
6	Regression	0.705	1	0.705	2.091	0.160
	Residual	8.763	26	0.337		
	Total	9.468	27			
7	Regression	.	.	.	.	.
	Residual	.	.	.	.	.
	Total	.	.	.	.	.

Coefficients

Model		Unstandardized	Standard Error	Standardized	t	p	Collinearity Statistics	
							Tolerance	VIF
1	(Intercept)	-24.540	43.873		-0.559	0.582		
	Double Support Mean	0.215	0.395	0.956	0.545	0.592	0.013	75.325
	Stance Mean	0.090	0.282	0.236	0.321	0.751	0.075	13.246
	Swing Mean	0.437	0.887	1.167	0.493	0.627	0.007	136.856
	Double Support CV	0.012	0.209	0.039	0.057	0.955	0.088	11.419
	Stance CV	1.758	9.277	0.802	0.189	0.852	0.002	437.828
	Swing CV	-1.644	6.617	-0.948	-0.248	0.806	0.003	356.683
2	(Intercept)	-22.757	30.088		-0.756	0.457		

Coefficients

Model		Unstandardized	Standard Error	Standardized	t	p	Collinearity Statistics	
							Tolerance	VIF
	Double Support Mean	0.197	0.231	0.876	0.854	0.402	0.037	26.964
	Stance Mean	0.090	0.275	0.234	0.326	0.747	0.076	13.215
	Swing Mean	0.402	0.629	1.074	0.640	0.529	0.014	72.051
	Stance CV	1.897	8.748	0.865	0.217	0.830	0.002	407.758
	Swing CV	-1.687	6.423	-0.973	-0.263	0.795	0.003	352.067
3	(Intercept)	-25.185	27.341		-0.921	0.367		
	Double Support Mean	0.218	0.206	0.968	1.058	0.301	0.045	22.363
	Stance Mean	0.051	0.203	0.132	0.249	0.806	0.132	7.549
	Swing Mean	0.506	0.402	1.349	1.257	0.221	0.032	30.799
	Swing CV	-0.296	0.337	-0.171	-0.878	0.389	0.988	1.012
4	(Intercept)	-19.967	17.216		-1.160	0.258		
	Double Support Mean	0.214	0.201	0.950	1.063	0.299	0.045	22.224
	Swing Mean	0.453	0.335	1.208	1.351	0.189	0.045	22.256
	Swing CV	-0.294	0.330	-0.170	-0.890	0.382	0.988	1.012
5	(Intercept)	-18.906	17.103		-1.105	0.280		
	Double Support Mean	0.196	0.200	0.871	0.984	0.335	0.045	22.009
	Swing Mean	0.421	0.332	1.124	1.269	0.216	0.045	22.009
6	(Intercept)	-2.343	3.016		-0.777	0.444		
	Swing Mean	0.102	0.071	0.273	1.446	0.160	1.000	1.000
7	(Intercept)	2.014	0.112		17.996	< .001		

Descriptives

	N	Mean	SD	SE
PCI	28	2.014	0.592	0.112
Double Support Mean	28	15.095	2.627	0.497
Stance Mean	28	57.471	1.546	0.292
Swing Mean	28	42.611	1.580	0.299
Double Support CV	28	7.886	1.935	0.366
Stance CV	28	1.379	0.270	0.051
Swing CV	28	1.855	0.342	0.065

Collinearity Diagnostics

				Variance Proportions	
Model	**Dimension**	**Eigenvalue**	**Condition Index**	**intercept**	**Swing Mean**
1	1	6.892	1.000	0.000	0.000
	2	0.080	9.268	0.000	0.000
	3	0.020	18.548	0.000	0.000
	4	0.008	29.385	0.000	0.000
	5	2.307e -4	172.847	0.000	0.002
	6	2.477e -5	527.468	0.040	0.032
	7	4.113e -6	1294.469	0.960	0.966
2	1	5.924	1.000	0.000	0.000
	2	0.055	10.342	0.000	0.000
	3	0.020	17.298	0.000	0.000
	4	3.207e -4	135.913	0.000	0.003
	5	2.554e -5	481.584	0.110	0.039
	6	8.121e -6	854.146	0.890	0.957
3	1	4.949	1.000	0.000	0.000
	2	0.032	12.513	0.000	0.000
	3	0.019	15.961	0.000	0.001
	4	1.412e -4	187.217	0.001	0.084
	5	1.151e -5	655.571	0.999	0.915
4	1	3.951	1.000	0.000	0.000
	2	0.031	11.266	0.000	0.000
	3	0.018	14.724	0.000	0.001
	4	2.385e -5	406.997	1.000	0.999
5	1	2.976	1.000	0.000	0.000
	2	0.024	11.163	0.000	0.001
	3	2.402e -5	351.992	1.000	0.999
6	1	1.999	1.000	0.000	0.000
	2	6.620e -4	54.954	1.000	1.000

Appendix 4 | Statistical Analysis: Bridging the Callosal Gap in Gait: A Mechanistic Evaluation of White Matter in Bilateral Coordination

Radial Diffusivity (RD)

Repeated Measures ANOVA

Within Subjects Effects

	Sum of Squares	df	Mean Square	F	p	η^2
Radial Diffusivity	4.032e -7	7	5.760e -8	113.307	< .001	0.323
Radial Diffusivity ✻ Type	4.750e -9	7	6.786e -10	1.335	0.232	0.004
Residual	1.921e -7	378	5.083e -10			

Note. Type III Sum of Squares

Between Subjects Effects

	Sum of Squares	df	Mean Square	F	p	η^2
Type	1.259e -7	1	1.259e -7	13.030	< .001	0.194
Residual	5.218e -7	54	9.664e -9			

Note. Type III Sum of Squares

PwMS: RD Correlation Matrix

Pearson Correlations

	Pearson's r	p
Normal PCI - CMA	0.395 *	0.021
Normal PCI - M1a	0.473 **	0.006
Normal PCI - M1p	0.308	0.059
Normal PCI - PMd	0.434 *	0.012
Normal PCI - PMv	0.355 *	0.034
Normal PCI - S1	0.360 *	0.033
Normal PCI - SMA	0.439 *	0.011
Normal PCI - preSMA	0.401 *	0.019

Neurotypical: RD Correlation Matrix

Pearson Correlations

	Pearson's r	p
Normal PCI - CMA	0.104	0.296
Normal PCI - M1a	0.122	0.264
Normal PCI - M1p	0.165	0.196
Normal PCI - PMd	0.108	0.288
Normal PCI - PMv	0.318 *	0.047
Normal PCI - S1	0.016	0.466
Normal PCI - SMA	0.158	0.206
Normal PCI - preSMA	0.065	0.369

Note . all tests one-tailed, for positive correlation

* p < .05, ** p < .01, *** p < .001, one-tailed

Fractional Anisotropy (FA)

Within Subjects Effects

	Sphericity Correction	Sum of Squares	df	Mean Square	F	p	η^2	η^2_p
Fractional Anisotropy	None	0.841[a]	7.000[a]	0.120[a]	149.751[a]	< .001[a]	0.500	0.735
	Greenhouse-Geisser	0.841[a]	4.940[a]	0.170[a]	149.751[a]	< .001[a]	0.500	0.735
Fractional Anisotropy ✻ Group	None	0.010[a]	7.000[a]	0.001[a]	1.812[a]	0.084[a]	0.006	0.032
	Greenhouse-Geisser	0.010[a]	4.940[a]	0.002[a]	1.812[a]	0.112[a]	0.006	0.032
Residual	None	0.303	378.000	8.027e -4				
	Greenhouse-Geisser	0.303	266.760	0.001				

Note. Type III Sum of Squares

[a] Mauchly's test of sphericity indicates that the assumption of sphericity is violated (p < .05).

Between Subjects Effects

	Sum of Squares	df	Mean Square	F	p	η^2	η^2_p
Group	0.067	1	0.067	7.902	0.007	0.128	0.128
Residual	0.461	54	0.009				

Note. Type III Sum of Squares

PwMS: FA Correlation Matrix

Pearson Correlations

		Pearson's r	p
Normal PCI	- CMA	-0.334**	0.006
Normal PCI	- M1a	-0.514***	< .001
Normal PCI	- M1p	-0.355**	0.004
Normal PCI	- PMd	-0.504***	< .001
Normal PCI	- PMv	-0.238*	0.039
Normal PCI	- S1	-0.346**	0.005
Normal PCI	- SMA	-0.401**	0.001
Normal PCI	- preSMA	-0.466***	< .001

Neurotypical: FA Correlation Matrix

Pearson Correlations

		Pearson's r	p
Normal PCI	- CMA	-0.102	0.300
Normal PCI	- M1a	-0.101	0.301
Normal PCI	- M1p	-0.047	0.405
Normal PCI	- PMd	-0.097	0.309
Normal PCI	- PMv	-0.172	0.187
Normal PCI	- S1	-0.100	0.302
Normal PCI	- SMA	-0.160	0.203
Normal PCI	- preSMA	-0.002	0.496

Note . all tests one-tailed, for negative correlation

* p < .05, ** p < .01, *** p < .001, one-tailed

Ipsilateral Silent Period (iSP)

Depth of Silent Period

Within Subjects Effects

	Sum of Squares	df	Mean Square	F	p	η^2	η^2_p
Hemisphere	0.005	1	0.005	4.907e -5	0.994	0.000	0.000
Hemisphere ✻ Group	0.140	1	0.140	0.001	0.971	0.000	0.000
Residual	4540.529	44	103.194				

Note. Type III Sum of Squares

Between Subjects Effects

	Sum of Squares	df	Mean Square	F	p	η^2	η^2_p
Group	18.343	1	18.343	0.068	0.796	0.002	0.002
Residual	11891.237	44	270.255				

Note. Type III Sum of Squares

Duration of Silent Period

Within Subjects Effects

	Sum of Squares	df	Mean Square	F	p	η^2	η^2_p
Hemisphere	429.000	1	429.000	0.372	0.545	0.002	0.008
Hemisphere ✻ Group	29.913	1	29.913	0.026	0.873	0.000	0.001
Residual	50719.739	44	1152.721				

Note. Type III Sum of Squares

Between Subjects Effects

	Sum of Squares	df	Mean Square	F	p	η^2	η^2_p
Group	1385.689	1	1385.689	0.511	0.479	0.011	0.011
Residual	119336.366	44	2712.190				

Note. Type III Sum of Squares

Appendix 5 | Statistical Analysis: Advanced Characterization of Static Postural Control Dysfunction in Persons with Multiple Sclerosis and Associated Neural Mechanisms

Neuroimaging Analysis

Radial Diffusivity: Independent Samples T-Test

	Test	Statistic	df	p	Cohen's d
CST_RD	Student	-2.569	54.000	0.006	-0.687
	Welch	-2.531	44.038	0.008	-0.682

Note. For all tests, the alternative hypothesis specifies that group *Neurotypical* is less than group *PwMS* .

Test of Equality of Variances (Levene's)

	F	df	p
CST_RD	10.536	1	0.002

Group Descriptives

	Group	N	Mean	SD	SE
CST_RD	Neurotypical	29	5.838e -4	4.241e -5	7.876e -6
	PwMS	27	6.215e -4	6.548e -5	1.260e -5

Fractional Anisotropy: Independent Samples T-Test

	t	df	p	Cohen's d
CST_FA	1.634	54.000	0.054	0.437

Note. Student's t-test.

Note. For all tests, the alternative hypothesis specifies that group *Neurotypical* is greater than group *PwMS* .

Group Descriptives

	Group	N	Mean	SD	SE
CST_FA	Neurotypical	29	0.343	0.021	0.004
	PwMS	27	0.333	0.022	0.004

Anterior-Posterior Results

AP: Repeated Measures ANOVA

Within Subjects Effects

	Sphericity Correction	Sum of Squares	df	Mean Square	F	p
mCTSIB	None	6804.637[a]	3.000[a]	2268.212[a]	214.403[a]	< .001[a]
	Greenhouse-Geisser	6804.637[a]	2.143[a]	3174.787[a]	214.403[a]	< .001[a]
mCTSIB ✻ Group	None	80.235[a]	3.000[a]	26.745[a]	2.528[a]	0.059[a]
	Greenhouse-Geisser	80.235[a]	2.143[a]	37.435[a]	2.528[a]	0.080[a]
Residual	None	1713.832	162.000	10.579		
	Greenhouse-Geisser	1713.832	115.740	14.808		

Note. Type III Sum of Squares

[a] Mauchly's test of sphericity indicates that the assumption of sphericity is violated (p < .05).

Between Subjects Effects

	Sum of Squares	df	Mean Square	F	p
Group	434.229	1	434.229	5.901	0.018
Residual	3973.432	54	73.582		

Note. Type III Sum of Squares

Descriptives

mCTSIB	Group	Mean	SD	N
Rigid Surface/Eyes Open	Neurotypical	20.632	7.019	29
	PwMS	16.001	6.820	27
Rigid Surface/Eyes Closed	Neurotypical	15.151	5.470	29
	PwMS	12.797	6.494	27
Compliant Surface/Eyes Open	Neurotypical	9.931	4.077	29
	PwMS	7.092	4.043	27
Compliant Surface/Eyes Closed	Neurotypical	4.369	2.000	29
	PwMS	3.048	2.493	27

PwMS RD-AP Correlations

Pearson Correlations

	Pearson's r	p
CST_RD - AP_TTB_Avg_RO	-0.303	0.063
CST_RD - AP_TTB_Avg_RC	-0.320	0.052
CST_RD - AP_TTB_Avg_CO	-0.370 *	0.029
CST_RD - AP_TTB_Avg_CC	-0.308	0.059

Note . all tests one-tailed, for negative correlation

* p < .05, ** p < .01, *** p < .001, one-tailed

Corrected Condition 3

Pearson Correlations

	Pearson's r	p
CST_RD - AP_TTB_Avg_CO	-0.431 *	0.016

Note . all tests one-tailed, for negative correlation
* p < .05, ** p < .01, *** p < .001, one-tailed

Corrected Condition 4

Pearson Correlations

	Pearson's r	p
CST_RD - AP_TTB_Avg_CC	-0.232	0.170

Note . all tests one-tailed, for negative correlation
* p < .05, ** p < .01, *** p < .001, one-tailed

Neurotypical RD-AP Correlations

Pearson Correlations

	Pearson's r	p
CST_RD - AP_TTB_Avg_RO	-0.247	0.098
CST_RD - AP_TTB_Avg_RC	-0.276	0.073
CST_RD - AP_TTB_Avg_CO	-0.155	0.211
CST_RD - AP_TTB_Avg_CC	-0.110	0.285

Note . all tests one-tailed, for negative correlation
* p < .05, ** p < .01, *** p < .001, one-tailed

Corrected Condition 4

Pearson Correlations

	Pearson's r	p
CST_RD - AP_TTB_Avg_CC	-0.143	0.478

Medial-Lateral Results

ML: Repeated Measures ANOVA

Within Subjects Effects

	Sphericity Correction	Sum of Squares	df	Mean Square	F	p
mCTSIB	None	2379.251[a]	3.000[a]	793.084[a]	209.092[a]	< .001[a]
	Greenhouse-Geisser	2379.251[a]	2.385[a]	997.608[a]	209.092[a]	< .001[a]
mCTSIB ✻ Group	None	10.091[a]	3.000[a]	3.364[a]	0.887[a]	0.449[a]
	Greenhouse-Geisser	10.091[a]	2.385[a]	4.231[a]	0.887[a]	0.430[a]
Residual	None	614.464	162.000	3.793		
	Greenhouse-Geisser	614.464	128.788	4.771		

Note. Type III Sum of Squares

[a] Mauchly's test of sphericity indicates that the assumption of sphericity is violated ($p < .05$).

Between Subjects Effects

	Sum of Squares	df	Mean Square	F	p
Group	49.202	1	49.202	1.751	0.191
Residual	1517.717	54	28.106		

Note. Type III Sum of Squares

Descriptives

mCTSIB	Group	Mean	SD	N
Rigid Surface/Eyes Open	Neurotypical	12.136	3.258	29
	PwMS	10.547	4.878	27
Rigid Surface/Eyes Closed	Neurotypical	8.807	2.715	29
	PwMS	8.409	4.245	27
Compliant Surface/Eyes Open	Neurotypical	6.328	2.071	29
	PwMS	5.440	3.353	27
Compliant Surface/Eyes Closed	Neurotypical	2.979	1.315	29
	PwMS	2.101	1.761	27

Step 1: Phase Coordination Index Calculations

```
 %Project: Mahoney.Richmond.Study (MRS)
 %Script Authors: Sutton Richmond, MS; Clayton Swanson, MS;
 %                & Zachary Haig, BS
 %Last Revised Date: 1/22/19
 %Coded for MAC use

 %Phase Coordination Index calculations originating authors and reference:

% Plotnik, M., Giladi, N., & Hausdorff, J. M. (2007). A new measure for
%    quantifying the bilateral coordination of human gait: effects of aging
%    and Parkinson's disease. Exp Brain Res, 181(4), 561-570.
%     doi:10.1007/s00221-007-0955-7

    %Script Equipment:APDM, Inc. Inertial Monitoring Units(6-sensor system)
    %Collection Parameters: Sampling rate: 128 Hz
    %Data Output: MobilityLab CSV files

%Script: will output the overall PCI score, accuracy,
%and consistency measures for three seperate (2-minute) walking conditions.
%Additionally, this script will generate a stride-by-stride graphical
%display of each of the walking conditions.

%Additional Functions .m files REQUIRED to be in the path:
% 1.)hline
% 2.)vline

%Experimental Procedure: (3) instrumented 2-minute walks at 1.)a
%self-selected pace, 2.)a self-selected pace and under a cognitive load
%(dual-task), & 3.) a fast pace.

%Pre-CSV preperation:
%1. Export APDM data (Export trial -> Check (only) the Detailed Results box
%->  click EXPORT
%2. In the .csv file, erase the following rows:
    %ID Rows 3 --> 5
    %Any gait data after Row #59 (60 +)
%3. Script is READY to be run!!!
%% Clear command window and workspace
clc
clear all
close all
GoBack = pwd;
%% Load Path Data
    %Alternative Load Option: Load the data from the designated (prompted by)
3 digit subject number;
    %make sure that the (3 digit subject numbers) files are located in the
    %designated root directory.
    % subnum = input('Enter 3 digit subject number: ', 's');
    % root_dir = ['/Users/suttonrichmond/Desktop/MRS_PCI_Data/'];
```

```
PATH = pwd
RootPath = uigetdir(PATH);
cd(RootPath)
%% Results Path
ResultDirS = [PATH '/PCIresults/SUBnumber/'];
ResultDirW = [PATH '/PCIresults/NORMALwalk/'];
ResultDirD = [PATH '/PCIresults/DUALwalk/'];
ResultDirF = [PATH '/PCIresults/FASTwalk/'];
PCIplotFolder = [PATH '/PCIplots/'];
%% PCI Equations
    %     phi_CV is the coefficient of variation of the mean of phi values
    %         for each subject.
    %         phi_CV = sigma_phi/mu_phi
    %     Pphi_ABS is the conversion of phi_ABS to a percentage.
    %         Pphi_ABS = 100*phi_ABS/180
    %     Finally,
    %         PCI = phi_CV + Pphi_ABS
%% Load the testing condition: Normal Walking Trial
STR1 = [RootPath,'/walk.csv'];
NWdata = dlmread(STR1, ',',16, 5);
%% Raw data from data sheet:
%Gait Cycle Duration [s] [L;R]:
Walk_GCD = [NWdata(7,:);NWdata(8,:)];
%Step Duration [s] [L;R];
Walk_StepDur = [NWdata(24,:);NWdata(25,:)];
%Lower Limb Swing [%GCT] [L;R]:
Walk_SwingGCT = [NWdata(28,:);NWdata(29,:)]./100; %Convert to decimal form.
%% Calculating True Swing Time [s] [L;R]:
Walk_SwingT = Walk_GCD.*Walk_SwingGCT;

Walk_n = length(Walk_SwingT(1,1:end));

Walk_phi = zeros(1,Walk_n-1);

%Determining Short and Long Swing Times:
Walk_tLft = Walk_SwingT(1,:); %Left Swing Time
Walk_tRt = Walk_SwingT(2,:); %Right Swing Time

if mean(Walk_tLft) < mean(Walk_tRt)
    Walk_tS = Walk_StepDur(1,:); tL = Walk_GCD(2,:);
else
    Walk_tS = Walk_StepDur(2,:); tL = Walk_GCD(1,:);
end

%% Calculating phi (degrees):
for i = 1:Walk_n-1
    Walk_phi(i) = 360*Walk_tS(i)/tL(i);
end

% figure (1);
% plot(Walk_phi,'MarkerSize',8,'Marker','o','LineStyle','none');%Create Plot
% ylim([90 270]); %Set Y-axis
% title('Normal Walking','FontSize',12,'FontName','Times New Roman');% Create
title
% xlabel('Stride Number','FontSize',12,'FontName','Times New Roman');% Create
xlabel
```

```
% ylabel('Stepping Phase','FontSize',12,'FontName','Times New Roman');%
Create ylabel
% hold on
% Xline = refline([0 180]);
% Xline.Color = 'r';
% Xline.LineWidth = 2
% % text(100,90,'PCI:'
Walk_phi_diff = abs(Walk_phi - 180); %Absolute difference of phi values
%% Calculate the Outcome Variables
%Mean value of absolute differences (degrees)
Walk_phi_abs = nanmean(Walk_phi_diff);
%Percentage-converted phi_ABS (%)
Walk_Pphi_abs = 100*Walk_phi_abs/180;
%Coefficient of variation of mean of phi (%)
Walk_phi_cv = (nanstd(Walk_phi)/nanmean(Walk_phi));
%Calculate PCI:
Walk_PCI = Walk_phi_cv + Walk_Pphi_abs;
%% Display the Outcomes
fprintf('Phase Coordination Index (PCI) for 2 minute normal walk:
%10.8f\n\n',Walk_PCI)
fprintf('ABS of PCI for 2 minute normal walk: %10.8f\n\n',Walk_Pphi_abs)
fprintf('CoV of PCI for 2 minute normal walk: %10.8f\n\n',Walk_phi_cv)
%% Write to Walk.csv
%PCI for the normal walking condition
fileID = fopen([ResultDirW,'Normal Walk PCI.csv'],'a+');
fprintf(fileID,'%s\n', Walk_PCI(:,1));
fclose(fileID);
%Percentage-converted phi_ABS (%)for the normal walking condition
fileID = fopen([ResultDirW,'Normal Walk Percent.csv'],'a+');
fprintf(fileID,'%s\n', Walk_Pphi_abs(:,1));
fclose(fileID);
%Coefficient of variation of mean of phi (%) for the normal walking
%condition
fileID = fopen([ResultDirW,'Normal Walk CoV.csv'],'a+');
fprintf(fileID,'%s\n', Walk_phi_cv(:,1));
fclose(fileID);
% [PCI(1),phi_cv(1),Pphi_abs(1)] = PCI_Function(data2min);
%
%
%
%% Load the testing condition: Dual Task Walking Trial
STR2 = [RootPath,'/dual.csv'];
DWdata = dlmread(STR2, ',',16, 5);
%% Raw data from data sheet:
%Gait Cycle Duration [s] [L;R]:
Dual_GCD = [DWdata(7,:);DWdata(8,:)];
%Step Duration [s] [L;R];
Dual_StepDur = [DWdata(24,:);DWdata(25,:)];
%Lower Limb Swing [%GCT] [L;R]:
Dual_SwingGCT = [DWdata(28,:);DWdata(29,:)]./100; %Convert to decimal form.
%% Calculating True Swing Time [s] [L;R]:
Dual_SwingT = Dual_GCD.*Dual_SwingGCT;

Dual_n = length(Dual_SwingT(1,1:end));

Dual_phi = zeros(1,Dual_n-1);

%Determining Short and Long Swing Times:
```

```
Dual_tLft = Dual_SwingT(1,:); %Left Swing Time
Dual_tRt = Dual_SwingT(2,:); %Right Swing Time

if mean(Dual_tLft) < mean(Dual_tRt)
    Dual_tS = Dual_StepDur(1,:); tL = Dual_GCD(2,:);
else
    Dual_tS = Dual_StepDur(2,:); tL = Dual_GCD(1,:);
end

%% Calculating phi (degrees):
for i = 1:Dual_n-1
    Dual_phi(i) = 360*Dual_tS(i)/tL(i);
end

Dual_phi_diff = abs(Dual_phi - 180); %Absolute difference of phi values
%% Calculate the Outcome Variables
%Mean value of absolute differences (degrees)
Dual_phi_abs = nanmean(Dual_phi_diff);
%Percentage-converted phi_ABS (%)
Dual_Pphi_abs = 100*Dual_phi_abs/180;
%Coefficient of variation of mean of phi (%)
Dual_phi_cv = (nanstd(Dual_phi)/nanmean(Dual_phi));
%Calculate PCI:
Dual_PCI = Dual_phi_cv + Dual_Pphi_abs;
%% Display the Outcomes
fprintf('Phase Coordination Index (PCI) for 2 minute dual-task walk:
%10.8f\n\n',Dual_PCI)
fprintf('ABS of PCI for 2 minute dual-task walk: %10.8f\n\n',Dual_Pphi_abs)
fprintf('CoV of PCI for 2 minute dual-task walk: %10.8f\n\n',Dual_phi_cv)
%% Write to Walk.csv
%PCI for the dual-task walking condition
fileID = fopen([ResultDirD,'Dual Task Walk PCI.csv'],'a+');
fprintf(fileID,'%s\n', Dual_PCI(:,1));
fclose(fileID);
%Percentage-converted phi_ABS (%)for the dual-task walking condition
fileID = fopen([ResultDirD,'Dual Task Walk Percent.csv'],'a+');
fprintf(fileID,'%s\n', Dual_Pphi_abs(:,1));
fclose(fileID);
%Coefficient of variation of mean of phi (%) for the dual-task walking
%condition
fileID = fopen([ResultDirD,'Dual Task Walk CoV.csv'],'a+');
fprintf(fileID,'%s\n', Dual_phi_cv(:,1));
fclose(fileID);
% [PCI(2),phi_cv(2),Pphi_abs(2)] = PCI_Function(data2min_1);
%
%
%
%% Load the testing condition: Fast Walking Trial
STR3 = [RootPath,'/fast.csv'];
FWdata = dlmread(STR3, ',',16, 5);
%% Raw data from data sheet:
%Gait Cycle Duration [s] [L;R]:
Fast_GCD = [FWdata(7,:);FWdata(8,:)];
%Step Duration [s] [L;R];
Fast_StepDur = [FWdata(24,:);FWdata(25,:)];
%Lower Limb Swing [%GCT] [L;R]:
Fast_SwingGCT = [FWdata(28,:);FWdata(29,:)]./100; %Convert to decimal form.
%% Calculating True Swing Time [s] [L;R]:
```

```
Fast_SwingT = Fast_GCD.*Fast_SwingGCT;

Fast_n = length(Fast_SwingT(1,1:end));

Fast_phi = zeros(1,Fast_n-1);

%Determining Short and Long Swing Times:
Fast_tLft = Fast_SwingT(1,:); %Left Swing Time
Fast_tRt = Fast_SwingT(2,:); %Right Swing Time

if mean(Fast_tLft) < mean(Fast_tRt)
    Fast_tS = Fast_StepDur(1,:); tL = Fast_GCD(2,:);
else
    Fast_tS = Fast_StepDur(2,:); tL = Fast_GCD(1,:);
end

%% Calculating phi (degrees):
for i = 1:Fast_n-1
    Fast_phi(i) = 360*Fast_tS(i)/tL(i);
end
Fast_phi_diff = abs(Fast_phi - 180); %Absolute difference of phi values
%% Calculate the Outcome Variables
%Mean value of absolute differences (degrees)
Fast_phi_abs = nanmean(Fast_phi_diff);
%Percentage-converted phi_ABS (%)
Fast_Pphi_abs = 100*Fast_phi_abs/180;
%Coefficient of variation of mean of phi (%)
Fast_phi_cv = (nanstd(Fast_phi)/nanmean(Fast_phi));
%Calculate PCI:
Fast_PCI = Fast_phi_cv + Fast_Pphi_abs;
%% Input the participant number for future refereence
SN = input('Enter 3 digit subject number: ', 's');
subnum = str2num(SN);
%% Display the Outcomes
fprintf('Phase Coordination Index (PCI) for 2 minute fast walk:
%10.8f\n\n',Fast_PCI)
fprintf('ABS of PCI for 2 minute fast walk: %10.8f\n\n',Fast_Pphi_abs)
fprintf('CoV of PCI for 2 minute fast walk: %10.8f\n\n',Fast_phi_cv)
%% Write to Walk.csv
%Participant number
fileID = fopen([ResultDirS,'SubjectNumber.csv'],'a+');
fprintf(fileID,'%d\n', subnum(:,1));
fclose(fileID);
%PCI for the fast walking condition
fileID = fopen([ResultDirF,'Fast Walk PCI.csv'],'a+');
fprintf(fileID,'%s\n', Fast_PCI(:,1));
fclose(fileID);
%Percentage-converted phi_ABS (%)for the fast walking condition
fileID = fopen([ResultDirF,'Fast Walk Percent.csv'],'a+');
fprintf(fileID,'%s\n', Fast_Pphi_abs(:,1));
fclose(fileID);
%Coefficient of variation of mean of phi (%) for the fast walking
%condition
fileID = fopen([ResultDirF,'Fast Walk CoV.csv'],'a+');
fprintf(fileID,'%s\n', Fast_phi_cv(:,1));
fclose(fileID);
% [PCI(3),phi_cv(3),Pphi_abs(3)] = PCI_Function(data2min_2);
```

```
%
%
cd(PATH)
%% Create a plot for the PCI
PCIplot = figure (1);
subplot(3,1,1);
plot(Walk_phi,'MarkerSize',8,'Marker','o','LineStyle','none');%Create Plot
ylim([90 270]); %Set Y-axis
title('Self-Selected Pace Walking','FontSize',12,'FontName','Times New
Roman');% Create title
xlabel('Stride Number','FontSize',12,'FontName','Times New Roman');% Create
xlabel
ylabel('Stepping Phase','FontSize',12,'FontName','Times New Roman');% Create
ylabel
hold on
Xline = refline([0 180]);
Xline.Color = 'r';
Xline.LineWidth = 2;
WPCI = num2str(Walk_PCI);
text(2.5,100,['PCI = ' WPCI]);
%Create Plot
subplot(3,1,2);
plot(Dual_phi,'MarkerSize',8,'Marker','o','LineStyle','none');
ylim([90 270]); %Set Y-axis
title('Dual-Task Walking','FontSize',12,'FontName','Times New Roman');%
Create title
xlabel('Stride Number','FontSize',12,'FontName','Times New Roman');% Create
xlabel
ylabel('Stepping Phase','FontSize',12,'FontName','Times New Roman');% Create
ylabel
hold on
Xline = refline([0 180]);
Xline.Color = 'r';
Xline.LineWidth = 2;
DPCI = num2str(Dual_PCI);
text(2.5,100,['PCI = ' DPCI]);
%Create Plot
subplot(3,1,3);
plot(Fast_phi,'MarkerSize',8,'Marker','o','LineStyle','none');%Create Plot
ylim([90 270]); %Set Y-axis
title('Fast Paced Walking','FontSize',12,'FontName','Times New Roman');%
Create title
xlabel('Stride Number','FontSize',12,'FontName','Times New Roman');% Create
xlabel
ylabel('Stepping Phase','FontSize',12,'FontName','Times New Roman');% Create
ylabel
hold on
Xline = refline([0 180]);
Xline.Color = 'r';
Xline.LineWidth = 2;
FPCI = num2str(Fast_PCI);
text(2.5,100,['PCI = ' FPCI]);
%Save figure...
PlotSaved = SN;
savefig(PCIplot,[PCIplotFolder,PlotSaved]);
    % PlotSaved = input('Enter the subject ID (example: 001):','s');
    % savefig(PCIplot,[PCIplotFolder,PlotSaved]);
%% Return to the main folder (cd)
```

```
cd(GoBack)
%% END of SCRIPT Step 1
%************************************************************************
%************************************************************************
%************************************************************************
```

Step 2: Phase Coordination Index Write Script

```
% Script Information
    % Originating Author:  Sutton B. Richmond, MS
    % Last updated: 10/05/18
% This script will allow you to compile the PCI metrics for each walking
% conditions for the MRS Dissertation Project.

%Additional Functions .m files REQUIRED to be in the path:
% 1.)csvwrite_with_headers

%REMEMBER: BEFORE running this script you should have ran each participant
%through the PCI Calculations script FIRST.

%% Set the retrieval path/directory
PATH = pwd
SN_PATH  = [PATH '/PCIresults/SUBnumber'];
NW_PATH  = [PATH '/PCIresults/NORMALwalk'];
DW_PATH  = [PATH '/PCIresults/DUALwalk'];
FW_PATH  = [PATH '/PCIresults/FASTwalk'];
addpath(SN_PATH);
addpath(NW_PATH);
addpath(DW_PATH);
addpath(FW_PATH);
%% Set the headers for the .csv file
headers = {'Participant Number','Normal PCI','Dual Task PCI','Fast
PCI','Normal CoV','Dual Task CoV','Fast CoV','Normal Pphi','Dual Task
Pphi','Fast Pphi'}
%% Compile the data
csv1 = csvread('SubjectNumber.csv');
csv2 = csvread('Normal Walk PCI.csv');
csv3 = csvread('Dual Task Walk PCI.csv');
csv4 = csvread('Fast Walk PCI.csv');
csv5 = csvread('Normal Walk CoV.csv');
csv6 = csvread('Dual Task Walk CoV.csv');
csv7 = csvread('Fast Walk CoV.csv');
csv8 = csvread('Normal Walk Percent.csv');
csv9 = csvread('Dual Task Walk Percent.csv');
csv10 = csvread('Fast Walk Percent.csv');

AllCsv1 = [csv1,csv2,csv3,csv4,csv5,csv6,csv7,csv8,csv9,csv10]; % Concatenate
vertically
csvwrite_with_headers ('Phase Coordination Index
Metrics.csv',AllCsv1,headers);
%% END of SCRIPT Step 2
%************************************************************************
%************************************************************************
%************************************************************************
```

Step 1: BTrackS File Converter

```
%% BTrackS automated converter for data files:.txt to .csv files
 %Script Author: Sutton Richmond, MS
 %Last Revised Date: 02/11/2020
 %Coded for MAC use

%This will open a dialog box to choose your directory (your folder) where
%the BTrackS data (.txt files) for your participant is stored.

%Additional Functions .m files REQUIRED to be in the path:
% 1.)txt2csv.m

GoBack = pwd
selpath = uigetdir(path)
cd(selpath)
%Converts the rigid surface with eyes open postural stabiity condition from
%a .txt to a .csv file.
data = importdata('rsEyesOpen.txt');
csvwrite('rsEyesOpen.csv',data.data);
%Converts the rigid surface with eyes closed postural stabiity condition
%from a .txt to a .csv file.
data = importdata('rsEyesClosed.txt');
csvwrite('rsEyesClosed.csv',data.data);
%Converts the compliant surface with eyes open postural stabiity condition
%from a .txt to a .csv file.
data = importdata('csEyesOpen.txt');
csvwrite('csEyesOpen.csv',data.data);
%Converts the compliant surface with eyes closed postural stabiity condition
%from a .txt to a .csv file.
data = importdata('csEyesClosed.txt');
csvwrite('csEyesClosed.csv',data.data);
cd(GoBack)
%% END of SCRIPT Step 1
%%%%%%%%%%%%%%%%%%%%%%%%%%%%%%%%%%%%%%%%%%%%%%%%%%%%%%%%%%%%%%%%%%%%%%%%%%%
%%%%%%%%%%%%%%%%%%%%%%%%%%%%%%%%%%%%%%%%%%%%%%%%%%%%%%%%%%%%%%%%%%%%%%%%%%%
%%%%%%%%%%%%%%%%%%%%%%%%%%%%%%%%%%%%%%%%%%%%%%%%%%%%%%%%%%%%%%%%%%%%%%%%%%%
```

Step 2: Time-To-Boundary Foot Parcellation

```
% Last Revised: 10/17/2018
% Script Authors: Sutton Richmond, MS & Tyler T. Whittier, MS

% Summary: This script imports an N x 4 matrix from an excel sheet with all
% participants foot measurements.  The first two columns are the dominant
% and non-dominant measurements from the MS group and the second 2 columns
% are the same from the control group.  Each participant takes up 2 rows
% with the length on the first row and width on the second as follows:

%        Column1                 Column2 .             Column3 .
Column 4
```

```
% Row 1:MS001 Dom. length   MS001 Non-dom. length    HC001 Dom. length
HC001 Non-dom. length
% Row 2:MS001 Dom. width    MS001 Non-dom. width     HC001 Dom.  width
HC001 Non-dom. width
% Row 3:MS002 Dom. length   MS002 Non-dom. length    HC002 Dom. length
HC002 Non-dom. length
% Row 4:MS002 Dom. width    MS002 Non-dom. width     HC002 Dom.  width
HC002 Non-dom. width
% etc.
% The specific measurements for each individual participant are exported as
% a .csv file into each participants folder

%% Start of Script: Step 1
%Clear command window and workspace
clear all
close all
clc
% Create a string with the filepath to the original excel file
PATH = pwd;
STR1 = [PATH '/Footmeasurements.xlsx'];
% Import data.  The specific range will depend on the sample size
DATA = xlsread(STR1, 'K:N');
%For each NaN value in the excel output--> Return in matrix a "0"
DATA(isnan(DATA))=0;
%Rotate the extracted data matrix
DOM = rot90(DATA(:,1:2));
N_DOM = rot90(DATA(:,3:4));
%Reshape the rotated matrix to fit the order needed.
DOM = reshape(DOM,[length(DOM(1,:))*2,1]);
N_DOM = reshape(N_DOM,[length(N_DOM(1,:))*2,1]);
%Place the reshaped data into DOMINATE and NON-DOMINATE columns for
%parcilation.
data(:,1) = DOM;
data(:,2) = N_DOM;
% Create a cell array of strings with each participants' identifier
for i = 1:9
    MRSTRINGS{i} = ['00' num2str(i)];
end
for i = 10:99
    MRSTRINGS{i} = ['0' num2str(i)];
end
%Identify where each participants measurements belong.
Start = [1:2:length(data)];
%Sort each participant into an individual cell in a cell array containing
%all participants measurements
for i = 1:length(Start)
    MS_dat{i} = data(Start(i):Start(i)+1,1:2);
end
%Export a .csv file with each individual participants' measurements into
%their specific folder.
for i = 1:length(Start)
    csvwrite([PATH '/' MRSTRINGS{i} '/FA.csv'], MS_dat{i})
end
%% END of SCRIPT Step 2
%************************************************************************
%************************************************************************
%************************************************************************
```

Step 3: Time-To-Boundary Calculations

```
 %Script Information

 %Clinical Exam: Modified Clinical Test of Sensory Interaction on Balance
 %(mCTSIB)
 %Project: Mahoney.Richmond.Study (MRS)
 %Script Authors: Sutton Richmond, MS & Kevin Dames, PhD
 %Last Revised Date: 06/19/2019
 %Coded for MAC use

 %Stability calculations originating authors and reference:

    %Hertel, J., & Olmsted-Kramer, L. C. (2007). Deficits in
        %time-to-boundary measures of postural control with chronic ankle
        %instability. Gait Posture, 25(1), 33-39.
        %doi:10.1016/j.gaitpost.2005.12.009

    %Script Equipment:Balance Tracking System (BTrackS)
    %Collection Parameters: Sampling rate: 25 Hz, Filtered: Lowpass
    %Butterworth filter at 4Hz (BTrackS Calculated)

%Additional Functions .m files REQUIRED to be in the path:
% 1.)deriv1.m

%Testing Procedure: Participant began in position (hands on the hips feet
%togeather (Dual Stance), looking straight ahead) on the plate and static
%stability was recorded for the duration of 30s for each mCTSIB testing
%condition. The participants remained on the plate for the entire duration
%of the trial.
    %mCTSIB testing condtion order (in order, in (4) seperate data files):
    %1. RO = Rigid Surface & Eyes Open
    %2. RC = Rigid Surface & Eyes Closed
    %3. CO = Compliant Surface & Eyes Open
    %4. CC = Compliant Surface & Eyes Closed
%Each BTrackS data file contains 30s (mCTSIB) of data in the
%comma-separated values format with 5 columns of data as follows:
    % Column 1: Time (sec)
    % Column 2: COPx (cm) filtered data
    % Column 3: COPy (cm) filtered data
    % Column 4: ufCOPx (cm) unfiltered data
    % Column 5: ufCOPy (cm) unfiltered data
%Foot Anthropometrics:The foot anthropometrics file should be placed in the
%same folder as the trial data; use the Footsorter.m script to divide
%everything up.

%% Start of Script: Step 2
%Clear command window and workspace
clc
clear all
close all
GoBack = pwd;
%% Set Frequency & Time to analyze
%Set the sampling frequency
Fs = 25;
dt = 1/Fs;
%% Select the Particpant & Load Data
```

```
    %Load the data from the prompted 3 digit subject number
    %Subject ID: C = Control subject or M = MS subject
    subnum = input('Enter 3 digit subject number: ', 's');
    %trial = input('Enter the trial type (RO, RC, CO or CC): ', 's');
    % root directory
    root_dir='/Volumes/SBR_CSU/Mobility/MRS_PS_Data/';
    %This string is the data file for the trials
    %Example for with trial input: STR1 =
[root_dir,subnum,'/rsEyesOpen',trial,'.csv'];
    STR1 = [root_dir,subnum,'/rsEyesOpen.csv'];
    STR2 = [root_dir,subnum,'/rsEyesClosed.csv'];
    STR3 = [root_dir,subnum,'/csEyesOpen.csv'];
    STR4 = [root_dir,subnum,'/csEyesClosed.csv'];
%Set the where the directory where the TTB plots will saved too.
TTBplotFolder1 =
'/Volumes/SBR_CSU/Mobility/MRS_PS_Data/TTBresults/TTBplots/Rigid_EO_Stabilogr
am/';
TTBplotFolder2 =
'/Volumes/SBR_CSU/Mobility/MRS_PS_Data/TTBresults/TTBplots/Rigid_EO_TTB_Plot/
';
TTBplotFolder3 =
'/Volumes/SBR_CSU/Mobility/MRS_PS_Data/TTBresults/TTBplots/Rigid_EC_Stabilogr
am/';
TTBplotFolder4 =
'/Volumes/SBR_CSU/Mobility/MRS_PS_Data/TTBresults/TTBplots/Rigid_EC_TTB_Plot/
';
TTBplotFolder5 =
'/Volumes/SBR_CSU/Mobility/MRS_PS_Data/TTBresults/TTBplots/Compliant_EO_Stabi
logram/';
TTBplotFolder6 =
'/Volumes/SBR_CSU/Mobility/MRS_PS_Data/TTBresults/TTBplots/Compliant_EO_TTB_P
lot/';
TTBplotFolder7 =
'/Volumes/SBR_CSU/Mobility/MRS_PS_Data/TTBresults/TTBplots/Compliant_EC_Stabi
logram/';
TTBplotFolder8 =
'/Volumes/SBR_CSU/Mobility/MRS_PS_Data/TTBresults/TTBplots/Compliant_EC_TTB_P
lot/';
%% Identification of the loaded data
% This section identifies if the data files exist in the directed folder
if exist(eval('STR1'),'file') == 2
    data1 = dlmread(STR1, ',',1, 0);
end
if exist(eval('STR2'),'file') == 2
    data2 = dlmread(STR2, ',',1, 0);
end
if exist(eval('STR3'),'file') == 2
    data3 = dlmread(STR3, ',',1, 0);
end
if exist(eval('STR4'),'file') == 2
    data4 = dlmread(STR4, ',',1, 0);
end
%% Foot anthropometrics
%This string is the data file for the foot anthropometrics
STR5= [root_dir,subnum,'/','FA.csv'];
%import data file containing feet anthropometrics
footdata=dlmread(STR5, ',',0,0);
%Define widths of the feet (D=dominant, ND=nondominant)
```

```
DWidth=footdata(2,1);
NDWidth=footdata(2,2);
DLength=footdata(1,1);
NDLength=footdata(1,2);
%% Initialize the designated Results Folders
%Identify where the data outputs will be stored
    ResultDirAP = '/Volumes/SBR_CSU/Mobility/MRS_PS_Data/TTBresults/AP/';
    ResultDirML = '/Volumes/SBR_CSU/Mobility/MRS_PS_Data/TTBresults/ML/';
    ResultDirRight =
'/Volumes/SBR_CSU/Mobility/MRS_PS_Data/TTBresults/Right/'
    ResultDirLeft = '/Volumes/SBR_CSU/Mobility/MRS_PS_Data/TTBresults/Left/'
    TTBstatsFolder
='/Volumes/SBR_CSU/Mobility/MRS_PS_Data/TTBresults/TTBstats/';
%% Initialize all outcome variables
%This section initializes all (48 of them) the output variables (adds them
%as blank sets) this allows the program to run fully, even if a condition
%(the data) is not present in the participant folder (i.e. they couldn't
%complete the condition).
TTBXROpeaks = [];
TTBXRCpeaks = [];
TTBXCOpeaks = [];
TTBXCCpeaks = [];
TTBXROpeaks_Right = [];
TTBXRCpeaks_Right = [];
TTBXCOpeaks_Right = [];
TTBXCCpeaks_Right = [];
TTBXROpeaks_Left = [];
TTBXRCpeaks_Left = [];
TTBXCOpeaks_Left = [];
TTBXCCpeaks_Left = [];
TTBYROpeaks = [];
TTBYRCpeaks = [];
TTBYCOpeaks = [];
TTBYCCpeaks = [];
TTBXaverageRO = [];
TTBXstdevRO = [];
TTBXaverageRC = [];
TTBXstdevRC = [];
TTBXaverageCO = [];
TTBXstdevCO = [];
TTBXaverageCC = [];
TTBXstdevCC = [];
TTBXaverageRO_Right = [];
TTBXstdevRO_Right = [];
TTBXaverageRC_Right = [];
TTBXstdevRC_Right = [];
TTBXaverageCO_Right = [];
TTBXstdevCO_Right = [];
TTBXaverageCC_Right = [];
TTBXstdevCC_Right = [];
TTBXaverageRO_Left = [];
TTBXstdevRO_Left = [];
TTBXaverageRC_Left = [];
TTBXstdevRC_Left = [];
TTBXaverageCO_Left = [];
TTBXstdevCO_Left = [];
TTBXaverageCC_Left = [];
TTBXstdevCC_Left = [];
```

```
TTBYaverageRO = [];
TTBYstdevRO = [];
TTBYaverageRC = [];
TTBYstdevRC = [];
TTBYaverageCO = [];
TTBYstdevCO = [];
TTBYaverageCC = [];
TTBYstdevCC = [];
%% Test Condition: mCTSIB: Rigid Surface & Eyes Open
%The if statement, initiaties the analysis of the section if data is
%present. If the data is not available, then the script will move on to the
%next condition analysis.
if exist('data1','var')== 1
    %Define borders of the feet. Wider of the two feet are used as the
    %length for TTB calculations. The width is the sum of the two feet.
    Width=DWidth+NDWidth;
    if DLength > NDLength;
        Length = DLength;
    else DLength < NDLength;
        Length = NDLength;
    end
    %Determine when the person steps onto the plate and wait five seconds
(125
    %samples) to start trial.

    %Segement out the X and Y data from the raw data; This data will include
    %the 30 sec of testing for the mCTSIB (when collecting at 25 Hz this will
    %be the next 750 frames)
    ROtrialxdata=data1(:,2);
    ROtrialydata=data1(:,3);
    %Define base of support for TTB reference based on anthropometrics. Set
the
    %borders of the feet relative to the center of the base of support. This
    %makes the centered stabiligram set in the center of the base of support
    %rectangle.
    %(1,1:2) = coordinate for left heel corner
    %(2,1:2) = coordinate for left heel toe corner
    %(3,1:2) = coordinate for right toe corner
    %(4,1:2) = coordinate for right heel corner
    edges=[Width*-.5 Length*-.5;
        Width*-.5 Length*.5;
        Width*.5 Length*.5;
        Width*.5 Length*-.5;
        Width*-.5 Length*-.5];
    %Center the stabilograms
    ROtrialxdata(:,1) = ROtrialxdata(:,1) - mean(ROtrialxdata(:,1));
    ROtrialydata(:,1) = ROtrialydata(:,1) - mean(ROtrialydata(:,1));
    %% Plot the stabiligram with borders identified.
    Stabilogram1 = figure(1)
    hold on
    plot(ROtrialxdata(:,1),ROtrialydata(:,1)), '-k';
    title('mCTSIB Stabiligram: Rigid Surface & Eyes Open');
    set(gca, 'FontSize', 18);
    xlabel('ML COP (cm)'); ylabel('AP COP (cm)');
    plot(edges(:,1), edges(:,2),'-k', 'LineWidth', 2);
    axis('square');
    hold off
    %Save figure 1...
```

```
PlotSaved = subnum;
savefig(Stabilogram1,[TTBplotFolder1,PlotSaved]);
%% Determine velocity of the COP in ML and AP directions
[copxvelRO]=deriv1(ROtrialxdata,dt);
[copyvelRO]=deriv1(ROtrialydata,dt);
%create vector for allocating distances between COP and boundary edge. A
%positive X means lateral movement and positive Y indicates anterior
%movement.
xboundarydistanceRO = [ ];
yboundarydistanceRO = [ ];
xboundarydistanceRO_Right = [ ];
xboundarydistanceRO_Left = [ ];
copxvelRO_Right = [ ];
copxvelRO_Left = [ ];
%Subtract right edge from laterally moving (+ velocity) COP and subtract
%position of left edge from medially moving (- velocity) COP
for i=1:length(ROtrialxdata);
    if copxvelRO(i) >= 0;
        xboundarydistanceRO(i) = edges(3,1) - ROtrialxdata(i);
        xboundarydistanceRO_Right(i) = edges(3,1) - ROtrialxdata(i);
        if copxvelRO(i) > 0
            copxvelRO_Right(i,1) = copxvelRO(i);
        else copxvelRO_Right(i,1) = inf;
        end
    else
        xboundarydistanceRO(i) = ROtrialxdata(i) - edges(1,1);
        xboundarydistanceRO_Left(i) = edges(3,1) - ROtrialxdata(i);
        copxvelRO_Left(i,1) = copxvelRO(i);
    end
end
xboundarydistanceRO_Right(xboundarydistanceRO_Right==0) = [];
xboundarydistanceRO_Left(xboundarydistanceRO_Left==0) = [];
copxvelRO_Right(copxvelRO_Right == 0) = [];
copxvelRO_Left(copxvelRO_Left == 0) = [];
for i = 1:length(copxvelRO_Right)
    if copxvelRO_Right(i) == Inf
        copxvelRO_Right(i) = 0;
    end
end
%Subtract toe edge from laterally moving (+ velocity) COP and subtract
%position of heel edge from medially moving (- velocity) COP
for i=1:length(ROtrialydata);
    if copyvelRO(i) >= 0;
        yboundarydistanceRO(i) = edges(2,2) - ROtrialydata(i);
    else
        yboundarydistanceRO(i) = ROtrialydata(i) - edges(1,2);
    end
end

TTBXRO = abs(xboundarydistanceRO'./copxvelRO);
TTBXRO_Right = abs(xboundarydistanceRO_Right'./copxvelRO_Right);
TTBXRO_Left = abs(xboundarydistanceRO_Left'./copxvelRO_Left);
TTBYRO = abs(yboundarydistanceRO'./copyvelRO);
%% Create a time vector for plotting the ML/AP TTBs
time_RO=1:length(TTBXRO);
time_RO=time_RO';
%Time for right TTB
time_RO_Right=1:length(TTBXRO_Right);
```

```
    time_RO_Right=time_RO_Right';
    %Time for left TTB
    time_RO_Left=1:length(TTBXRO_Left);
    time_RO_Left=time_RO_Left';
    %Find local minima (valleys) by first multiplying both series by -1 and
use
    %the findpeaks function to get the time index of these peaks. Then
rectify
    %the signal to convert back to valleys. Convert from time to sample of
the
    %peaks by multiplying the time index by sampling rate (25 Hz).
    %Findpeaks commands:
    %These can be used individually or in combination to achieve desired
    %results.
    %MinPeakHeight: minimum value needed to be considered a "peak". This
    %can be positive or negative.
    %Threshold: minimum difference in magnitude between two possible peaks
    %to consider a second value a peak. This must be a positive integer.
    %MinPeakDistance: minimum separation in time between a peak and
    %surrounding potential peaks. This searches from largest magnitude
    %first and continues until no more peaks are available.
    %Flip to negative values so valleys become peaks.
    TTBXRO=TTBXRO*-1;
    TTBXRO_Right=TTBXRO_Right*-1;
    TTBXRO_Left=TTBXRO_Left*-1;
    %find the peaks
    [TTBXROpeaks,TTBXROlocs]=findpeaks(TTBXRO,Fs);
    [TTBXROpeaks_Right,TTBXROlocs_Right]=findpeaks(TTBXRO_Right,Fs);
    [TTBXROpeaks_Left,TTBXROlocs_Left]=findpeaks(TTBXRO_Left,Fs);
    %Flip back to positive numbers for array of times.
    TTBXRO=TTBXRO*-1;
    TTBXRO_Right=TTBXRO_Right*-1;
    TTBXRO_Left=TTBXRO_Left*-1;
    %Flip peak values also to positive numbers
    TTBXROpeaks=TTBXROpeaks*-1;
    TTBXROpeaks_Right=TTBXROpeaks_Right*-1;
    TTBXROpeaks_Left=TTBXROpeaks_Left*-1;
    %Convert from sample number to time by multiplying time index of peaks by
    %sampling frequency.
    TTBXROlocs=TTBXROlocs*25;
    TTBXROlocs_Right=TTBXROlocs_Right*25;
    TTBXROlocs_Left=TTBXROlocs_Left*25;
    %Duplicate above steps for the anterior-posterior data
    TTBYRO=TTBYRO*-1;
    [TTBYROpeaks,TTBYROlocs]=findpeaks(TTBYRO,Fs);
    TTBYRO=TTBYRO.*-1;
    TTBYROpeaks=TTBYROpeaks.*-1;
    TTBYROlocs=TTBYROlocs*25;
    %Calculate average, standard deviation, and 2X the standard deviation of
    %the time to boundary sequence for mediolateral COP
    TTBXaverageRO=mean(TTBXROpeaks);
    TTBXstdevRO=std(TTBXROpeaks);
    TTBXthresholdRO=TTBXaverageRO + 2*TTBXstdevRO;
    TTBXaverageRO_Right=mean(TTBXROpeaks_Right);
    TTBXstdevRO_Right=std(TTBXROpeaks_Right);
    TTBXthresholdRO_Right=TTBXaverageRO_Right + 2*TTBXstdevRO_Right;
    TTBXaverageRO_Left=mean(TTBXROpeaks_Left);
    TTBXstdevRO_Left=std(TTBXROpeaks_Left);
```

```
    TTBXthresholdRO_Left=TTBXaverageRO_Left + 2*TTBXstdevRO_Left;
    %Calculate average, standard deviation, and 2X the standard deviation of
    %the time to boundary sequence for anterior-posterior COP
    TTBYaverageRO=mean(TTBYROpeaks);
    TTBYstdevRO=std(TTBYROpeaks);
    TTBYthresholdRO=TTBYaverageRO + 2*TTBYstdevRO;
    %Create vector of maximum peak height that warrants a TTB minimum.
    TTBXthresholdlineRO(1:length(time_RO),1)=TTBXthresholdRO;

TTBXthresholdlineRO_Right(1:length(time_RO_Right),1)=TTBXthresholdRO_Right;
    TTBXthresholdlineRO_Left(1:length(time_RO_Left),1)=TTBXthresholdRO_Left;
    TTBYthresholdlineRO(1:length(time_RO),1)=TTBYthresholdRO;
    %Plot TTBs for AP and ML series and label the local minima where the
    %minimum TTB occurs. Plot the threshold as a black dashed line across the
figures.
    TTBplot1 = figure(2)
    subplot(2,1,1);plot(time_RO, TTBYthresholdlineRO, '--k',time_RO,TTBYRO,'-
k', TTBYROlocs,TTBYROpeaks, 'xr','MarkerSize',12);
    title('mCTSIB: Rigid Surface & Eyes Open');
    ylabel('AP Time to Boundary (s)');
    text(TTBYROlocs,TTBYROpeaks,num2str((1:numel(TTBYROpeaks))'));
    legend('+2 SD of average TTB Events', 'TTB', 'Min TTB');
    set(gca,'FontSize', 18);
    subplot(2,1,2);plot(time_RO, TTBXthresholdlineRO, '--k',time_RO,TTBXRO,
'-k', TTBXROlocs,TTBXROpeaks, 'xr','MarkerSize',12);
    text(TTBXROlocs,TTBXROpeaks,num2str((1:numel(TTBXROpeaks))'));
    ylabel('ML Time to Boundary (s)');
    xlabel('Sample');
    legend('+2 SD of average TTB Events', 'TTB', 'Min TTB');
    set(gca,'FontSize', 18);
    %Save TTB figure1...
    PlotSaved = subnum;
    savefig(TTBplot1,[TTBplotFolder2,PlotSaved]);

    %Since the data series are all different lengths these are written out as
    %separate data files by trial and ML/AP directions. Each of these files
    %contains two columns: Column 1 = location (sample #, Fs = 25 Hz) of the
    %TTB event and column two is the value of the TTB in seconds.

    %ML Outputs
    fname = [ResultDirML,'/',subnum,'_ML_RO_mCTSIB.csv'];
    RO_mCTSIB_ML = [TTBXROlocs TTBXROpeaks];
    writefile(fname,RO_mCTSIB_ML);
        fname = [ResultDirRight,'/',subnum,'_ML_RO_mCTSIB_Right.csv'];
        RO_mCTSIB_ML_Right = [TTBXROlocs_Right TTBXROpeaks_Right];
        writefile(fname,RO_mCTSIB_ML_Right);
            fname = [ResultDirLeft,'/',subnum,'_ML_RO_mCTSIB_Left.csv'];
            RO_mCTSIB_ML_Left = [TTBXROlocs_Left TTBXROpeaks_Left];
            writefile(fname,RO_mCTSIB_ML_Left);
    %AP Outputs
    fname = [ResultDirAP,'/',subnum,'_AP_RO_mCTSIB.csv'];
    RO_mCTSIB_AP = [TTBYROlocs TTBYROpeaks];
    writefile(fname,RO_mCTSIB_AP);
end
%END processing of mCTSIB: Rigid Surface & Eyes Open condition

%% Test Condition: mCTSIB: Rigid Surface & Eyes Closed
if exist('data2','var')== 1
```

```
    %Segement out the X and Y data from the raw data; This data will include
    %the 30 sec of testing for the mBESS (when collecting at 25 Hz this will
    %be the next 750 frames)
    RCtrialxdata=data2(:,2);
    RCtrialydata=data2(:,3);
    %Center the stabilograms
    RCtrialxdata(:,1) = RCtrialxdata(:,1) - mean(RCtrialxdata(:,1));
    RCtrialydata(:,1) = RCtrialydata(:,1) - mean(RCtrialydata(:,1));
    %% Plot the base of support and stabiligram
    Stabilogram2 = figure(3)
    hold on
    plot(RCtrialxdata(:,1),RCtrialydata(:,1)), '-k';
    title('mCTSIB Stabiligram: Rigid Surface & Eyes Closed');
    set(gca, 'FontSize', 18);
    xlabel('ML COP (cm)'); ylabel('AP COP (cm)');
    plot(edges(:,1), edges(:,2),'-k', 'LineWidth', 2);
    axis('square');
    hold off
    %Save figure...
    PlotSaved = subnum;
    savefig(Stabilogram2,[TTBplotFolder3,PlotSaved]);
    %% Calculate distances between position of COP and the boundary the COP
is
    %approaching. Calculate the velocity during the interval and divide the
    %distance to the border by the velocity of approach to get the TTB. This
    %portion is the mediolateral direction.
    %determine velocity of the COP in ML and AP directions
    [copxvelRC]=deriv1(RCtrialxdata,dt);
    [copyvelRC]=deriv1(RCtrialydata,dt);
    %create vector for allocating distances between COP and boundary edge. A
    %positive X means lateral movement and positive Y indicates anterior
    %movement.
    xboundarydistanceRC = [ ];
    yboundarydistanceRC = [ ];
    xboundarydistanceRC_Right = [ ];
    xboundarydistanceRC_Left = [ ];
    copxvelRC_Right = [ ];
    copxvelRC_Left = [ ];
    %Subtract right edge from laterally moving (+ velocity) COP and subtract
    %position of left edge from medially moving (- velocity) COP
    for i=1:length(RCtrialxdata);
        if copxvelRC(i) >= 0;
            xboundarydistanceRC(i) = edges(3,1) - RCtrialxdata(i);
            xboundarydistanceRC_Right(i) = edges(3,1) - RCtrialxdata(i);
            if copxvelRC(i) > 0
                copxvelRC_Right(i,1) = copxvelRC(i);
            else copxvelRC_Right(i,1) = inf;
            end
        else
            xboundarydistanceRC(i) = RCtrialxdata(i) - edges(1,1);
            xboundarydistanceRC_Left(i) = edges(3,1) - RCtrialxdata(i);
            copxvelRC_Left(i,1) = copxvelRC(i);
        end
    end
    xboundarydistanceRC_Right(xboundarydistanceRC_Right==0) = [];
    xboundarydistanceRC_Left(xboundarydistanceRC_Left==0) = [];
    copxvelRC_Right(copxvelRC_Right == 0) = [];
    copxvelRC_Left(copxvelRC_Left == 0) = [];
```

```
    for i = 1:length(copxvelRC_Right)
        if copxvelRC_Right(i) == Inf
            copxvelRC_Right(i) = 0;
        end
    end
    %Subtract toe edge from laterally moving (+ velocity) COP and subtract
    %position of heel edge from medially moving (- velocity) COP
    for i=1:length(RCtrialydata);
        if copyvelRC(i) >= 0;
            yboundarydistanceRC(i) = edges(2,2) - RCtrialydata(i);
        else
            yboundarydistanceRC(i) = RCtrialydata(i) - edges(1,2);
        end
    end

    TTBXRC = abs(xboundarydistanceRC'./copxvelRC);
    TTBXRC_Right = abs(xboundarydistanceRC_Right'./copxvelRC_Right);
    TTBXRC_Left = abs(xboundarydistanceRC_Left'./copxvelRC_Left);
    TTBYRC = abs(yboundarydistanceRC'./copyvelRC);
    %% Create a time vector for plotting the ML/AP TTBs
    time_RC=1:length(TTBXRC);
    time_RC=time_RC';
    %Time for right TTB
    time_RC_Right=1:length(TTBXRC_Right);
    time_RC_Right=time_RC_Right';
    %Time for left TTB
    time_RC_Left=1:length(TTBXRC_Left);
    time_RC_Left=time_RC_Left';
    %Find local minima (valleys) by first multiplying both series by -1 and
use
    %the findpeaks function to get the time index of these peaks. Then
rectify
    %the signal to convert back to valleys. Convert from time to sample of
the
    %peaks by multiplying the time index by sampling rate (25 Hz).
    %Findpeaks commands:
    %These can be used individually or in combination to achieve desired
    %results.
        %MinPeakHeight: minimum value needed to be considered a "peak". This
        %can be positive or negative.
        %Threshold: minimum difference in magnitude between two possible
peaks
        %to consider a second value a peak. This must be a positive integer.
        %MinPeakDistance: minimum separation in time between a peak and
        %surrounding potential peaks. This searches from largest magnitude
        %first and continues until no more peaks are available.
    %Flip to negative values so valleys become peaks.
    TTBXRC=TTBXRC*-1;
    TTBXRC_Right=TTBXRC_Right*-1;
    TTBXRC_Left=TTBXRC_Left*-1;
    %find the peaks
    [TTBXRCpeaks,TTBXRClocs]=findpeaks(TTBXRC,Fs);
    [TTBXRCpeaks_Right,TTBXRClocs_Right]=findpeaks(TTBXRC_Right,Fs);
    [TTBXRCpeaks_Left,TTBXRClocs_Left]=findpeaks(TTBXRC_Left,Fs);
    %Flip back to positive numbers for array of times.
    TTBXRC=TTBXRC*-1;
    TTBXRC_Right=TTBXRC_Right*-1;
    TTBXRC_Left=TTBXRC_Left*-1;
```

```
    %Flip peak values also to positive numbers
    TTBXRCpeaks=TTBXRCpeaks*-1;
    TTBXRCpeaks_Right=TTBXRCpeaks_Right*-1;
    TTBXRCpeaks_Left=TTBXRCpeaks_Left*-1;
    %Convert from sample number to time by multiplying time index of peaks by
    %sampling frequency.
    TTBXRClocs=TTBXRClocs*25;
    TTBXRClocs_Right=TTBXRClocs_Right*25;
    TTBXRClocs_Left=TTBXRClocs_Left*25;
    %Duplicate above steps for the anterior-posterior data
    TTBYRC=TTBYRC*-1;
    [TTBYRCpeaks,TTBYRClocs]=findpeaks(TTBYRC,Fs);
    TTBYRC=TTBYRC.*-1;
    TTBYRCpeaks=TTBYRCpeaks.*-1;
    TTBYRClocs=TTBYRClocs*25;
    %Calculate average, standard deviation, and 2X the standard deviation of
    %the time to boundary sequence for mediolateral COP
    TTBXaverageRC=mean(TTBXRCpeaks);
    TTBXstdevRC=std(TTBXRCpeaks);
    TTBXthresholdRC=TTBXaverageRC + 2*TTBXstdevRC;
        TTBXaverageRC_Right=mean(TTBXRCpeaks_Right);
        TTBXstdevRC_Right=std(TTBXRCpeaks_Right);
        TTBXthresholdRC_Right=TTBXaverageRC_Right + 2*TTBXstdevRC_Right;
            TTBXaverageRC_Left=mean(TTBXRCpeaks_Left);
            TTBXstdevRC_Left=std(TTBXRCpeaks_Left);
            TTBXthresholdRC_Left=TTBXaverageRC_Left + 2*TTBXstdevRC_Left;
    %Calculate average, standard deviation, and 2X the standard deviation of
    %the time to boundary sequence for anterior-posterior COP
    TTBYaverageRC=mean(TTBYRCpeaks);
    TTBYstdevRC=std(TTBYRCpeaks);
    TTBYthresholdRC=TTBYaverageRC + 2*TTBYstdevRC;
    %Create vector of maximum peak height that warrants a TTB minimum.
    TTBXthresholdlineRC(1:length(time_RC),1)=TTBXthresholdRC;

TTBXthresholdlineRC_Right(1:length(time_RC_Right),1)=TTBXthresholdRC_Right;

TTBXthresholdlineRC_Left(1:length(time_RC_Left),1)=TTBXthresholdRC_Left;
    TTBYthresholdlineRC(1:length(time_RC),1)=TTBYthresholdRC;

    %Plot TTBs for AP and ML series and label the local minima where the
    %minimum TTB occurs
    TTBplot2 = figure(4)
    subplot(2,1,1);plot(time_RC, TTBYthresholdlineRC, '--k',time_RC,TTBYRC,
'-k', TTBYRClocs,TTBYRCpeaks, 'xr','MarkerSize',12);
    ylabel('AP Time to Boundary (s)');
    title('mCTSIB: Rigid Surface & Eyes Closed');
    text(TTBYRClocs,TTBYRCpeaks,num2str((1:numel(TTBYRCpeaks))'));
    legend('+2 SD of average TTB Events', 'TTB', 'Min TTB');
    set(gca,'FontSize', 18);
    subplot(2,1,2);plot(time_RC, TTBXthresholdlineRC, '--k',time_RC,TTBXRC,
'-k', TTBXRClocs,TTBXRCpeaks, 'xr','MarkerSize',12);
    text(TTBXRClocs,TTBXRCpeaks,num2str((1:numel(TTBXRCpeaks))'));
    ylabel('ML Time to Boundary (s)');
    xlabel('Sample');
    legend('+2 SD of average TTB Events', 'TTB', 'Min TTB');
    set(gca,'FontSize', 18);
    %Save figure...
    PlotSaved = subnum;
```

```
    savefig(TTBplot2,[TTBplotFolder4,PlotSaved]);

    %ML Outputs
    fname = [ResultDirML,'/',subnum,'_ML_RC_mCTSIB.csv'];
    RC_mCTSIB_ML = [TTBXRClocs TTBXRCpeaks];
    writefile(fname,RC_mCTSIB_ML);
        fname = [ResultDirRight,'/',subnum,'_ML_RC_mCTSIB_Right.csv'];
        RC_mCTSIB_ML_Right = [TTBXRClocs_Right TTBXRCpeaks_Right];
        writefile(fname,RC_mCTSIB_ML_Right);
            fname = [ResultDirLeft,'/',subnum,'_ML_RC_mCTSIB_Left.csv'];
            RC_mCTSIB_ML_Left = [TTBXRClocs_Left TTBXRCpeaks_Left];
            writefile(fname,RC_mCTSIB_ML_Left);
    %AP Outputs
    fname = [ResultDirAP,'/',subnum,'_AP_RC_mCTSIB.csv'];
    RC_mCTSIB_AP = [TTBYRClocs TTBYRCpeaks];
    writefile(fname,RC_mCTSIB_AP);
end
%% END processing of mCTSIB: Rigid Surface & Eyes Closed condition
%% Test Condition: mCTSIB: Compliant Surface & Eyes Open
if exist('data3','var')== 1
    %Segement out the X and Y data from the raw data; This data will include
    %the 30 sec of testing for the mBESS (when collecting at 25 Hz this will
    %be the next 750 frames)
    COtrialxdata=data3(:,2);
    COtrialydata=data3(:,3);
    %Center the stabilograms
    COtrialxdata(:,1) = COtrialxdata(:,1) - mean(COtrialxdata(:,1));
    COtrialydata(:,1) = COtrialydata(:,1) - mean(COtrialydata(:,1));
    %% Plot the base of support and stabiligram
    Stabilogram3 = figure(5)
    hold on
    plot(COtrialxdata(:,1),COtrialydata(:,1)), '-k';
    title('mCTSIB Stabiligram: Compliant Surface & Eyes Open');
    set(gca, 'FontSize', 18);
    xlabel('ML COP (cm)'); ylabel('AP COP (cm)');
    plot(edges(:,1), edges(:,2),'-k', 'LineWidth', 2);
    axis('square');
    hold off
    %Save figure...
    PlotSaved = subnum;
    savefig(Stabilogram3,[TTBplotFolder5,PlotSaved]);
    %% Calculate distances between position of COP and the boundary the COP
is
    %approaching. Calculate the velocity during the interval and divide the
    %distance to the border by the velocity of approach to get the TTB. This
    %portion is the mediolateral direction.
    %determine velocity of the COP in ML and AP directions
    [copxvelCO]=deriv1(COtrialxdata,dt);
    [copyvelCO]=deriv1(COtrialydata,dt);
    %create vector for allocating distances between COP and boundary edge. A
    %positive X means lateral movement and positive Y indicates anterior
    %movement.
    xboundarydistanceCO = [ ];
    yboundarydistanceCO = [ ];
    xboundarydistanceCO_Right = [ ];
    xboundarydistanceCO_Left = [ ];
    copxvelCO_Right = [ ];
    copxvelCO_Left = [ ];
```

```
    %Subtract right edge from laterally moving (+ velocity) COP and subtract
    %position of left edge from medially moving (- velocity) COP
    for i=1:length(COtrialxdata);
        if copxvelCO(i) >= 0;
            xboundarydistanceCO(i) = edges(3,1) - COtrialxdata(i);
            xboundarydistanceCO_Right(i) = edges(3,1) - COtrialxdata(i);
            if copxvelCO(i) > 0
                copxvelCO_Right(i,1) = copxvelCO(i);
            else copxvelCO_Right(i,1) = inf;
            end
        else
            xboundarydistanceCO(i) = COtrialxdata(i) - edges(1,1);
            xboundarydistanceCO_Left(i) = edges(3,1) - COtrialxdata(i);
            copxvelCO_Left(i,1) = copxvelCO(i);
        end
    end
    xboundarydistanceCO_Right(xboundarydistanceCO_Right==0) = [];
    xboundarydistanceCO_Left(xboundarydistanceCO_Left==0) = [];
    copxvelCO_Right(copxvelCO_Right == 0) = [];
    copxvelCO_Left(copxvelCO_Left == 0) = [];
    for i = 1:length(copxvelCO_Right)
        if copxvelCO_Right(i) == Inf
            copxvelCO_Right(i) = 0;
        end
    end
    %Subtract toe edge from laterally moving (+ velocity) COP and subtract
    %position of heel edge from medially moving (- velocity) COP
    for i=1:length(COtrialydata);
        if copyvelCO(i) >= 0;
            yboundarydistanceCO(i) = edges(2,2) - COtrialydata(i);
        else
            yboundarydistanceCO(i) = COtrialydata(i) - edges(1,2);
        end
    end

    TTBXCO = abs(xboundarydistanceCO'./copxvelCO);
    TTBXCO_Right = abs(xboundarydistanceCO_Right'./copxvelCO_Right);
    TTBXCO_Left = abs(xboundarydistanceCO_Left'./copxvelCO_Left);
    TTBYCO = abs(yboundarydistanceCO'./copyvelCO);
    %% Create a time vector for plotting the ML/AP TTBs
    time_CO=1:length(TTBXCO);
    time_CO=time_CO';
    %Time for right TTB
    time_CO_Right=1:length(TTBXCO_Right);
    time_CO_Right=time_CO_Right';
    %Time for left TTB
    time_CO_Left=1:length(TTBXCO_Left);
    time_CO_Left=time_CO_Left';
    %Find local minima (valleys) by first multiplying both series by -1 and
use
    %the findpeaks function to get the time index of these peaks. Then
rectify
    %the signal to convert back to valleys. Convert from time to sample of
the
    %peaks by multiplying the time index by sampling rate (25 Hz).
    %Findpeaks commands:
    %These can be used individually or in combination to achieve desired
    %results.
```

```
        %MinPeakHeight: minimum value needed to be considered a "peak". This
        %can be positive or negative.
        %Threshold: minimum difference in magnitude between two possible
peaks
        %to consider a second value a peak. This must be a positive integer.
        %MinPeakDistance: minimum separation in time between a peak and
        %surrounding potential peaks. This searches from largest magnitude
        %first and continues until no more peaks are available.
    %Flip to negative values so valleys become peaks.
    TTBXCO=TTBXCO*-1;
    TTBXCO_Right=TTBXCO_Right*-1;
    TTBXCO_Left=TTBXCO_Left*-1;
    %find the peaks
    [TTBXCOpeaks,TTBXCOlocs]=findpeaks(TTBXCO,Fs);
    [TTBXCOpeaks_Right,TTBXCOlocs_Right]=findpeaks(TTBXCO_Right,Fs);
    [TTBXCOpeaks_Left,TTBXCOlocs_Left]=findpeaks(TTBXCO_Left,Fs);
    %Flip back to positive numbers for array of times.
    TTBXCO=TTBXCO*-1;
    TTBXCO_Right=TTBXCO_Right*-1;
    TTBXCO_Left=TTBXCO_Left*-1;
    %Flip peak values also to positive numbers
    TTBXCOpeaks=TTBXCOpeaks*-1;
    TTBXCOpeaks_Right=TTBXCOpeaks_Right*-1;
    TTBXCOpeaks_Left=TTBXCOpeaks_Left*-1;
    %Convert from sample number to time by multiplying time index of peaks by
    %sampling frequency.
    TTBXCOlocs=TTBXCOlocs*25;
    TTBXCOlocs_Right=TTBXCOlocs_Right*25;
    TTBXCOlocs_Left=TTBXCOlocs_Left*25;
    %Duplicate above steps for the anterior-posterior data
    TTBYCO=TTBYCO*-1;
    [TTBYCOpeaks,TTBYCOlocs]=findpeaks(TTBYCO,Fs);
    TTBYCO=TTBYCO.*-1;
    TTBYCOpeaks=TTBYCOpeaks.*-1;
    TTBYCOlocs=TTBYCOlocs*25;
    %Calculate average, standard deviation, and 2X the standard deviation of
    %the time to boundary sequence for mediolateral COP
    TTBXaverageCO=mean(TTBXCOpeaks);
    TTBXstdevCO=std(TTBXCOpeaks);
    TTBXthresholdCO=TTBXaverageCO + 2*TTBXstdevCO;
        TTBXaverageCO_Right=mean(TTBXCOpeaks_Right);
        TTBXstdevCO_Right=std(TTBXCOpeaks_Right);
        TTBXthresholdCO_Right=TTBXaverageCO_Right + 2*TTBXstdevCO_Right;
            TTBXaverageCO_Left=mean(TTBXCOpeaks_Left);
            TTBXstdevCO_Left=std(TTBXCOpeaks_Left);
            TTBXthresholdCO_Left=TTBXaverageCO_Left + 2*TTBXstdevCO_Left;
    %Calculate average, standard deviation, and 2X the standard deviation of
    %the time to boundary sequence for anterior-posterior COP
    TTBYaverageCO=mean(TTBYCOpeaks);
    TTBYstdevCO=std(TTBYCOpeaks);
    TTBYthresholdCO=TTBYaverageCO + 2*TTBYstdevCO;
    %Create vector of maximum peak height that warrants a TTB minimum.
    TTBXthresholdlineCO(1:length(time_CO),1)=TTBXthresholdCO;

TTBXthresholdlineCO_Right(1:length(time_CO_Right),1)=TTBXthresholdCO_Right;

TTBXthresholdlineCO_Left(1:length(time_CO_Left),1)=TTBXthresholdCO_Left;
    TTBYthresholdlineCO(1:length(time_CO),1)=TTBYthresholdCO;
```

```
    %Plot TTBs for AP and ML series and label the local minima where the
    %minimum TTB occurs
    TTBplot3 = figure(6)
    subplot(2,1,1);plot(time_CO, TTBYthresholdlineCO, '--k',time_CO,TTBYCO,
'-k', TTBYCOlocs,TTBYCOpeaks, 'xr','MarkerSize',12);
    ylabel('AP Time to Boundary (s)');
    title('mCTSIB: Compliant Surface & Eyes Open');
    text(TTBYCOlocs,TTBYCOpeaks,num2str((1:numel(TTBYCOpeaks))'));
    legend('+2 SD of average TTB Events', 'TTB', 'Min TTB');
    set(gca,'FontSize', 18);
    subplot(2,1,2);plot(time_CO, TTBXthresholdlineCO, '--k',time_CO,TTBXCO,
'-k', TTBXCOlocs,TTBXCOpeaks, 'xr','MarkerSize',12);
    text(TTBXCOlocs,TTBXCOpeaks,num2str((1:numel(TTBXCOpeaks))'));
    ylabel('ML Time to Boundary (s)');
    xlabel('Sample');
    legend('+2 SD of average TTB Events', 'TTB', 'Min TTB');
    set(gca,'FontSize', 18);
    %Save figure...
    PlotSaved = subnum;
    savefig(TTBplot3,[TTBplotFolder6,PlotSaved]);

    % ML Outputs
    fname = [ResultDirML,'/',subnum,'_ML_CO_mCTSIB.csv'];
    CO_mCTSIB_ML = [TTBXCOlocs TTBXCOpeaks];
    writefile(fname,CO_mCTSIB_ML);
        fname = [ResultDirRight,'/',subnum,'_ML_CO_mCTSIB_Right.csv'];
        CO_mCTSIB_ML_Right = [TTBXCOlocs_Right TTBXCOpeaks_Right];
        writefile(fname,CO_mCTSIB_ML_Right);
            fname = [ResultDirLeft,'/',subnum,'_ML_CO_mCTSIB_Left.csv'];
            CO_mCTSIB_ML_Left = [TTBXCOlocs_Left TTBXCOpeaks_Left];
            writefile(fname,CO_mCTSIB_ML_Left);
    % AP Outputs
    fname = [ResultDirAP,'/',subnum,'_AP_CO_mCTSIB.csv'];
    CO_mCTSIB_AP = [TTBYCOlocs TTBYCOpeaks];
    writefile(fname,CO_mCTSIB_AP);
end
% END processing of mCTSIB: Compliant Surface & Eyes Open condition
%% Test Condition: mCTSIB: Compliant Surface & Eyes Closed
if exist('data4','var')== 1
    %Segement out the X and Y data from the raw data; This data will include
    %the 30 sec of testing for the mBESS (when collecting at 25 Hz this will
    %be the next 750 frames)
    CCtrialxdata=data4(:,2);
    CCtrialydata=data4(:,3);
    %Center the stabilograms
    CCtrialxdata(:,1) = CCtrialxdata(:,1) - mean(CCtrialxdata(:,1));
    CCtrialydata(:,1) = CCtrialydata(:,1) - mean(CCtrialydata(:,1));
    %% Plot the base of support and stabiligram
    Stabilogram4 = figure(7)
    hold on
    plot(CCtrialxdata(:,1),CCtrialydata(:,1)), '-k';
    title('mCTSIB Stabiligram: Compliant Surface & Eyes Closed');
    set(gca, 'FontSize', 18);
    xlabel('ML COP (cm)'); ylabel('AP COP (cm)');
    plot(edges(:,1), edges(:,2),'-k', 'LineWidth', 2);
    axis('square');
    hold off
```

```
    PlotSaved = subnum;
    savefig(Stabilogram4,[TTBplotFolder7,PlotSaved]);
    %% Calculate distances between position of COP and the boundary the COP
is
    %approaching. Calculate the velocity during the interval and divide the
    %distance to the border by the velocity of approach to get the TTB. This
    %portion is the mediolateral direction.
    %determine velocity of the COP in ML and AP directions
    [copxvelCC]=deriv1(CCtrialxdata,dt);
    [copyvelCC]=deriv1(CCtrialydata,dt);
    %create vector for allocating distances between COP and boundary edge. A
    %positive X means lateral movement and positive Y indicates anterior
    %movement.
    xboundarydistanceCC = [ ];
    yboundarydistanceCC = [ ];
    xboundarydistanceCC_Right = [ ];
    xboundarydistanceCC_Left = [ ];
    copxvelCC_Right = [ ];
    copxvelCC_Left = [ ];
    %Subtract right edge from laterally moving (+ velocity) COP and subtract
    %position of left edge from medially moving (- velocity) COP
    for i=1:length(CCtrialxdata);
        if copxvelCC(i) >= 0;
            xboundarydistanceCC(i) = edges(3,1) - CCtrialxdata(i);
            xboundarydistanceCC_Right(i) = edges(3,1) - CCtrialxdata(i);
            if copxvelCC(i) > 0
                copxvelCC_Right(i,1) = copxvelCC(i);
            else copxvelCC_Right(i,1) = inf;
            end
        else
            xboundarydistanceCC(i) = CCtrialxdata(i) - edges(1,1);
            xboundarydistanceCC_Left(i) = edges(3,1) - CCtrialxdata(i);
            copxvelCC_Left(i,1) = copxvelCC(i);
        end
    end
    xboundarydistanceCC_Right(xboundarydistanceCC_Right==0) = [];
    xboundarydistanceCC_Left(xboundarydistanceCC_Left==0) = [];
    copxvelCC_Right(copxvelCC_Right == 0) = [];
    copxvelCC_Left(copxvelCC_Left == 0) = [];
    for i = 1:length(copxvelCC_Right)
        if copxvelCC_Right(i) == Inf
            copxvelCC_Right(i) = 0;
        end
    end
    %Subtract toe edge from laterally moving (+ velocity) COP and subtract
    %position of heel edge from medially moving (- velocity) COP
    for i=1:length(CCtrialydata);
        if copyvelCC(i) >= 0;
            yboundarydistanceCC(i) = edges(2,2) - CCtrialydata(i);
        else
            yboundarydistanceCC(i) = CCtrialydata(i) - edges(1,2);
        end
    end

    TTBXCC = abs(xboundarydistanceCC'./copxvelCC);
    TTBXCC_Right = abs(xboundarydistanceCC_Right'./copxvelCC_Right);
    TTBXCC_Left = abs(xboundarydistanceCC_Left'./copxvelCC_Left);
    TTBYCC = abs(yboundarydistanceCC'./copyvelCC);
```

```
    %% Create a time vector for plotting the ML/AP TTBs
    time_CC=1:length(TTBXCC);
    time_CC=time_CC';
    %Time for right TTB
    time_CC_Right=1:length(TTBXCC_Right);
    time_CC_Right=time_CC_Right';
    %Time for left TTB
    time_CC_Left=1:length(TTBXCC_Left);
    time_CC_Left=time_CC_Left';
    %Find local minima (valleys) by first multiplying both series by -1 and
use
    %the findpeaks function to get the time index of these peaks. Then
rectify
    %the signal to convert back to valleys. Convert from time to sample of
the
    %peaks by multiplying the time index by sampling rate (25 Hz).
    %Findpeaks commands:
    %These can be used individually or in combination to achieve desired
    %results.
        %MinPeakHeight: minimum value needed to be considered a "peak". This
        %can be positive or negative.
        %Threshold: minimum difference in magnitude between two possible
peaks
        %to consider a second value a peak. This must be a positive integer.
        %MinPeakDistance: minimum separation in time between a peak and
        %surrounding potential peaks. This searches from largest magnitude
        %first and continues until no more peaks are available.
    %Flip to negative values so valleys become peaks.
    TTBXCC=TTBXCC*-1;
    TTBXCC_Right=TTBXCC_Right*-1;
    TTBXCC_Left=TTBXCC_Left*-1;
    %find the peaks
    [TTBXCCpeaks,TTBXCClocs]=findpeaks(TTBXCC,Fs);
    [TTBXCCpeaks_Right,TTBXCClocs_Right]=findpeaks(TTBXCC_Right,Fs);
    [TTBXCCpeaks_Left,TTBXCClocs_Left]=findpeaks(TTBXCC_Left,Fs);
    %Flip back to positive numbers for array of times.
    TTBXCC=TTBXCC*-1;
    TTBXCC_Right=TTBXCC_Right*-1;
    TTBXCC_Left=TTBXCC_Left*-1;
    %Flip peak values also to positive numbers
    TTBXCCpeaks=TTBXCCpeaks*-1;
    TTBXCCpeaks_Right=TTBXCCpeaks_Right*-1;
    TTBXCCpeaks_Left=TTBXCCpeaks_Left*-1;
    %Convert from sample number to time by multiplying time index of peaks by
    %sampling frequency.
    TTBXCClocs=TTBXCClocs*25;
    TTBXCClocs_Right=TTBXCClocs_Right*25;
    TTBXCClocs_Left=TTBXCClocs_Left*25;
    %Duplicate above steps for the anterior-posterior data
    TTBYCC=TTBYCC*-1;
    [TTBYCCpeaks,TTBYCClocs]=findpeaks(TTBYCC,Fs);
    TTBYCC=TTBYCC.*-1;
    TTBYCCpeaks=TTBYCCpeaks.*-1;
    TTBYCClocs=TTBYCClocs*25;
    %Calculate average, standard deviation, and 2X the standard deviation of
    %the time to boundary sequence for mediolateral COP
    TTBXaverageCC=mean(TTBXCCpeaks);
    TTBXstdevCC=std(TTBXCCpeaks);
```

```
    TTBXthresholdCC=TTBXaverageCC + 2*TTBXstdevCC;
        TTBXaverageCC_Right=mean(TTBXCCpeaks_Right);
        TTBXstdevCC_Right=std(TTBXCCpeaks_Right);
        TTBXthresholdCC_Right=TTBXaverageCC_Right + 2*TTBXstdevCC_Right;
            TTBXaverageCC_Left=mean(TTBXCCpeaks_Left);
            TTBXstdevCC_Left=std(TTBXCCpeaks_Left);
            TTBXthresholdCC_Left=TTBXaverageCC_Left + 2*TTBXstdevCC_Left;
    %Calculate average, standard deviation, and 2X the standard deviation of
    %the time to boundary sequence for anterior-posterior COP
    TTBYaverageCC=mean(TTBYCCpeaks);
    TTBYstdevCC=std(TTBYCCpeaks);
    TTBYthresholdCC=TTBYaverageCC + 2*TTBYstdevCC;
    %Create vector of maximum peak height that warrants a TTB minimum.
    TTBXthresholdlineCC(1:length(time_CC),1)=TTBXthresholdCC;

TTBXthresholdlineCC_Right(1:length(time_CC_Right),1)=TTBXthresholdCC_Right;

TTBXthresholdlineCC_Left(1:length(time_CC_Left),1)=TTBXthresholdCC_Left;
    TTBYthresholdlineCC(1:length(time_CC),1)=TTBYthresholdCC;

    %Plot TTBs for AP and ML series and label the local minima where the
    %minimum TTB occurs
    TTBplot4 = figure(8)
    subplot(2,1,1);plot(time_CC, TTBYthresholdlineCC, '--k',time_CC,TTBYCC,
'-k', TTBYCClocs,TTBYCCpeaks, 'xr','MarkerSize',12);
    ylabel('AP Time to Boundary (s)');
    title('mCTSIB: Compliant Surface & Eyes Closed');
    text(TTBYCClocs,TTBYCCpeaks,num2str((1:numel(TTBYCCpeaks))'));
    legend('+2 SD of average TTB Events', 'TTB', 'Min TTB');
    set(gca,'FontSize', 18);
    subplot(2,1,2);plot(time_CC, TTBXthresholdlineCC, '--k',time_CC,TTBXCC,
'-k', TTBXCClocs,TTBXCCpeaks, 'xr','MarkerSize',12);
    text(TTBXCClocs,TTBXCCpeaks,num2str((1:numel(TTBXCCpeaks))'));
    ylabel('ML Time to Boundary (s)');
    xlabel('Sample');
    legend('+2 SD of average TTB Events', 'TTB', 'Min TTB');
    set(gca,'FontSize', 18);
    %Save figure...
    PlotSaved = subnum;
    savefig(TTBplot4,[TTBplotFolder8,PlotSaved]);

    % ML Outputs
    fname = [ResultDirML,'/',subnum,'_ML_CC_mCTSIB.csv'];
    CC_mCTSIB_ML = [TTBXCClocs TTBXCCpeaks];
    writefile(fname,CC_mCTSIB_ML);
        fname = [ResultDirRight,'/',subnum,'_ML_CC_mCTSIB_Right.csv'];
        CC_mCTSIB_ML_Right = [TTBXCClocs_Right TTBXCCpeaks_Right];
        writefile(fname,CC_mCTSIB_ML_Right);
            fname = [ResultDirLeft,'/',subnum,'_ML_CC_mCTSIB_Left.csv'];
            CC_mCTSIB_ML_Left = [TTBXCClocs_Left TTBXCCpeaks_Left];
            writefile(fname,CC_mCTSIB_ML_Left);
    % AP Outputs
    fname = [ResultDirAP,'/',subnum,'_AP_CC_mCTSIB.csv'];
    CC_mCTSIB_AP = [TTBYCClocs TTBYCCpeaks];
    writefile(fname,CC_mCTSIB_AP);
end
% END processing of mCTSIB: Compliant Surface & Eyes Closed condition
%%%%%%%%%%%%%%%%%%%%%%%%%%%%%%%%%%%%%%%%%%%%%%%%%%%%%%%%%%%%%%%%%%%%%%%%%%%%
```

```
%% Output the data set
%Export the statistics for each trial and direction. These are exported as
%a single csv file. These variables are in two columns. Column 1 contains
%ML data: rows 1, 4, 7, and 10 are Rigid-Eyes Open, Rigid-Eyes Closed,
%Compliant-Eyes Open, and Compliant-Eyes Closed TTB events.
%Rows 2, 5, and 8, 11 are the average TTB values (in seconds).
%Rows 3, 6, 9, and 12 are the standard deviations of the TTB values.
%Column 2 has similar data organization but for the AP direction.
TTBMLSeries = [length(TTBXROpeaks) length(TTBXRCpeaks) length(TTBXCOpeaks)
length(TTBXCCpeaks)];
    TTBMLSeries_Right = [length(TTBXROpeaks_Right) length(TTBXRCpeaks_Right)
length(TTBXCOpeaks_Right) length(TTBXCCpeaks_Right)];
    TTBMLSeries_Left = [length(TTBXROpeaks_Left) length(TTBXRCpeaks_Left)
length(TTBXCOpeaks_Left) length(TTBXCCpeaks_Left)];
TTBAPSeries = [length(TTBYROpeaks) length(TTBYRCpeaks) length(TTBYCOpeaks)
length(TTBYCCpeaks)];
MLStatistics = [TTBMLSeries(1,1); TTBXaverageRO; TTBXstdevRO;
TTBMLSeries(1,2);...
    TTBXaverageRC; TTBXstdevRC; TTBMLSeries(1,3); TTBXaverageCO; TTBXstdevCO;
TTBMLSeries(1,4); TTBXaverageCC; TTBXstdevCC];
        MLStatistics_Right = [TTBMLSeries_Right(1,1); TTBXaverageRO_Right;
TTBXstdevRO_Right; TTBMLSeries_Right(1,2);...
            TTBXaverageRC_Right; TTBXstdevRC_Right; TTBMLSeries_Right(1,3);
TTBXaverageCO_Right; TTBXstdevCO_Right; TTBMLSeries_Right(1,4);
TTBXaverageCC_Right; TTBXstdevCC_Right];
        MLStatistics_Left = [TTBMLSeries_Left(1,1); TTBXaverageRO_Left;
TTBXstdevRO_Left; TTBMLSeries_Left(1,2);...
            TTBXaverageRC_Left; TTBXstdevRC_Left; TTBMLSeries_Left(1,3);
TTBXaverageCO_Left; TTBXstdevCO_Left; TTBMLSeries_Left(1,4);
TTBXaverageCC_Left; TTBXstdevCC_Left];

APStatistics = [TTBAPSeries(1,1); TTBYaverageRO; TTBYstdevRO;
TTBAPSeries(1,2);...
    TTBYaverageRC; TTBYstdevRC; TTBAPSeries(1,3); TTBYaverageCO; TTBYstdevCO;
TTBAPSeries(1,4); TTBYaverageCC; TTBYstdevCC];
%Antero-Posterior output values
    AP_AllStats = [APStatistics];
    fname = [TTBstatsFolder,'/',subnum,'AP_TTBstatistics.csv'];
    writefile(fname,AP_AllStats);
%Medio-Lateral output values
    ML_AllStats = [MLStatistics];
    fname = [TTBstatsFolder,'/',subnum,'ML_TTBstatistics.csv'];
    writefile(fname,ML_AllStats);
 %Right output values
    Right_AllStats = [MLStatistics_Right];
    fname = [TTBstatsFolder,'/',subnum,'Right_ML_TTBstatistics.csv'];
    writefile(fname,Right_AllStats);
 %Leftl output values
    Left_AllStats = [MLStatistics_Left];
    fname = [TTBstatsFolder,'/',subnum,'Left_ML_TTBstatistics.csv'];
    writefile(fname,Left_AllStats);

%% END of SCRIPT Step 3
%*************************************************************************
%*************************************************************************
%*************************************************************************
```

Step 4: Time-To-Boundary Write Script

```
%Script Author: Sutton B. Richmond
    %Last Revised Script: 10/20/2018
    %Parent Script: MRS_TTB_mCTSIB
    %Additional Functions .m files REQUIRED to be in the path:
    % 1.)writefile.m

%Original output files achieved from the MRS_TTB_mCTSIB (AP_TTBstatistics &
%ML_TTBstatistics)info:

%Trials for each subject will be exported as TTB statistics for each
%direction. These are exported as a single csv file. These variables are in
%one columns.
%ML data:
%Rows 1, 4, 7, and 10 are TTB events.
%Rows 2, 5, and 8, 11 are the average TTB values (in seconds).
%Rows 3, 6, 9, and 12 are the standard deviations of the TTB values.

%AP data:
%Rows 1, 4, 7, and 10 are TTB events.
%Rows 2, 5, and 8, 11 are the average TTB values (in seconds).
%Rows 3, 6, 9, and 12 are the standard deviations of the TTB values.

%Clear the MATLAB spaces
clc
clear all
close all
%This will allow the script to return to the main directory.
GoBack = pwd;
%% AP TTB Evaluation
cd('/Volumes/SBR_CSU/Mobility/MRS_PS_Data/TTBresults/TTBstats/');
uiwait(msgbox('Choose the ###AP_TTBstatistics.csv'));
APfile = uigetfile('*.csv');
PATH = pwd
STR1 = APfile;
APdata = dlmread([PATH,'/', STR1], ',',0, 0);
% Input the desired location where you would like to input the data within
% the new sheet = the right side of the parameter is the location from
% where in the original data output.

%Column 1: subject ID
    % subnum = input('Enter 3 digit subject number: ', 's');
    % avgTTB(1,1)= subnum;
%Column 2: TTB Average (seconds) for Rigid Surface-Eyes Open (mCTSIB)
%Column 3: TTB Average (seconds) for Rigid Surface-Eyes Closed (mCTSIB)
%Column 4: TTB Average (seconds) for Compliant Surface-Eyes Open (mCTSIB)
%Column 5: TTB Average (seconds) for Compliant Surface-Eyes Closed (mCTSIB)
AP_TTB(1,2)= APdata(2,1);
AP_TTB(1,3)= APdata(5,1);
AP_TTB(1,4)= APdata(8,1);
AP_TTB(1,5)= APdata(11,1);
%Column 6: TTB Standard Deviation of TTB Avg for Rigid Surface-Eyes Open
(mCTSIB)
%Column 7: TTB Standard Deviation of TTB Avg Rigid Surface-Eyes Closed
(mCTSIB)
```

```
%Column 8: TTB Standard Deviation of TTB Avg Compliant Surface-Eyes Open
(mCTSIB)
%Column 9: TTB Standard Deviation of TTB Avg Compliant Surface-Eyes Closed
(mCTSIB)
AP_TTB(1,6)= APdata(3,1);
AP_TTB(1,7)= APdata(6,1);
AP_TTB(1,8)= APdata(9,1);
AP_TTB(1,9)= APdata(12,1);
%Column 6: TTB Events (number) for Rigid Surface-Eyes Open (mCTSIB)
%Column 7: TTB Events (Number) for Rigid Surface-Eyes Closed (mCTSIB)
%Column 8: TTB Events (Number) for Compliant Surface-Eyes Open (mCTSIB)
%Column 9: TTB Events (Number) for Compliant Surface-Eyes Closed (mCTSIB)
AP_TTB(1,10)= APdata(1,1);
AP_TTB(1,11)= APdata(4,1);
AP_TTB(1,12)= APdata(7,1);
AP_TTB(1,13)= APdata(10,1);
%Write AP Outcomes
dlmwrite('APttbSummary.csv',AP_TTB,'delimiter',',','-append');
%% ML TTB Evaluation
cd(pwd);
uiwait(msgbox('Choose the ###ML_TTBstatistics.csv'));
MLfile = uigetfile('*.csv');
PATH = pwd
STR2 = MLfile;
MLdata = dlmread([PATH,'/', STR2], ',',0, 0);
%     subnum = input('Enter 3 digit subject number: ', 's');
%     avgTTB(1,1)= subnum;
ML_TTB(1,2)= MLdata(2,1);
ML_TTB(1,3)= MLdata(5,1);
ML_TTB(1,4)= MLdata(8,1);
ML_TTB(1,5)= MLdata(11,1);
    ML_TTB(1,6)= MLdata(3,1);
    ML_TTB(1,7)= MLdata(6,1);
    ML_TTB(1,8)= MLdata(9,1);
    ML_TTB(1,9)= MLdata(12,1);
        ML_TTB(1,10)= MLdata(1,1);
        ML_TTB(1,11)= MLdata(4,1);
        ML_TTB(1,12)= MLdata(7,1);
        ML_TTB(1,13)= MLdata(10,1);
dlmwrite('MLttbSummary.csv',ML_TTB,'delimiter',',','-append');
%% Right Side TTB Evaluation
cd(pwd);
uiwait(msgbox('Choose the ###Right_ML_TTBstatistics.csv'));
Right_MLfile = uigetfile('*.csv');
PATH = pwd
STR3 = Right_MLfile;
Right_MLdata = dlmread([PATH,'/', STR3], ',',0, 0);
%     subnum = input('Enter 3 digit subject number: ', 's');
%     avgTTB(1,1)= subnum;
Right_ML_TTB(1,2)= Right_MLdata(2,1);
Right_ML_TTB(1,3)= Right_MLdata(5,1);
Right_ML_TTB(1,4)= Right_MLdata(8,1);
Right_ML_TTB(1,5)= Right_MLdata(11,1);
    Right_ML_TTB(1,6)= Right_MLdata(3,1);
    Right_ML_TTB(1,7)= Right_MLdata(6,1);
    Right_ML_TTB(1,8)= Right_MLdata(9,1);
    Right_ML_TTB(1,9)= Right_MLdata(12,1);
        Right_ML_TTB(1,10)= Right_MLdata(1,1);
```

```
        Right_ML_TTB(1,11)= Right_MLdata(4,1);
        Right_ML_TTB(1,12)= Right_MLdata(7,1);
        Right_ML_TTB(1,13)= Right_MLdata(10,1);
dlmwrite('Right_MLttbSummary.csv',Right_ML_TTB,'delimiter',',','-append');
%% Left Side TTB Evaluation
cd(pwd);
uiwait(msgbox('Choose the ###Left_ML_TTBstatistics.csv'));
Left_MLfile = uigetfile('*.csv');
PATH = pwd
STR4 = Left_MLfile;
Left_MLdata = dlmread([PATH,'/', STR4], ',',0, 0);
%     subnum = input('Enter 3 digit subject number: ', 's');
%     avgTTB(1,1)= subnum;
Left_ML_TTB(1,2)= Left_MLdata(2,1);
Left_ML_TTB(1,3)= Left_MLdata(5,1);
Left_ML_TTB(1,4)= Left_MLdata(8,1);
Left_ML_TTB(1,5)= Left_MLdata(11,1);
    Left_ML_TTB(1,6)= Left_MLdata(3,1);
    Left_ML_TTB(1,7)= Left_MLdata(6,1);
    Left_ML_TTB(1,8)= Left_MLdata(9,1);
    Left_ML_TTB(1,9)= Left_MLdata(12,1);
        Left_ML_TTB(1,10)= Left_MLdata(1,1);
        Left_ML_TTB(1,11)= Left_MLdata(4,1);
        Left_ML_TTB(1,12)= Left_MLdata(7,1);
        Left_ML_TTB(1,13)= Left_MLdata(10,1);
dlmwrite('Left_MLttbSummary.csv',Left_ML_TTB,'delimiter',',','-append');

cd(GoBack);

%% END of SCRIPT Step 4
%*************************************************************************
%*************************************************************************
%*************************************************************************
```